Progress Report for FY 1988-89

on Grant DE-FG05-85ER60285

DOE/ER/60285--6

DE89 015814

# Simulation Analysis of Moored Fluorometer Time Series from the Mid-Atlantic Bight

Principal Investigator: John J. Walsh

Co-Investigators: D. A. Dieterle, W. W. Gregg, J. R. Pribble

---

During 1988-89, I compiled a planning document for a major DOE particle flux experiment off Cape Hatteras as a complement to the NSF GOFS program and the ONR Biosynop program. The plan, entitled "A prospectus for a Department of Energy COMFS-I Cape Hatteras Flux Experiment," was sent to Dr. George W. Saunders of the Ecological Research Division. As outlined in our research plan of last year, I also initiated collaboration with Dr. Wilton Sturges of Florida State University to run some of our simulation models on the ETA-10 supercomputer at SCRI in Tallahassee. A proposal for computer time entitled "A Gulf Stream biophysical model: supercomputer access to the FSU/SCRI ETA-10" was just submitted to Dr. George D. Duda of the Health Effects Research Division.

To begin an analysis of the export of energy-related by-products from coastal zones by western boundary currents, we successfully coupled a two-layered baroclinic model of Loop Current penetration and eddy shedding in the Gulf of Mexico over a simulated period of one year on the ECOS modeling facility at USF. Model estimates of upward nitrate fluxes across the basin pycnocline and of sinking particle fluxes in slope waters approximate those of other oligotrophic regimes, while simulated nitrate and chlorophyll abundances match shipboard and satellite observations in the Gulf of Mexico. These results are described in the attached manuscript, "Nitrogen exchange at the continental margin: a numerical study of the Gulf of Mexico," which has been accepted for publication in Progress in Oceanography.

Over the last year with partial DOE support, we have also initiated a simulation analysis of the time-dependent sources of algal

phytodetritus to sediment traps, moored for one year during SEEP-I on the continental slope and rise of the Mid-Atlantic Bight. In this model, phytodetritus with respective sinking rates of 1 m $day^{-1}$, 10 m $day^{-1}$, and 100 m $day^{-1}$ represents the residues of picoplankton, diatom, and macro-aggregate populations at the bottom of the euphotic zone. Preliminary results suggest a time dependency of the macro-aggregate size class centered around the spring bloom, which must be kept resuspended within a benthic boundary layer to survive descent to depths of 1000-2000 m on the slope. This work will constitute part of the dissertation research of Mr. J. R. Pribble.

Another student, Mr. W. W. Gregg, has completed a first draft of his dissertation on a simulation model of plankton dynamics within shelf and slope waters of the Mid-Atlantic Bight. Specifically, his research involves a two-layer baroclinic, wind-forced circulation field, "new" production and that based on regenerated ammonium through herbivore grazing, high depth resolution to adequately resolve depth-dependent light and biological processes (10 layers), two phytoplankton size fractions -- netplankton and nanoplankton -- to simulate spatially dependent phytoplankton distributions of diatoms in shelf and flagellates in slope waters, with the spectral composition of the surface light fields determined as a function of Rayleigh, ozone, and aerosol scattering and absorption. He is able to replicate both algal species succession from shelf to slope waters and CZCS satellite estimates of algal biomass.

Over the last year of this research, we will begin to adapt the biological dynamics of the above Gulf of Mexico model to a GFDL/NCAR

physical model residing on the ETA-10 computer at SCRI, which will extend from a depth of 40 m off Miami to Cape Hatteras, along the U.S. east coast, with an offshore extent to the deep sea (>3000 m) near Bermuda at 25-km grid resolution. The interactions of four algal functional groups (diatom, flagellate, cyanobacterial and coccolithophorid) will then be incorporated into surface waters of the coupled biophysical model of Gulf Stream plankton dynamics. Finally, the more detailed fate of phytodetritus within the aphotic zone, i.e. oxidation or burial, will also be added from our ongoing analysis of the fate of picoplankton, diatoms, and macro-aggregates within slope waters of the Mid-Atlantic Bight as part of Mr. Pribble's dissertation.

# Nitrogen exchange at the continental margin: a numerical study of the Gulf of Mexico

by

John J. Walsh, Dwight A. Dieterle, Mark B. Meyers, and Frank E. Muller-Karger

Department of Marine Science
University of South Florida
140 Seventh Avenue South
St. Petersburg, Florida 33701

## ABSTRACT

A two-layered baroclinic circulation model and a 21-layered biochemical model are used to explore the consequences of Loop Current-induced upwelling and terrestrial eutrophication on "new" production within the Gulf of Mexico. During a quasi-annual penetration and eddy-shedding cycle of the Loop Current, the simulated seasonal changes of incident radiation, wind stress, and surface mixed layer depth induce an annual cycle of algal biomass that corresponds to *in situ* and satellite time series of chlorophyll. The simulated nitrate fields match those of shipboard surveys, while fallout of particulate matter approximates that caught in sediment traps and accumulating in bottom sediments. Assuming an f ratio of 0.06-0.12, the total primary production of the Gulf of Mexico might be 105-210 g C $m^{-2}$ $yr^{-1}$ in the absence of anthropogenic nutrient loadings, i.e., 2-3 fold that of oligotrophic regions not impacted by western boundary currents. Less than 25% of the nitrogen effluent of the Mississippi River may be stored in bottom sediments, with most of this input dispersed in dissolved form beneath the pycnocline, after remineralization of particulate detritus within several production cycles derived from riverine loading. At a sinking rate of 3 m $day^{-1}$, however, sufficient phytodetritus survives oxidation in the water column to balance estimates of bottom metabolism and burial at the margins.

## Introduction

The major nitrogen sources for the Gulf of Mexico are advection of nitrate in through Yucatan Strait, nitrogen fixation by cyanobacteria, and river discharge of sewage and fertilizers. Similarly, the significant nitrogen sinks for the Gulf of Mexico are presumably advection of water out through Florida Strait, denitrification by other bacteria, and burial of organic matter. Rainfall, dry deposition, and exchange of nitrous oxide are considered to be small sources and sinks of nitrogen, compared to the above processes. To explore the consequences of altered fluxes of nitrogen across the oceanic, atmospheric, and terrestrial boundaries of the Gulf of Mexico, we combined a 2-layered model of water motion with a 21-layered model of nutrient cycling in the basin.

Such coupled models require specification of boundary conditions of flow, dissolved nitrogen, and particulate matter; but synoptic nitrate, current, and plankton data from both the Yucatan and Florida Straits are scarce. During January 1952, two sections were taken across these Straits by the R/V Alaska (Fig. 1) within 5-6 days of each other. To construct consistent depth profiles of nitrate distribution from the NODC files of this cruise, we deleted 20 apparently spurious observations from the available 136 measurements of $NO_3$ at these 11 stations (Fig. 2). The questionable data indicated a local decline of $NO_3$ with depth, before encountering the subsurface maximum of 35-40 μg-at $NO_3$ $\ell^{-1}$ at depths of 500-1000 m (Fig. 2), i.e., just below the oxygen minimum layer and within the salinity minimum of Antarctic Intermediate Water.

The edited 1952 data set displays the same vertical structure of $NO_3$ within Yucatan Strait (Fig. 2a) as subsequently observed 20-25 yr later during October 1972 (Berberian and Starr, 1978) and July 1977 (Furnas and Smayda, 1987). A more recent nutrient data set, taken across Yucatan and Florida Straits during November 1976 and October 1977 (G. Berberian, personal communication; Maul et al., 1979) by the R/V Researcher (Fig. 1), provides a further quality check on our editing of the 1952 data. Autoanalyzer determination of nitrate distribution from the 1976-1977 frozen samples (G. Berberian, personal communication) provided similar subsurface maxima of >35 μg-at $NO_3$ $\ell^{-1}$ at the same depths (Figs. 3-4) of the 1952 sections (Fig. 2), while impoverished nitrate stocks (<1 μg-at $NO_3$ $\ell^{-1}$) were found in the euphotic zone of mid-strait stations, sampled 25 yr apart (Figs. 2-4). We did not use nutrient data from the Researcher sampling of the western Gulf in October 1976, however, when poor nutrient standards on a separate leg of the cruise evidently led to erroneously high nitrate values within the subsurface maxima.

1. Flow

At a sill depth of 768 m in the eastern part of Florida Strait, efflux of nitrogen must be restricted to the upper half of the water column, sampled upstream and north of Havana within the deeper part of this channel on 19-20 January 1952, 14 November 1976, and 29 October 1977 (Figs. 2b-4b). During May 1972, 13 direct measurements of the Florida Current, south of Key West, suggested a mean eastward flow of $21.4 \times 10^6$ $m^3$ $sec^{-1}$ (Sv). This

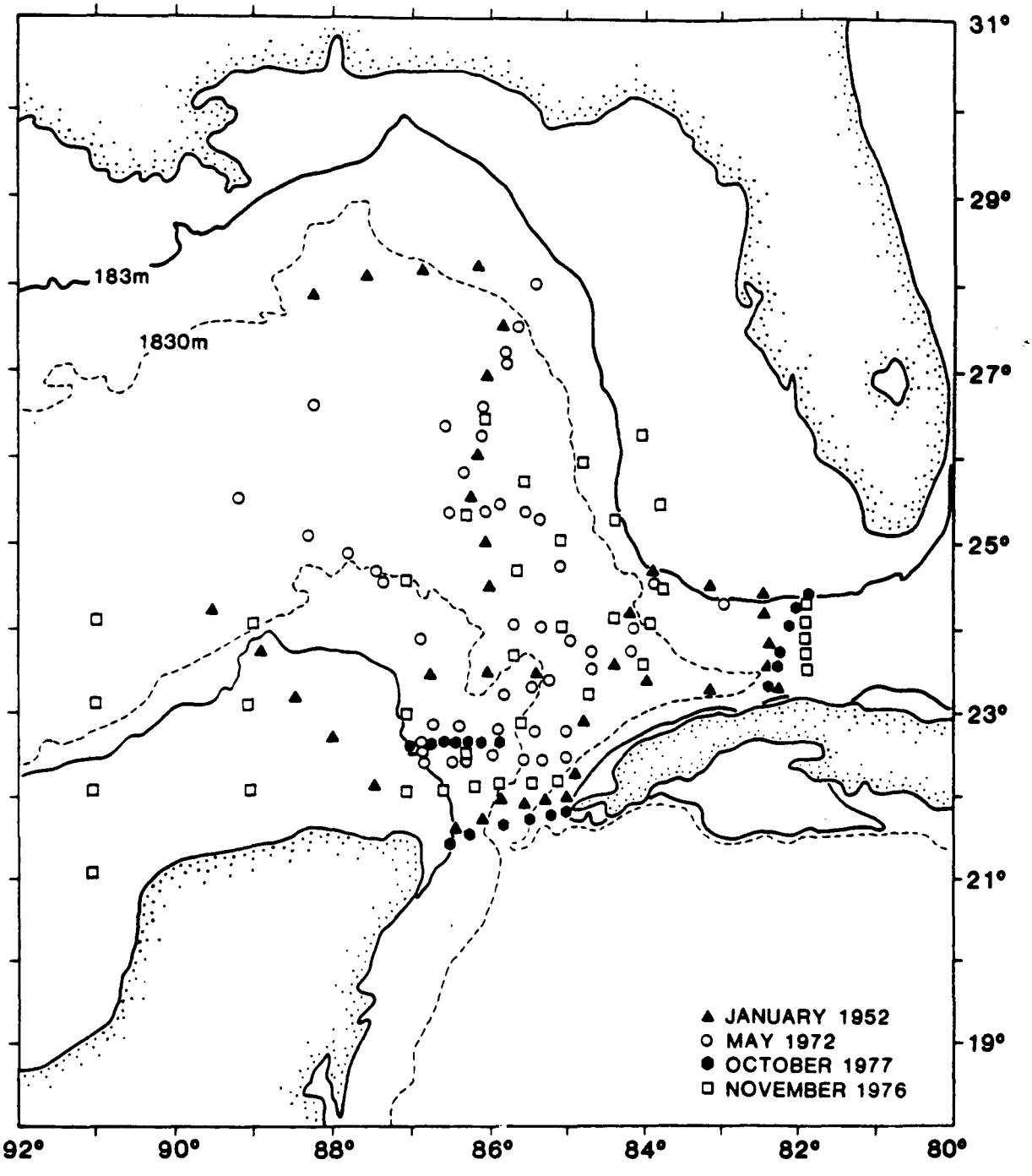


Fig. 1. Station location of nutrient surveys within the eastern Gulf of Mexico during January 1952 (▲), May 1972 (o), November 1976 (□), and October 1977 (•).

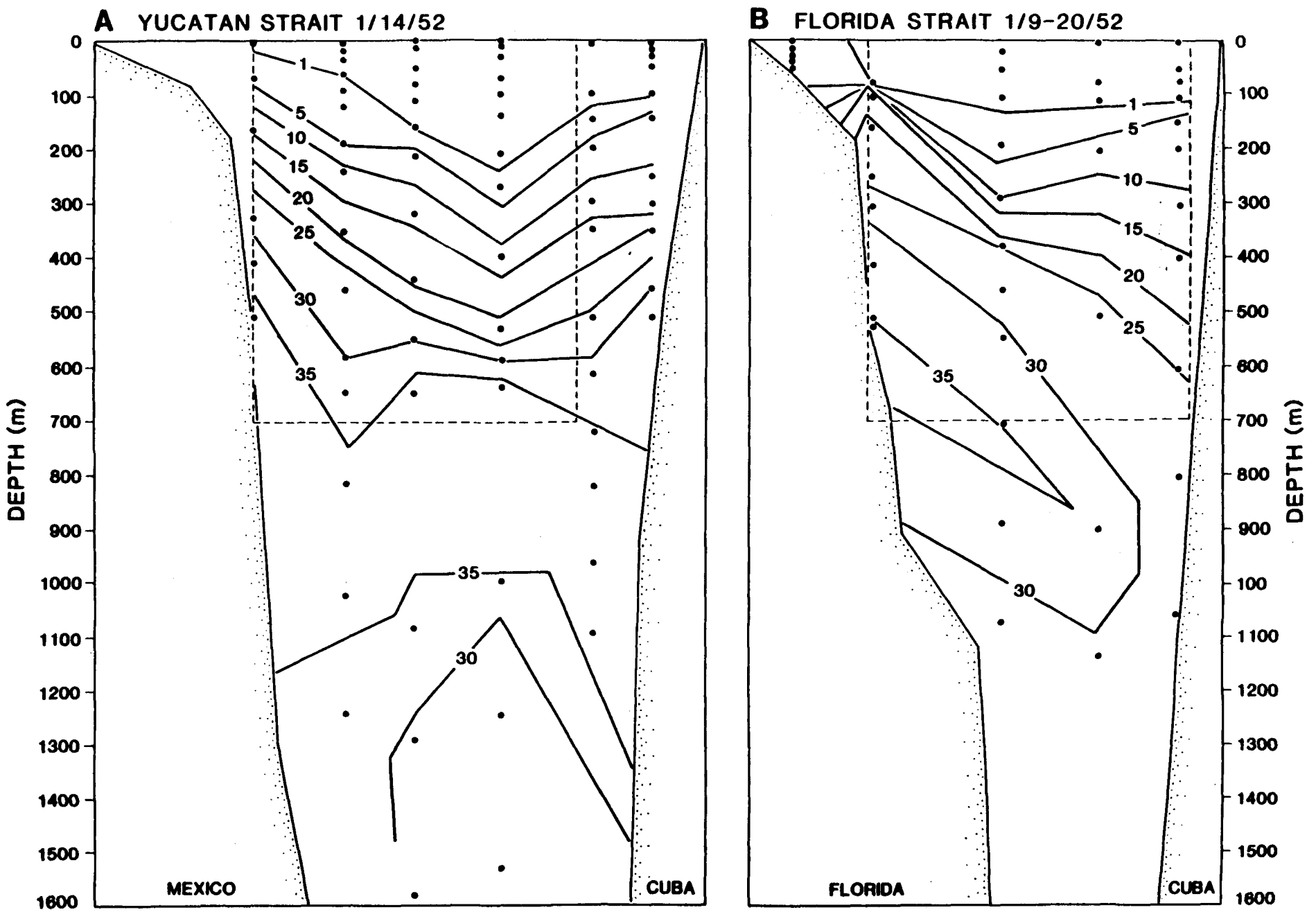


Fig. 2. Nitrate distribution (μg-at $\ell^{-1}$) within the upper 1600 m during a) January 14, 1952 in Yucatan Strait and b) January 19-20, 1952 in Florida Strait.

average includes both the baroclinic and barotropic components of transport in the Florida Strait above a $\sigma_t$ surface of 27.0, i.e., above depths of 160-460 m near respectively Florida and Cuba (Brooks and Niiler, 1975). The 1972 dropsonde transects terminated at 35 km north of Havana, however, perhaps missing a significant part of the eastward transport. The 25 μg-at $\ell^{-1}$ isopleths of nitrate in Figures 2b-4b approximated the 27.0 $\sigma_t$ interfaces of these 1952, 1976, and 1977 sections. At these times, the nitrate profiles of the nearshore Alaska (Fig. 2b) and Researcher (Fig. 3b) stations were taken within ∿10 km of Havana on the Cuban coast, where the 27.0 $\sigma_t$ layer was deeper at depths of 600-620 m.

Recalculation (Maul, 1978) of the baroclinic contribution to flow in the Florida Strait above 700 m and closer to Cuba during March 1938 (Montgomery, 1941), suggests a geostrophic transport of 22.8 Sv. But 27% of the flow was then located within 23 km of the Cuban coast. Another 3.2 Sv of eastward transport occurred between 700 m and 1200 m, where this flow was sampled by a station taken 7 km north of Havana in 1938 (Montgomery, 1941). Presumably some of this deeper flow in the western part of Florida Strait did not exit above the shallow sill to the east. Additional complexities of transport in this strait are flow reversals, for example, with shallow westward flow observed south of Key West in March 1938 (Montgomery, 1941), March 1962 (Hofmann and Worley, 1986) and May 1972 (Brooks and Niiler, 1975).

In a series of monthly hydrographic transects, taken between August 1972 and September 1973 from the 50-m isobath off Key West to 22 km north of Cuba, the eastward geostrophic transport above 700 m varied from 12.4 to 29.0 Sv,

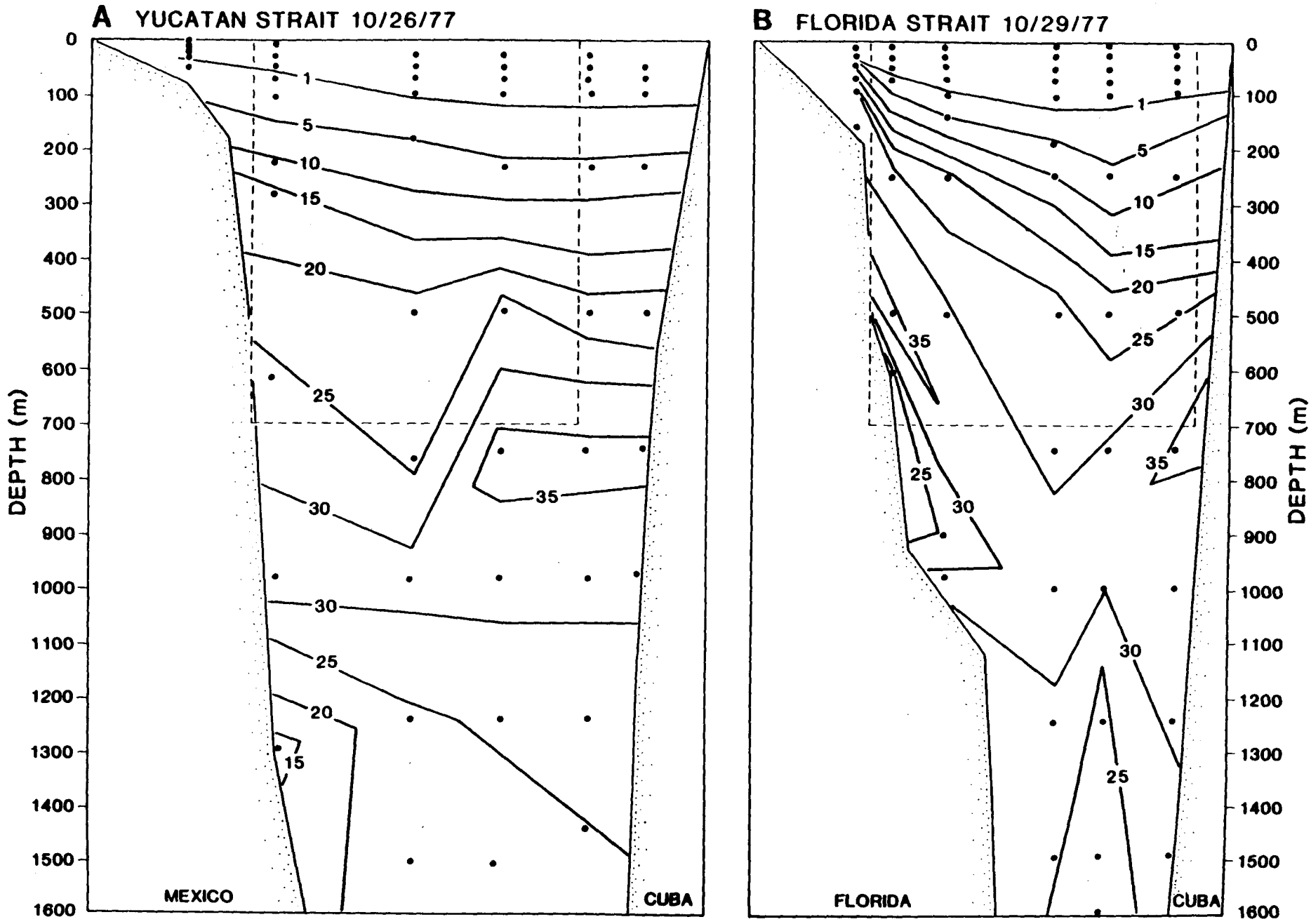


Fig. 3. Nitrate distribution (μg-at $\ell^{-1}$) within the upper 1600 m during a) October 26, 1977 in Yucatan Strait and b) October 29, 1977 in Florida Strait.

with a mean of 19.5 Sv (Maul, 1978). Resident Gulf of Mexico water (Nowlin and McLellan, 1967), i.e., not water of immediate Yucatan or Caribbean origin (Wüst, 1964) and also termed Continental Edge Water (Wennekens, 1959), exits Florida Strait in varying amounts (Fig. 5). It constituted as much as 8.3 Sv of the monthly geostrophic transport through Florida Strait in 1972-73, with a mean flux of 2.7 Sv, i.e., 14% of the outflow (Maul, 1978). When the precursor of the Florida Current, e.g. the Loop Current, penetrates farther north into the Gulf of Mexico from Yucatan Strait, displacing resident waters, the outflow of Continental Edge Water increases along the northern wall of the Florida Strait (Maul, 1977; 1978).

The precursor of the Loop Current in the Gulf of Mexico is termed the Yucatan Current when this western boundary flow is south of and within Yucatan Strait. Measurements of surface flow and hydrographic transects in May 1972 suggested a northward transport above the 27.0 $\sigma_t$ interface of 22.3 Sv within the Yucatan Current between Isla Mujeres, Mexico, and Cabo San Antonio, Cuba (Molinari and Yager, 1977). Similarly 24.0 Sv of northward transport were found above this interface within 6 crossings of the Loop Current, taken north of Yucatan Strait in the same experiment (Morrison and Nowlin, 1977). The depths of the 27.0 $\sigma_t$ surface in Yucatan Strait ranged from 300 m near Mexico to 600 m near Cuba in 1952 and 1977, and were again mainly coincident with the 25 $\mu$g-at $NO_3$ $\ell^{-1}$ isopleths of Figures 2a and 3a.

Southward counterflow has been observed both at greater depths and to the east within Yucatan Strait (Gordon, 1967; Hansen and Molinari, 1979). Between Contoy Island, Mexico, and Cabo San Antonio, Cuba, for example, the

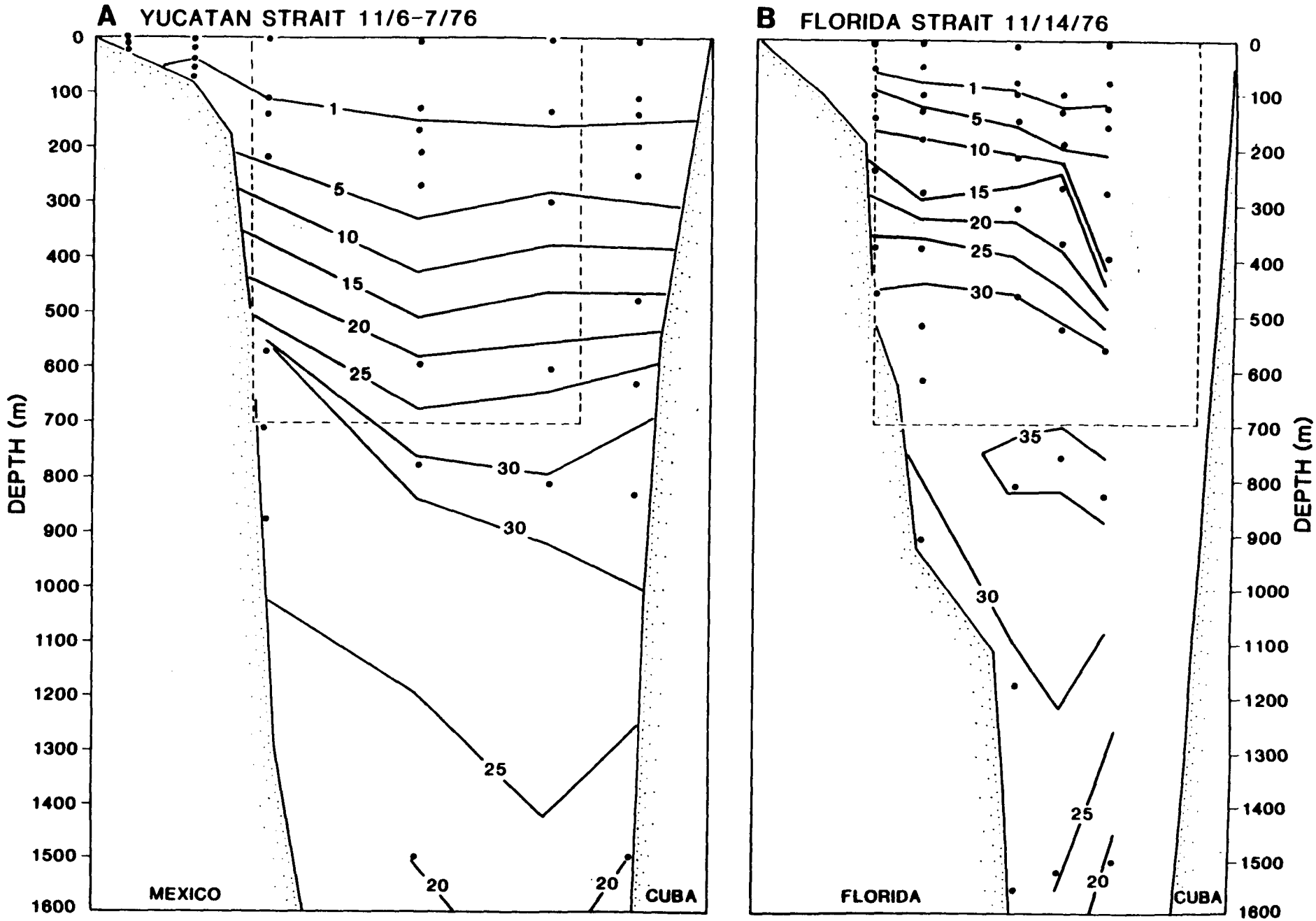


Fig. 4. Nitrate distribution (μg-at $\ell^{-1}$) within the upper 1600 m during a) November 6-7, 1976 in Yucatan Strait and b) November 14, 1976 in Florida Strait.

Table 1. Nitrogen flux through the upper 700 m of Yucatan and Florida Straits during 14-20 January 1952/26-29 October 1977.

| Nitrate Layer ($\mu$g-at $NO_3$ $\ell^{-1}$) | Average Concentration (mg $NO_3$-N $m^{-3}$) | Layer Area ($10^6$ $m^2$) | Nitrate Stock (kg $NO_3$-N $m^{-1}$) | Mean Flow (m $sec^{-1}$) | Nitrate Flux ($10^3$ kg $NO_3$-N $sec^{-1}$) |
|---|---|---|---|---|---|
| Yucatan Strait: | | | | | |
| 0-1 | 7 | 13.52/10.52 | 94.64/ 73.64 | .44 | 0.04/0.03 |
| 1-5 | 42 | 6.76/ 8.26 | 283.92/ 346.92 | .44 | 0.13/0.15 |
| 5-10 | 105 | 5.41/ 6.01 | 568.05/ 631.05 | .44 | 0.25/0.28 |
| 10-15 | 175 | 6.08/ 7.51 | 1064.00/ 1314.25 | .44 | 0.47/0.58 |
| 15-20 | 245 | 8.11/ 9.01 | 1986.95/ 2207.25 | .44 | 0.87/0.97 |
| 20-25 | 315 | 4.73/17.28 | 1489.95/ 5443.20 | .44 | 0.66/2.40 |
| 25-30 | 385 | 7.44/ 6.76 | 2864.40/ 2602.60 | .44 | 1.26/1.15 |
| 30-35 | 455 | 8.79/ 2.25 | 3999.45/ 1023.75 | .44 | 1.76/0.45 |
| 35-40 | 525 | 6.76/ 0.00 | 3549.00/ 0.00 | .44 | 1.56/0.00 |
| Total: | | 67.60/67.60 | 15900.36/13642.66 | | 7.00/6.01 |
| Florida Strait: | | | | | |
| 0-1 | 7 | 10.82/11.14 | 75.74/ 77.98 | .44 | 0.03/0.03 |
| 1-5 | 42 | 5.41/ 6.69 | 227.22/ 280.98 | .44 | 0.10/0.12 |
| 5-10 | 105 | 6.08/ 6.69 | 638.40/ 702.45 | .44 | 0.28/0.31 |
| 10-15 | 175 | 5.41/ 4.46 | 946.75/ 780.50 | .44 | 0.42/0.34 |
| 15-20 | 245 | 6.08/ 5.20 | 1489.60/ 1274.00 | .44 | 0.66/0.56 |
| 20-25 | 315 | 6.76/ 8.17 | 2129.40/ 2573.55 | .44 | 0.94/1.13 |
| 25-30 | 385 | 14.20/15.60 | 5467.00/ 6006.00 | .44 | 2.41/2.64 |
| 30-35 | 455 | 9.46/ 8.91 | 4304.30/ 4054.05 | .44 | 1.89/1.78 |
| 35-40 | 525 | 3.38/ 0.74 | 1774.50/ 388.50 | .44 | 0.78/0.17 |
| Total: | | 67.60/67.60 | 17052.91/16138.01 | | 7.51/7.08 |

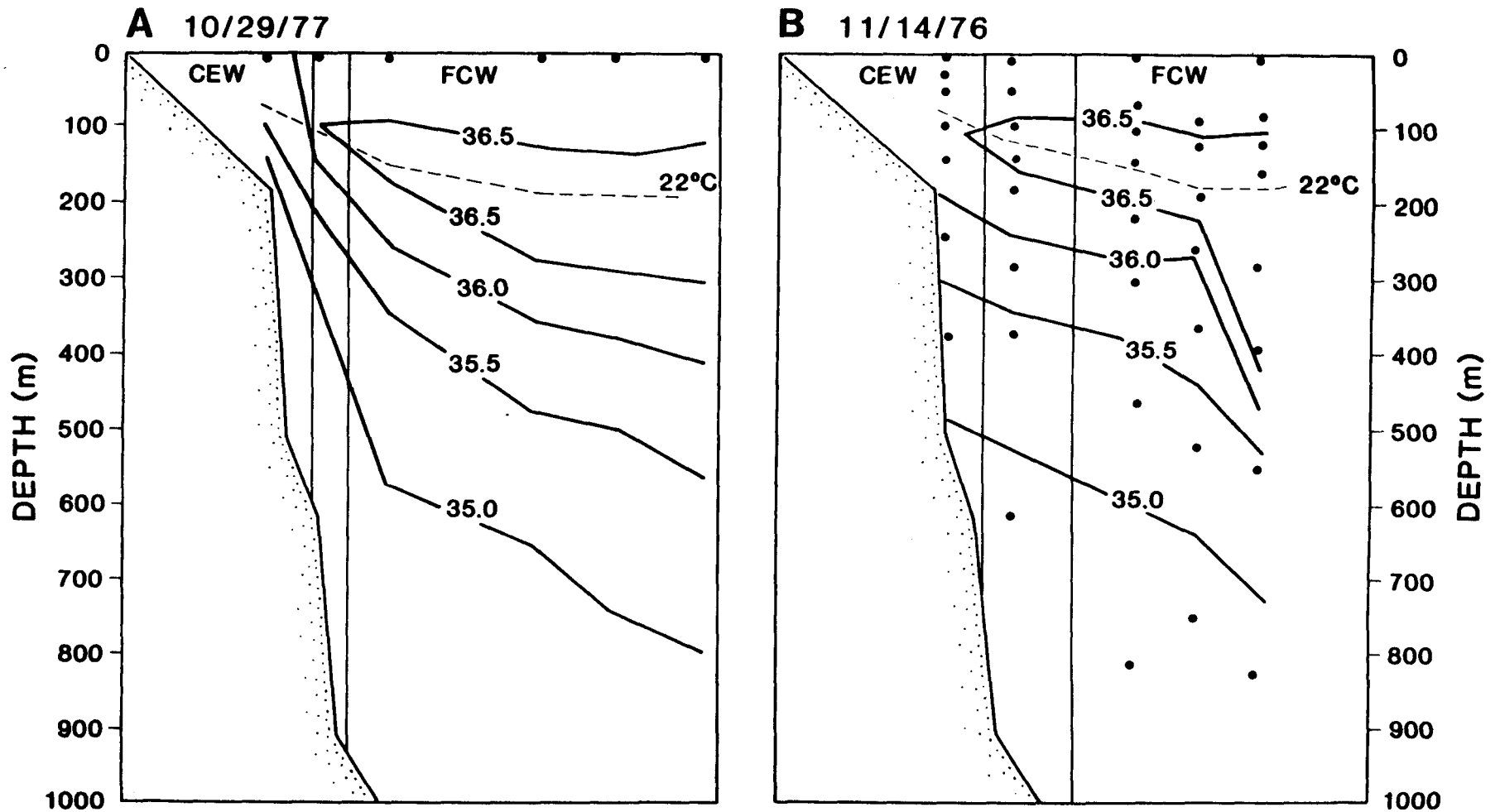


Fig. 5. The depth of the 22°C isotherm in relation to both salinity fields and boundaries of Continental Edge Water and of Florida Current Water within Florida Strait during a) October 29, 1977 and b) November 14, 1976.

geostrophic transport within the upper 700 m in Yucatan Strait varied from 17.5 to 31.1 Sv between August 1972 and September 1973, with a mean of 25.4 Sv (Maul, 1978). With such variance of the transport of water in and out of the Gulf of Mexico, three daily realizations of the nitrate fields within the Yucatan (Figs. 2a-4a) and Florida (Figs. 2b-4b) Straits provide only a departure point for possible assessment of the oceanic boundary fluxes of nitrogen.

2. Dissolved nitrogen

To provide a perspective on the following numerical results, however, we computed the flux of nitrate through Yucatan and Florida Straits assuming an average transport of 30 Sv within the upper 700 m of 97-km-long portions of the sections made during 14-20 January 1952 (Fig. 2) and 26-29 October 1977 (Fig. 3). The 1976 section in Florida Strait (Fig. 4b) was not taken close enough to the Cuban coast to allow a third calculation. To estimate these fluxes, we measured the area between each set of $NO_3$ isopleths, e.g., 0 and 1 μg-at $NO_3$ $\ell^{-1}$, of Figures 2 and 3 with a planimeter. We then multiplied the mean concentration of each nitrate layer by a mean flow of 44 cm $sec^{-1}$ to yield the flux estimates of Table 1.

A total of $7.0 \times 10^3$ kg $NO_3$-N $sec^{-1}$ entered the Gulf of Mexico via Yucatan Strait on 14 January 1952, with an efflux of $7.5 \times 10^3$ kg $NO_3$-N $sec^{-1}$ through Florida Strait on 19-20 January 1952, i.e., an increment of 7%. Similarly, a nitrate influx of $6.0 \times 10^3$ kg $NO_3$-N $sec^{-1}$ on 26 October 1977 and

an efflux of 7.1 x $10^3$ kg $NO_3$-N $sec^{-1}$ on 29 October 1977 suggests a larger nitrate increment of 18% between surface layers of the Yucatan and Florida Straits. Within the uncertainties of smoothing the nutrient data and of estimating the width, depth, and speed of the Yucatan and Florida Currents, the above scenario may or may not indicate a net nutrient loss from the Gulf of Mexico.

The mean salinities of the 8 Alaska stations within the upper 700 m of Figure 2 were 35.98% for the 42 discrete bottle samples taken during 1952 in Florida Strait, and 35.94% for the 46 samples taken ~400 km upstream in Yucatan Strait. They suggest little addition of estuarine water to the Atlantic Ocean from the Gulf of Mexico at the time of these sections. The increased salt and nutrient contents of the 1952 surface layer (<700 m) of the Florida Current, compared to the Yucatan Current (Fig. 2), instead suggest that upwelling occurred during the mean transit time of about 10 days from Yucatan Strait (i.e., over a distance of ∿500 km at a speed of 44 cm $sec^{-1}$).

However, the mean salinities of 8 comparable Researcher stations within the upper 700 m of Figure 3 were 35.85‰ for the 150 CSTD samples taken during 1977 in Florida Strait, compared to 35.99‰ for 143 samples in Yucatan Strait. The larger increase of nitrate stocks between Florida and Yucatan Straits in 1977 was instead associated with a freshening of surface waters. From a much larger data base, Maul (1978) determined that the Yucatan Current has 0.05‰ higher salinity than the Florida Current, with both being as much as 0.40‰ saltier than Continental Edge Water at a temperature of 22°C.

The lower salt content of Continental Edge Water is derived from either upwelling of Antarctic Intermediate Water (Fig. 5) or from land runoff. Higher nutrients can similarly result from either coastal discharge or upwelling at the cyclonic edge of these western boundary currents (Figs. 2 and 3). Note that, while the depth integral of $NO_3$ over 0 and 700 m only increased 7-18% (Table 1) between the 1952 and 1977 sections across Yucatan Strait and those across Florida Strait, the vertical structure of $NO_3$ changed significantly. For example, the 5-15 μg-at $NO_3$ $\ell^{-1}$ isopleths were all grouped at or above the 100-m depth on the Florida shelf-break, compared to deeper levels off Mexico, while the 20 μg-at $NO_3$ $\ell^{-1}$ isopleth was found at depths of 80-140 m off Florida (Figs. 2a-3a), compared to depths of 220-380 m near Mexico (Figs. 2b-3b).

The average depth change in the latter isopleth suggests continued upwelling, at perhaps 20 m $day^{-1}$, if the water flowed directly northeast at 44 cm $sec^{-1}$ over 500 km within the successive Yucatan, Loop, and Florida Currents. Northward excursions of the Loop Current into the Gulf of Mexico would increase the time over which upwelling occurs, thereby decreasing the estimate of upward movement. The depth of the 22°C isotherm can be used (Leipper, 1970; Maul, 1977; 1978) to demarcate the boundaries of the respective Yucatan, Loop, and Florida Currents (>100 m) with resident Gulf of Mexico water, where the nearshore, shallower depth (<100 m) of this isotherm at their cyclonic edge reflects the upwelling process as well.

A plot of the depths of the 22°C isotherm during the 1952 cruise of the R/V Alaska suggests that the Loop Current penetrated to 24°30'N (Fig. 6),

implying minimal occupation of the Florida Strait by Continental Edge Water at this time (Maul, 1978). As in May 1972 (Merrell et al., 1978), there appears to be a previously-shed anticyclonic eddy just to the northwest of the Loop Current during January 1952 (Fig. 6). Synoptic infrared imagery of surface temperature gradients from the NOAA VHRR suggests that the Loop Current had similarly penetrated to only 24°30'N on 28 October 1977, compared to 28°N between 14 October 1976 and 4 December 1976 (Vukovich et al., 1979). With a large northward excursion, the inclined front between Loop Current and resident Gulf of Mexico water extended over 1500 km between Yucatan and Florida Straits in the fall of 1976, compared to ∿500 km in the fall of 1977.

Over a longer travel distance of ∿1500 km for water parcels observed in the 6-7 and 14 November 1976 sections across Yucatan and Florida Straits (Fig. 4), an upward movement of the 20 μg-at $NO_3$ $\ell^{-1}$ isopleth, from respectively 440 m off Mexico to 280 m off Florida, implies an upwelling velocity of only ∿5 m $day^{-1}$. A decline in the upwelling rate, from 20 to 5 m $day^{-1}$, and increase of residence time, from 10 to 30 days, would allow phytoplankton to take up more of the upwelled nitrate within the euphotic zone at the cyclonic edge of these currents. Note that both the 1 and 5 μg-at $\ell^{-1}$ isopleths of nitrate have the same slope, between depths of 100 and 200 m in the middle of Florida Strait, during October 1977 (Fig. 3b) and November 1976 (Fig. 4b). Near the shelf-break, however, the 5 μg-at $NO_3$ $\ell^{-1}$ isopleth is at 60 m depth in 1977, compared to 100 m depth in 1976, presumably as a result of enhanced nutrient uptake within the lower part of the >100 m euphotic zone during 1976. Within the deeper aphotic zone, increased upwelling during 1977

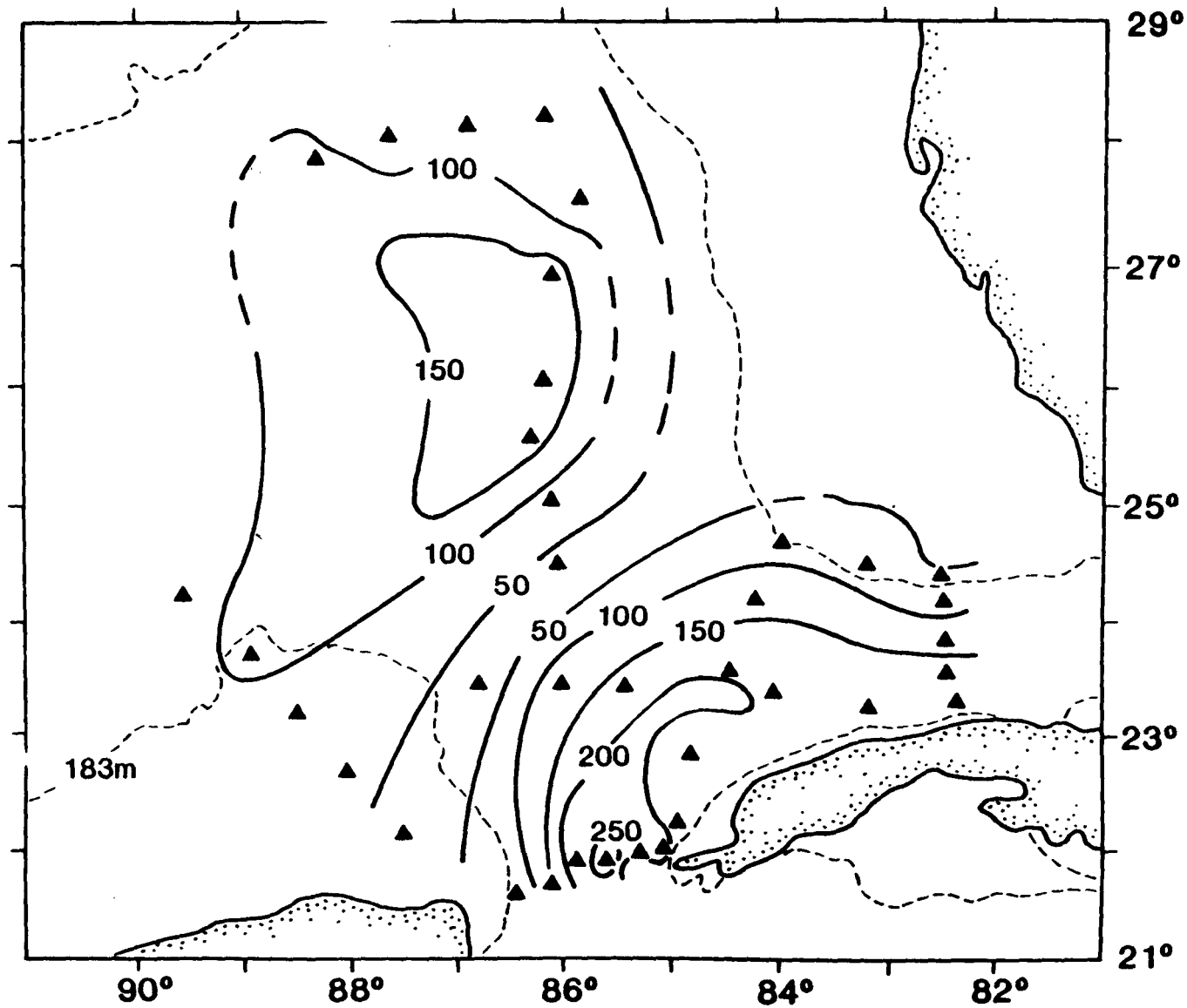


Fig. 6. The depth of the 22°C isotherm within the eastern Gulf of Mexico during January 1952.

led to a shoaling of other isopleths, e.g., the 10, 15, and 20 μg-at $NO_3$ $\ell^{-1}$ (Fig. 3b), previously found ∿120 m deeper on the upper slope in 1976 (Fig. 4b).

The rates of upwelling and nutrient uptake in Florida Strait, as well as the lateral extent of Continental Edge Water, appear to be affected by the extent of northward penetration of the Loop Current into the Gulf of Mexico. Using water type criteria of Continental Edge Water, as the 22°C isotherm ≦ 100 m depth, and of Florida Current Water, as 36.70‰ salinity at 22°C (Maul, 1978), the respective locations of these water types in Florida Strait are shown in Figure 5, before (Fig. 5a) and during (Fig. 5b) an excursion of the Loop Current into the Gulf of Mexico. When the Loop Current flows directly into Florida Strait, the Florida Current Water is located 49 km south of the U.S. coast, with isopleths of salinity sharply inclined shoreward (Fig. 5a). The 25 μg-at $\ell^{-1}$ isopleth of nitrate coincides with the 35.5‰ isopleth of salinity (Fig. 3b). With a northward intrusion of the Loop Current, the Florida Current Water is instead located 65 km south of the coast, with the strongest vertical gradient of salinity found at mid-channel (Fig. 5b), similar to the nitrate structure (Fig. 4b).

Depression of nearshore upwelling at the Florida Keys during intrusions of the Loop Current and greater export of Continental Edge Water, with possible offshore and/or upstream shifts in loci of nutrient input, are the local result of southward movement of the Dry Tortugas meander (Vukovich and Maul, 1985). During northward penetration of the Loop Current, sporadic

upwelling also occurs along the West Florida shelf, until southerly retreat of the Current and/or shedding of an anticyclonic eddy. In the western half of the Gulf of Mexico, these shed eddies may induce further upwelling at the Texas-Mexican shelf-break. Based on salinity budgets, about 10% of the transport of the inflowing Yucatan Current is annually exchanged with resident water in the Gulf of Mexico via the Loop Current upwelling and eddy shedding (Maul, 1978). From Table 1, this exchange rate suggests that about 700 kg $NO_3$-N $sec^{-1}$ may be supplied at the oceanic boundary of the Gulf.

3. Particulate matter

Part or all of the oceanic nitrate input must fuel the primary production of the interior basin and shelves of the Gulf of Mexico. Assuming a maximal nitrate concentration of 150 mg-at $m^{-3}$ and a mean flow of $1.8 \times 10^4$ $m^3$ $sec^{-1}$ for the Mississippi River (Walsh et al., 1981), an equivalent anthropogenic terrestrial flux of nitrogen to the Gulf might be as much as 38 kg $NO_3$-N $sec^{-1}$, i.e., ∿5% of the oceanic source. Finally, applying open-ocean nitrogen fixation rates of 16.1-32.3 kg N $km^{-2}$ $yr^{-1}$ (Capone and Carpenter, 1982; Fogg, 1982) over the surface area of the Gulf ($1.53 \times 10^6$ $km^2$), a possible atmospheric nitrogen input to the Gulf might be only 1-2 kg $NO_3$-N $sec^{-1}$.

Because the atmospheric input of nitrogen is small (∿ <1%), compared to oceanic and terrestrial inputs of nitrogen to the Gulf of Mexico, we ignored $N_2$ fixation by cyanobacteria in our calculations. Redistribution of the oceanic and terrestrial boundary inputs of nitrogen of 738 kg $NO_3$-N $sec^{-1}$

within the interior of the Gulf over the life cycle of a Loop Current intrusion, their possible loss to the sediments and atmosphere via burial and $N_2$ evasion, as well as their possible export to the Atlantic Ocean are the subjects of our simulation models.

The burial and denitrification losses of nitrogen in the Gulf of Mexico can be constrained a priori from the abundance of organic-rich sediments, their porosity, C/N ratio, and sedimentation rates. Using values of organic carbon (% dw) measured in surficial sediments over the last 30 yr (Stetson and Trask, 1953; Trask, 1953; Scholl, 1963; Upshaw et al., 1966; Vasilev and Torin, 1969; Hathaway, 1971; Rowe and Menzel, 1971; Armstrong, 1974; Gearing, 1975; Gearing et al., 1976; Hedges and Parker, 1976; Berryhill, 1977; SUSIO, 1977; ESE and LGL, 1985; LGL, 1986), we constructed a composite (Fig. 7) of the distribution of organic matter in recent sediments of the Gulf. Typically, regions of 1-2% organic carbon have C/N ratios of 6/1, whereas those of 0.5-1.0% carbon have higher C/N ratios of 10/1 (Walsh, 1983), reflecting increased remineralization and lower accumulation rates, since the $\delta^{13}C$ signature of these sediments is mainly marine (Hedges and Parker, 1976; Gearing et al., 1977).

The burial rate of organic matter on a unit area basis can then be obtained (Muller and Suess, 1979) from

$$A = S \cdot G \cdot C \cdot N/C \cdot (1 - P) \qquad (1)$$

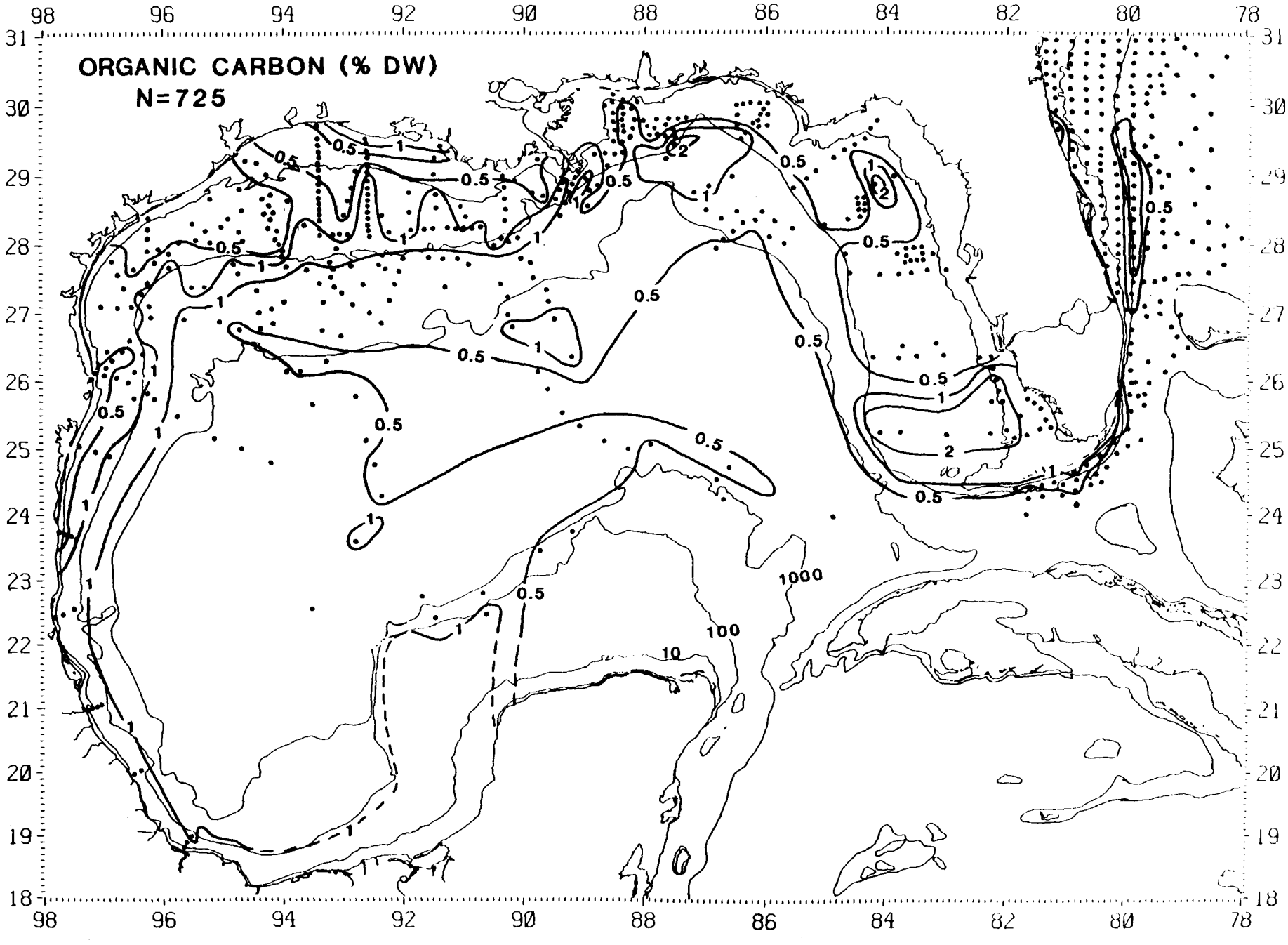


Fig. 7. The composite distribution of organic carbon (% dw) within surficial sediments of the Gulf of Mexico over the last 30 years.

where A is the accumulation rate of nitrogen in the sediment (g N $cm^{-2}$ $yr^{-1}$); S is the sedimentation rate (cm $yr^{-1}$); G is the specific gravity of sediment (2.6 g $cc^{-1}$); C is the % dw carbon content (more frequently measured); N/C is the ratio of nitrogen and carbon within the surviving organic matter of the sediment; and P is the porosity, providing an estimate of the volume of water within the sediment column. At the shelf-break off the Mississippi River Delta, sedimentation rates as high as 1.0 cm $yr^{-1}$ have been observed near the 100-m isobath (Shokes, 1976; Parker, 1977), but more typical rates in other shelf and slope regions are 0.01-0.10 cm $yr^{-1}$ (Walsh et al., 1985).

Using a specific gravity of 2.6 g $cc^{-1}$, a porosity of 0.8, a sedimentation rate of 0.10 cm $yr^{-1}$, a N/C ratio of 0.17, and a mean carbon content of 1.5% dw for the area (0.24 x $10^{12}$ $m^2$) enclosed by the 1.0% dw isopleth of sediment carbon (Fig. 7), as well as a rate of 0.01 cm $yr^{-1}$, a ratio of 0.10, and a mean content of 0.75% dw for the area (0.70 x $10^{12}$ $m^2$) enclosed by the 0.5%-1.0% isopleths (Fig. 7), we obtain a hypothetical Gulf burial rate, from eq. (1) and Figure 7, of 3.5 x $10^8$ kg N $yr^{-1}$. We assume that "new" nitrogen, in the form of either nitrate or anthropogenic input (Eppley and Peterson, 1980; Walsh, 1983), sets the limit for export of nitrogen fixed in the Gulf's euphotic zone. Such a burial estimate then implies, in a steady state, that at least 3.5 x $10^8$ kg $NO_3$-N $yr^{-1}$ must be supplied to the overlying water column, without consideration of either shunts of recycled nitrogen (ammonium, urea, amino acids), or of gaseous losses of nitrogen ($N_2$).

Assuming a denitrification rate of 1.1 x $10^3$ kg N $km^{-2}$ $yr^{-1}$ (Christensen, 1981; Haines et al., 1981) for the richer carbon (>1% dw) sediments of the outer shelf and upper slope of the Gulf of Mexico, the area (0.24 x $10^6$ $km^2$) enclosed by the 1.0% isopleth of carbon (Fig. 7) yields an estimated $N_2$ loss to the atmosphere of 2.6 x $10^8$ kg N $yr^{-1}$. On an annual basis, the above estimated rate of nitrogen fixation of atmospheric $N_2$ in surface waters of the Gulf by cyanobacteria is evidently much lower, 2.5-5.0 x $10^7$ kg N $yr^{-1}$, implying a net loss of nitrogen gas from the Gulf to the local atmosphere. Man's fixation of atmospheric nitrogen for fertilizer, its leaching from fields into the drainage basin of the Mississippi River, as well as addition of sewage as another by-product of agricultural activities, lead, however, to a circuitous return from the global atmosphere of 8.5 x $10^8$ kg N $yr^{-1}$ within the mean plume of the Mississippi River.

A total mean nitrogen input of 738 kg $NO_3$-N $sec^{-1}$ to the Gulf of Mexico, or 231 x $10^8$ kg N $yr^{-1}$, from the oceanic and terrestrial boundaries appears to more than offset a combined loss of perhaps 6 x $10^8$ kg N $yr^{-1}$ from our preliminary estimates of the burial of organic nitrogen and evasion of $N_2$. We have thus far not included possible export of nitrogen via the Florida Strait. Also, our estimate of the oceanic input of nitrate to the southern Gulf of Mexico is a depth integral over 700 m, which may not all be utilized by phytoplankton, nor by the rest of the food web.

For example, low near-surface chlorophyll concentrations of 0.10-0.15 µg chl $\ell^{-1}$ resulted in a 1% light depth of 115 m during an intrusion of the Loop Current in early February 1981 (Ortner et al., 1984). During this study, the

nitrate content of the euphotic zone within the Loop Current was <0.4 μg-at $NO_3$ $\ell^{-1}$. Even after local wind forcing, the depth of the 3 μg-at $NO_3$ $\ell^{-1}$ isopleth only shoaled from 240 m to 140 m within the center of the Loop Current. This is in contrast to nutrient conditions at the cyclonic edge of these western boundary currents, where 20 μg-at $NO_3$ $\ell^{-1}$ are found at this same depth near the Florida shelf-break (Fig. 2b).

Conversion of the oceanic input of nitrate by organisms to organic nitrogen and $N_2$ would thus be enhanced by upwelling, in addition to diffusion supply to the euphotic zone. Such a kinetic energy supplement is not required for consumption of the terrestrial input of nitrogen which occurs within a low-salinity lens at the surface of the northern Gulf of Mexico. Our assumptions about the factors controlling the biochemical conversion process of nitrate uptake, i.e., light and nutrient limitation, upwelling velocities, vertical mixing, and horizontal dispersion, are discussed in the next section.

## Methods

### 1. Circulation formulation

Initial barotropic simulations of western boundary currents, e.g., the Loop Current (Paskausky and Reid, 1972), the Kuroshio (O'Brien, 1971) and the Gulf Stream (Holland and Hirschman, 1972), underestimated their transports of respectively 30, 90, and 150 Sv by about 30-90%. Addition of baroclinicity and realistic bottom topography to numerical models generates larger transports, e.g., 81 Sv for the Gulf Stream (Holland and Hirschman, 1972).

Use of large horizontal eddy viscosities on grids of poor spatial resolution over whole ocean or basin domains, however, damps the nonlinear acceleration terms of the Navier-Stokes equations. The models then lead to smaller transports, for example, of 60 Sv within the Gulf Stream (Cox, 1975). The large horizontal viscosities over these grids of world ocean models (Bryan and Cox, 1972; Cox, 1975) are also unable to resolve the formation of mesoscale eddies, shed from these western boundary currents by latitudinal variation of the Coriolis term (Hulburt and Thompson, 1980).

The simplest baroclinic formulation of flow within these currents is a "reduced gravity" model, which assumes no motion in the lower part of a two-layered ocean. Early (Stommel, 1965) and more recent (Csanady and Hamilton, 1988) analytical studies of the Gulf Stream, as well as numerical studies of the Loop Current (Hulburt and Thompson, 1980), invoked such oversimplification of time-invariant buoyancy fluxes within a stratified water column. The most complex baroclinic models of western boundary currents utilize 16-21 layers to approximate the vertical structure of density and associated time-dependent thermodynamics, vertical mixing, and advection within the Loop Current (Blumberg and Mellor, 1985) and the Gulf Stream (Blumberg and Mellor, 1983). These models did not resolve eddy shedding from the Loop Current, however. To provide an initial assessment of the consequences of nutrient injection by western boundary currents, we thus employed a simple baroclinic circulation model which was still capable of shedding eddies.

Of particular interest in our present study was the shedding of cyclonic eddies (Vukovich and Maul, 1985), which induces upwelling here and in the South Atlantic Bight (Atkinson et al., 1985), as opposed to the anticyclonic, warm core eddies (Elliott, 1982) within the Gulf of Mexico. Lateral movement of a western boundary current and/or wind stress can also induce upwelling at the shelf-break. Eddy-resolving simulation models of this region require small grid spacing (10-25 km), and associated low viscosities (1-10 x $10^6$ $cm^2$ $sec^{-1}$). With appropriate parameterization, they allow formation of cyclonic eddies both at the shoreward wall of the Loop Current in the eastern Gulf and as part of an eddy pair in the western Gulf (Hulburt and Thompson, 1980; Blumberg and Mellor, 1985; Wallcraft, 1986).

Natural boundary conditions for simulating the circulation, in which these eddies are embedded, within the Gulf of Mexico might be the time-dependent influx of the order of ~30 Sv through Yucatan Strait and an outflow of about the same magnitude through Florida Strait. The cycle of northward penetration of the Loop Current into the eastern Gulf of Mexico, release of an anticyclonic eddy, and southward retreat, may have less of periodic signal than originally hypothesized (Maul, 1977), however. There is evidently a seasonal amplitude of 4.1 Sv for the Florida Current off Miami from 7 yr of observations made during 1964-1970, when a mean transport of 29.5 Sv was found (Niiler and Richardson, 1973). A similar seasonal signal of the Loop Current may be masked upstream by counterflows within Yucatan Strait, since most of the continuity requirement of a Loop Current intrusion may be met by outflow of Yucatan Bottom Water south through this Strait (Maul, 1978).

Hulburt and Thompson (1980), as well as Wallcraft (1986), were able to produce quasi-annual cycles of Loop Current penetration and eddy shedding, however, with time-invariant boundary conditions of flow within Yucatan and Florida Straits. We have adopted their approach, using a steady input through Yucatan Strait of a transport of 20 Sv above, and 10 Sv below, an initial interface (pycnocline) depth of 200 m, embedded in a two-layered model of constant densities, $\rho_1$ and $\rho_2$. This interface is impermeable. The Boussinesq approximation is used and a mean density, $\rho_o$, replaces $\rho_1$ or $\rho_2$, except for the buoyancy term described below by eq. (8).

In a cartesian coordinate system (x,y,z), with z positive upwards and t denoting time, the vertically-integrated equations for the flow (u,v) within each layer are:

$$\frac{\partial U_i}{\partial t} + \frac{\partial\left(U_i u_i\right)}{\partial x} + \frac{\partial\left(V_i u_i\right)}{\partial y} = fV_i - h_i \frac{\partial P_i}{\partial x}$$

$$+ \frac{\left(\tau_i^x - \tau_{i+1}^x\right)}{\rho_o} + K_x h_i \nabla^2 u_i \qquad (2)$$

$$\frac{\partial V_i}{\partial t} + \frac{\partial\left(U_i v_i\right)}{\partial x} + \frac{\partial\left(V_i v_i\right)}{\partial y} = -fU_i - h_i \frac{\partial P_i}{\partial y}$$

$$+ \frac{\left(\tau_i^y - \tau_{i+1}^y\right)}{\rho_o} + K_y h_i \nabla^2 v_i \qquad (3)$$

$$\text{and} \quad \frac{\partial h_i}{\partial t} = - \frac{\partial U_i}{\partial x} - \frac{\partial V_i}{\partial y} \tag{4}$$

where the index, i = 1,2 indicates the upper and lower layers of the model. The variable $u_i$ is the x (positive to the east) component of the velocity, $v_i$ is the y (positive to the north) component, $h_i$ is the thickness, and $U_i = u_i h_i$, $V_i = v_i h_i$ are the depth-integrated transports in each layer.

The pressure term, $P_i$, of eqs. (2)-(3) is defined additionally (Hulburt and Thompson, 1980) by

$$P_1 = g\eta \tag{5}$$

$$\text{and} \quad P_2 = g\eta - g'h_1 \tag{6}$$

where g is the acceleration due to gravity, $\eta$ is the sea surface elevation, and g' is the reduced gravity, or buoyancy effect. Without stratification of the water column, $P_1 = P_2$, and the circulation model is barotropic. The free surface, $\eta$, is defined by

$$\eta = h_1 + h_2 - D \tag{7}$$

where D is the local depth. The baroclinic shear of the model is incorporated in the reduced gravity term as

$$g' = g(\rho_2 - \rho_1)/\rho_o \tag{8}$$

which we set to 3 cm $sec^{-2}$.

The Coriolis parameter, f, is assumed to vary with latitude. We follow the β-plane approximation of

$$f = f_o + \beta(Y - Y_o) \tag{9}$$

Using a central latitude of 24.5°N, $f_o$ is 6.03 x $10^{-5}$ $sec^{-1}$ and β is 2.08 x $10^{-13}$ $cm^{-1}$ $sec^{-1}$.

The stress terms, $\tau_i^{x,y}$ of this type of Lagrangian model (O'Brien and Hulburt, 1972) lead to numerical instabilities, if the interface depth either surfaces or intersects the bottom. Wind stress, for example, generates rapid upwelling in this Gulf of Mexico model, with consequent abortion of the numerical solution as the upper layer approaches zero thickness (Wallcraft, 1986). In the circulation model, both wind stress and interfacial stresses are thus ignored; wind forcing is considered in the vertical mixing term of the biological model, however.

The bottom stress is defined in quadratic form by

$$\tau^x = \rho_o cqu_2 \tag{10}$$

$$\tau^y = \rho_o cqv_2 \tag{11}$$

where $q = (u_2^2 + v_2^2)^{1/2}$ and c is a drag coefficient of $2.0 \times 10^{-3}$. To avoid intersection of the interface depth with the bottom, a minimum bottom depth, D, of 500 m was assumed for the continental shelf regions. Other bottom topography was digitized from NOS Chart 411 and smoothed to eliminate small-scale features (Fig. 8).

The last term on the right-hand side of eqs. (2) and (3) represents horizontal mixing of momentum, where $\nabla^2 = \frac{\partial^2()}{\partial x^2} + \frac{\partial^2()}{\partial y^2}$ is the Laplacian operator and $K_x = K_y = 2.5 \times 10^6$ cm$^2$ sec$^{-1}$ are the horizontal eddy viscosities. Our formulation differs somewhat from Hulburt and Thompson (1980), because we use the Laplacian of the horizontal velocities, rather than the transports, to simulate the horizontal mixing processes. A full derivation of this term is given by Thompson (1974).

The computational grid for the two-layered circulation model involves a horizontal resolution of 1/4° x 1/4°. Such spatial resolution yields a rectangular grid increment in the x-dimension of 25.4 km and of 27.8 km in the y-dimension. The model grid covers the entire Gulf to avoid specification of other open boundary conditions, besides those of Yucatan and Florida Straits. The inflow port has a 175-km width across Yucatan Strait and the outflow port is 125-km wide across Florida Strait. The land boundaries of the models were chosen to conform to the coastlines of the Gulf (Fig. 8).

At these coastal boundaries, a no-flow constraint was imposed on the velocity component normal to the shore. Use of the Laplacian horizontal friction term, i.e., Munk (1950), in eqs. (2)-(3) requires the tangential component of the flow to also be specified at the coast. A simple method,

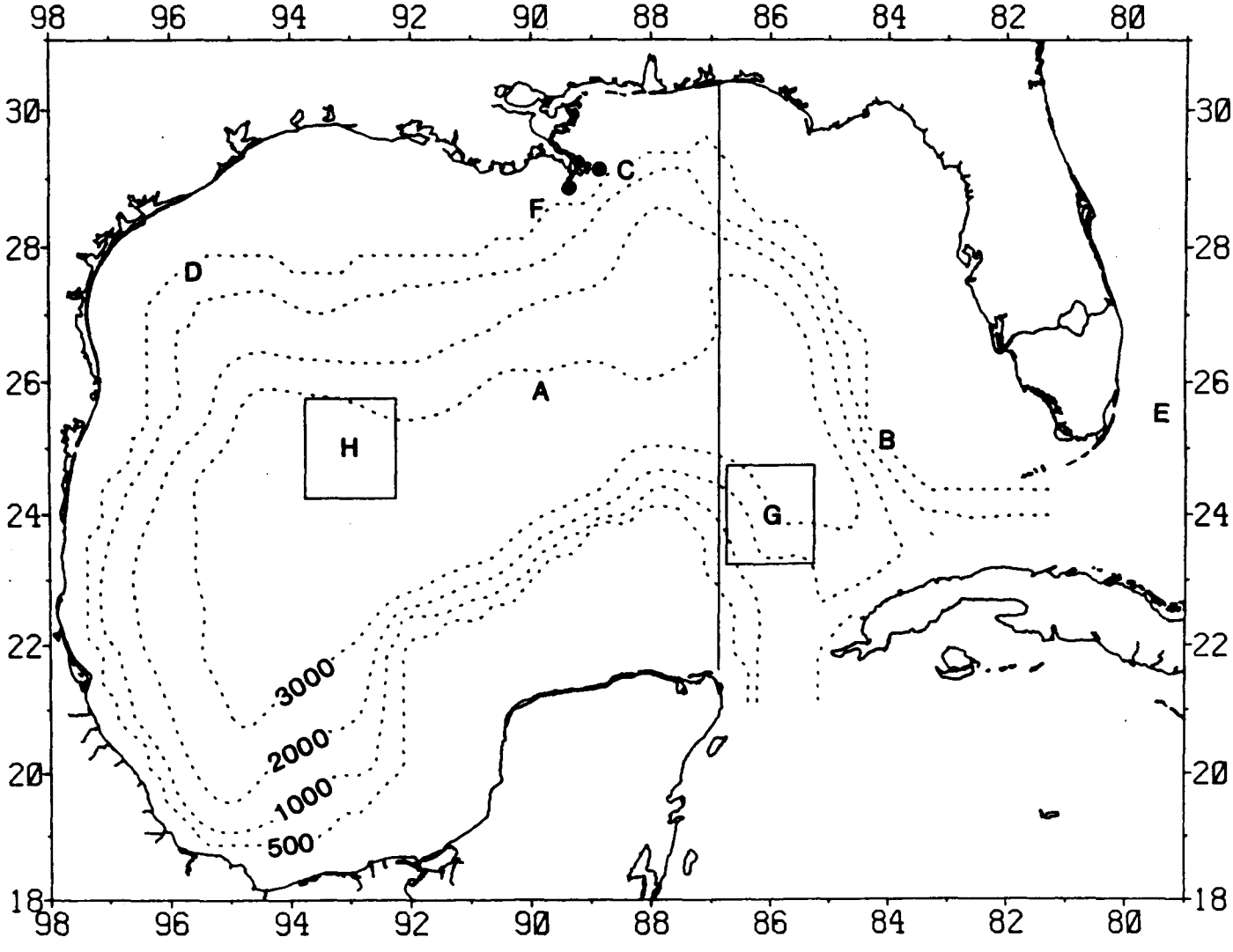


Fig. 8. Locations of a latitudinal section of the circulation model, of anthropogenic sources of nitrogen (•), and of simulated time series from both the biological model (E) and from the coupled physical/biological models (A-D), with respect to shipboard (F) and aggregated satellite (G-H) data.

parameterizing vorticity generation at solid boundaries, is the no-slip boundary condition. The no-slip condition is achieved by assigning an equivalent velocity, at each boundary grid point, of opposite sign to that of the tangential component (Holland and Lin, 1975).

A steady northward flow, with a quadratic profile in the upper layer and uniform flow in the lower layer, was prescribed at the inflow open boundary of Yucatan Strait. Outflow through Florida Strait was constrained to match the volume inflow from Yucatan Strait, in a manner similar to Hulburt and Thompson (1980), i.e., the latitudinal pressure gradient of eq. (2) is assumed constant along the outflow boundary. It is determined by imposing the constraint that the outflow of water in each layer must match the corresponding inflow from Yucatan Strait. In addition, the tangential component of the flow was set to zero for grid points just outside the inflow and outflow ports.

2. Vertical mixing

As a result of the impermeable nature of the interface between the two layers of the model, complex formulations of wind stress, heat flux, and vertical stratification have been added to simulate vertical mixing of momentum and temperature (Thompson, 1974; O'Brien and Heburn, 1983). Similarly, without a term for description of nutrient exchange across this interface, no renewal of nitrogen would occur in the upper layer, except for river discharge and remineralization. Uncertainties in the actual wind curl (Wallcraft, 1986) and heat flux (Etter, 1983) within the Gulf of Mexico, together with a poor resolution of vertical stratification within a

two-layered circulation model preclude a complex description of vertical mixing for use in the companion biological model.

We instead prescribed an empirical depth profile of the vertical eddy diffusivity, $K_z$, over the upper layer of the circulation model as additional input to the twenty-layer biological model, which is nestled in this upper part of the water column. At the depth of the interface, i.e., $z_1 = h_1 - \eta$, $K_z$ is taken to be 0.1 $cm^2$ $sec^{-1}$, reflecting low turbulent mixing of nutrients across the pycnocline (Eppley et al., 1979; King and Devol, 1979). Within the surface mixed layer, $K_z$ is much greater, with variation of both $K_z$ and the mixed layer depth, $h_m$, at time scales ranging from wind events to seasons.

Using a one-dimensional model of time-dependent, wind-induced mixing (Niiler, 1975) and a turbulence closure scheme (Mellor and Yamada, 1974), a $K_z$ of 188.0 $cm^2$ $sec^{-1}$ can be calculated for a 44-m thick surface mixed layer of weak vertical stratification (0.4 $\sigma_t$ 50 $m^{-1}$) after ~9 hr of wind forcing at 10 m $sec^{-1}$ (Wroblewski and Richman, 1987). A day after cessation of the simulated wind impulse in their model, $K_z$ had declined to 22.0 $cm^2$ $sec^{-1}$, however. Since exogenous factors of the biological model change at the 30-day time scale (Table 2), we chose to average over such wind events using field estimates of mean wind stress and the thickness of the surface mixed layer.

A surface mixed layer of 50-m thickness ($\leqq \Delta 0.13$ $\sigma_t$ criterion), measured at the Researcher stations within Florida Strait near the end of October 1977, for example, is quite similar to a climatological monthly average of 48-m thickness (Table 2) for October in the middle of the Atlantic Ocean at 25.5°N, 40.5°W (Levitus, 1982). The mixed layer depths, $h_m$, in January at the Alaska

Table 2. The monthly wind stress and photosynthetically active radiation (PAR) at the sea surface, in relation to the vertical eddy diffusivity and depth of the mixed layer in the simulated Gulf of Mexico.

| | $\tau$ (dyne $cm^{-2}$) | $K_o$ ($cm^2$ $sec^{-1}$) | $h_m$ at 25.5°N, 40.5°W (m) | Maximum $I_o$ (1200 hr) at 25° N ($\mu$Ein $cm^{-2}$ $hr^{-1}$) |
|---|---|---|---|---|
| Jan | .61 | 49 | 100 | 731 |
| Feb | .62 | 50 | 93 | 827 |
| Mar | .72 | 58 | 86 | 930 |
| Apr | .77 | 62 | 62 | 997 |
| May | .69 | 56 | 41 | 1016 |
| Jun | .59 | 48 | 24 | 1016 |
| Jul | .42 | 34 | 24 | 1016 |
| Aug | .32 | 26 | 24 | 1005 |
| Sep | .56 | 45 | 45 | 956 |
| Oct | .81 | 66 | 48 | 860 |
| Nov | .77 | 62 | 59 | 752 |
| Dec | .70 | 57 | 78 | 696 |

stations within the eastern Gulf of Mexico (Fig. 1) were also similar to those of the mid-Atlantic, while the Alaminos stations in May suggested shallower depths than the climatological mean (Table 2). Finally, a compilation of these and other temperature data over the whole Gulf (> $0.5 \times 10^6$ stations prior to 1979) yields a seasonal cycle of vertical temperature structure (Fig. 11a of Blumberg and Mellor, 1985), which confirms our assumed seasonal cycle of the depth of the surface mixed layer.

From monthly estimates (> $1 \times 10^6$ observations) of wind stress on a 1° square grid of the Gulf of Mexico, the area-averaged wind stress vector (Fig. 3a of Blumberg and Mellor, 1985) was used to obtain the magnitude of the surface wind stress, $\tau$, in Table 2. A number of relationships (Sverdrup et al., 1942; Munk and Anderson, 1948; Csanady, 1976; Kullenberg, 1976) have been derived for estimation of the vertical eddy viscosity within the mixed layer, $K_o$, from the surface wind stress. Using dye experiments and classical Ekman theory (Kullenberg, 1976), the early estimates of $K_o$ have been reduced by an order of magnitude to

$$K_o = \rho_a c_a \tau (\rho_o^2 \zeta^2 f)^{-1} \tag{12}$$

where $\rho_a$ and $\rho_o$ are the densities of air and seawater, $c_a$ is another drag coefficient, and $\zeta$ is a proportionality constant. Assuming values of $1.23 \times 10^{-3}$ for $\rho_a$, 1.0 for $\rho_o$, $1.3 \times 10^{-3}$ for $c_a$, and $1.8 \times 10^{-2}$ for $\zeta$, eq. (12) reduces to

$$K_o = 4.9 \times 10^{-3} \tau/f \qquad (13)$$

which is identical to the relationship of Csanady (1979). Using eq. (13), the wind stresses in Table 2, and the value of the Coriolis parameter at 24.5°N, we computed monthly entries for $K_o$ (Table 2). The monthly wind stress, vertical eddy coefficient, and mixed layer depth range from respective maxima of 0.81 dynes $cm^{-2}$, 66 $cm^2$ $sec^{-1}$, and 100 m to minima of 0.32 dynes $cm^{-2}$, 26 $cm^2$ $sec^{-1}$, and 24 m (Table 2).

The vertical profile of $K_z$ is completed by assuming an exponential decay, from the uniform monthly value in the surface mixed layer, $K_o$, to the smaller value of 0.1 $cm^2$ $sec^{-1}$ at the interface, $K_f$, described by

$$K_z(z) = K_o e^{b(|z| - h_m)} \qquad (14)$$

where $h_m$ is the depth of the mixed layer, b is log $(K_f/K_o)/(z_1 - h_m)$, and $z_1$ is the interface depth. The overall shape of our $K_z$ profile with depth is similar to the Richardson number-dependent profiles calculated by Hamilton and Rattray (1978).

The depth of the interface, $z_1 = h_1 - \eta$, varied over time and space from 100 to 400 m in separate runs of the circulation model. Therefore, a vertical resolution of 20 levels for the biological model over $h_1$ insured that at least the $K_z$ of the topmost layer reflected the value of $K_o$ during each time step. The 21st layer of the biological model extended over $h_2$, the lower

layer of the circulation model. The value of $K_z$ over each of the 20 depth intervals of the upper water column was the average over each respective depth integral, similar to the following calculations for estimation of the in situ light field.

3. Biochemical formulation

With both upwelling/downwelling motion of the interface between layers and vertical mixing within the upper layer of the physical model, phytoplankton, M, experience large temporal and spatial changes in the gradients of light, I, and nutrient, N, over the domains of the coupled biological/physical models. Since little ammonium, urea, or even chlorophyll data exist for the Gulf, our validation data consist mainly of dissolved nitrate in the water column (Fig. 1), particulate carbon in the sediment (Fig. 7), and satellite estimates of pigment within the first optical depth (Fig. 25). Accordingly, we chose to model the "new" production of the system, employing nitrate as the nutrient state variable, N.

The tempo-spatial distributions of nitrate ($\mu$g-at $NO_3$ $\ell^{-1}$) can be described on an Eulerian grid by

$$\frac{\partial N}{\partial t} = - u \frac{\partial N}{\partial x} - v \frac{\partial N}{\partial y} - w \frac{\partial N}{\partial z} + \frac{\partial}{\partial z} K_z \frac{\partial N}{\partial z} - aMs^{-1} + oMs^{-1} \qquad (15)$$

where u and v are the depth-averaged flows of the upper layer of the physical model, as calculated from eqs. (2)-(4). The third term is the vertical

advection of nitrate, which does not appear explicitly in the Lagrangian formulation of eq. (18). The horizontal eddy diffusivities, $K_x$ and $K_y$ of eqs. (2)-(3) are ignored, since the advective terms are much larger than the diffusive terms in the horizontal dispersion of nitrate. The vertical eddy diffusivity, $K_z$, is obtained at each grid point by the procedure described above. The fifth term of eq. (15) is the uptake of nitrogen by phytoplankton, expanded in the more complex expression of eq. (20), where s = 1.68 relates either pigment formation ($\mu g\ \ell^{-1}\ hr^{-1}$) to nitrogen uptake ($\mu g\text{-at}\ \ell^{-1}\ hr^{-1}$), or pigment degradation during nitrification, assuming a C/chl ratio of 50/1 and a C/N ratio by weight of 6/1. The last term of eq. (15) is nitrification in the water column, where o = 0.0050-0.0025 $day^{-1}$ are the remineralization rates of phytoplankton within respectively the upper and lower layers of the circulation model.

Phytoplankton biomass ($\mu g$ chl $\ell^{-1}$), M, in the simulated Gulf of Mexico is similarly described by

$$\frac{\partial M}{\partial t} = - u \frac{\partial M}{\partial x} - v \frac{\partial M}{\partial y} - w \frac{\partial M}{\partial z} + \frac{\partial}{\partial z} K_z \frac{\partial M}{\partial z} + aM - w_s \frac{\partial M}{\partial z} - oM \qquad (16)$$

where the first four terms have been defined. The last two terms are the sinking and oxidative losses of phytoplankton. In steady state, the sinking loss should be equivalent to the supply of "new" production, i.e., river discharge within the first two terms of eq. (15), and vertical input within the fourth term of eq. (15). Oxidation in the model will result in some

recycling of particulate nitrogen (ammonification and nitrification) within the upper and lower layers.

Decomposition of organic matter within the open ocean eventually liberates $CO_2$ and $NO_3$ from sinking particles, forming the nitrate subsurface maximum at 500-1000 m (recall Figures 2-4). In the Pacific Ocean, the particulate carbon and nitrogen fluxes at a depth of 1000 m are 10% of those at 100 m (Martin et al., 1987). At sinking velocities, $w_s$, of 10 m $day^{-1}$ for large phytoplankton and 100 m $day^{-1}$ for fecal pellets, the mean daily decomposition rates, o, of falling particles over the 900-m depth interval would be respectively 0.01 and 0.10 $day^{-1}$.

Sinking rates of phytoplankton may accelerate during nutrient depletion (Cullen and Eppley, 1981; Bienfang et al., 1983) and cell aggregation (Smetacek, 1985), or decelerate during particle decomposition (Csanady, 1986), however. During formulation of the initial conditions of the biological model, we thus explored a range in both sinking and decomposition rates of eq. (16) -- a rate of 3 m $day^{-1}$ was chosen. Such a sinking rate of 3 m $day^{-1}$ over $h_1$ and $h_2$ layer thickness of 100 m and 800 m, together with upper and lower layer decomposition rates of 0.005-0.0025 $day^{-1}$ to simulate the increased refractory nature of organic matter in the aphotic zone (Berger et al., 1987), yield, for example, a survival rate of 16.7% for phytoplankton at a depth of 900 m after 300 days in the model. Under certain situations, however, much higher sinking rates of 30-300 m $day^{-1}$ may prevail for aggregated picoplankton (Lochte and Turley, 1988).

Since the circulation model is a Lagrangian formulation with depth, the vertical velocity, w, is not an explicit term of eqs. (18)-(19). Transformation of eqs. (15)-(16) into the vertical coordinate of the circulation model by

$$\phi = (z - \eta)/h_1 \tag{17}$$

leads to

$$\frac{\partial h_1 N}{\partial t} = - \frac{\partial h_1 uN}{\partial x} - \frac{\partial h_1 vN}{\partial y} + \frac{1}{h_1^2} \frac{\partial}{\partial \phi} K_z \frac{\partial h_1 N}{\partial \phi} + h_1 \left( - aMs^{-1} + oMs^{-1} \right) \tag{18}$$

and

$$\frac{\partial h_1 M}{\partial t} = - \frac{\partial h_1 uM}{\partial x} - \frac{\partial h_1 vM}{\partial y} + \frac{1}{h_1^2} \frac{\partial}{\partial \phi} K_z \frac{\partial h_1 M}{\partial \phi} - \frac{w_s}{h_1} \frac{\partial h_1 M}{\partial \phi} + h_1 (aM - oM) \tag{19}$$

where $\eta$ and $h_1$ were previously defined as the sea surface elevation and the thickness of the upper layer.

The movement of the depth of the interface, $z_1 = h_1 - \eta$, is recorded in eqs. (18)-(19) by the changing vertical gradients of nitrate and chlorophyll at each grid point and time step, with respect to both the nitrate boundary condition at the pycnocline and the light regime at the surface. The sinking

and decomposition terms of eq. (16) are also computed over $h_2$, the lower layer of the circulation model, to allow input of the surviving particles to the sea floor of the model. The circulation field of the lower layer is not applied to particles within $h_2$, i.e., the sinking debris falls in place after passing through the interface. The biological model thus consists of 20 layers within the upper layer of the circulation model and 1 additional layer of sinking, oxidizing particles within the stationary lower layer of this coupled physical-biological model.

The effects of temperature, light, and recycled nitrogen on algal growth are expressed in the fifth term of eq. (16) by

$$a = \mu_T \tanh \left[\alpha \frac{chl}{C} I(z)\mu_T^{-1}\right]\chi \qquad (20)$$

where $\mu_T$ is the maximum, carbon-specific growth rate of phytoplankton, taken here as 4 cell divisions $day^{-1}$ for a temperature of 25°C (Eppley, 1972). This is an exponential growth rate of 0.12 $hr^{-1}$ over a 24-hr day, and is adjusted to the simulated photoperiod by eq. (27). We have not corrected this maximum growth rate for lower temperatures with depth or season.

The hyperbolic tangent function of light (Platt and Jassby, 1976) in eq. (20) does not contain a photoinhibition effect, as did our previous model of the Mid-Atlantic shelf (Walsh et al., 1988a). Since most of the nitrate-based, "new" production would take place at depth in the deeper water column of the Gulf of Mexico model, however, we assumed that depression of

algal growth by photoinhibition would be minimal. At the surface of the mouth of the Mississippi River, self-shading by phytoplankton in eq. (21) was similarly considered to be more important than photoinhibition.

The initial slope, $\alpha$, of the general photosynthesis-light relationship (Walsh, 1988) in eq. (20) is taken to be 0.05 $\frac{\mu g\ C\ \mu g\ chl^{-1}\ hr^{-1}}{\mu Ein\ cm^{-2}\ hr^{-1}}$ (Jassby and Platt, 1976; Platt and Jassby, 1976; Malone and Neale, 1981). This parameter can be considered as the product of the maximum photon efficiency and the chlorophyll-specific, light absorption cross-section of the algal cell (Bannister and Weidemann, 1984; Geider and Osborne, 1986). The latter property of the algal population is considered in the depth dependence of the in situ light field.

At depth, variation of light is effected by extinction due to water, $k_w$, absorption due to chlorophyll, $k_m$, and scattering due to particulates (including phytoplankton) over an average cosine light path. These processes are parameterized by

$$I(z) = I_o\, e^{-1.33\left[k_w z + k_m \int_o^z M(z)dz\right]} \qquad (21)$$

Towards the blue end of the spectrum of photosynthetically-active radiation (PAR), the diffuse attenuation coefficient for water is taken as $k_w = 0.03\ m^{-1}$. The spectral average of chlorophyll-specific absorption for an open-ocean community of phytoplankton in the Pacific is $k_m = 0.055\ (mg\ chl)^{-1}\ m^2$ (K. Carder, personal communication).

We assume this value typifies the algal communities of the Gulf of Mexico and multiply the product of this coefficient and the chlorophyll biomass by an average cosine value of 1/0.75 to obtain the diffuse attenuation coefficient of phytoplankton in our model. Using the chlorophyll biomass from a depth profile taken within the Loop Current by El-Sayed and Trees (1980) and eq. (21), we obtained a 1% light depth, at the bottom of the conventional euphotic zone, of 88.5 m, which is similar to their secchi-disk estimated value within ± 5 m. To include growth and nutrient uptake at the 0.1% light depths, we integrated "new" production down to the depth of the interface.

Since the coupled physical-biological models explore the consequences of an annual cycle of Loop Current penetration into the Gulf of Mexico, seasonal changes in surface light intensity and photoperiod must also be specified. Accordingly, the surface daily PAR value, $I_o$, was computed each day, d, from

$$I_o(d) = 4.46\delta I_r \tag{22}$$

where $\delta = 0.43$ is the assumed ratio of PAR to total incident solar irradiance, $I_r$, determined daily at 25°N from the Smithsonian meteorological tables (Reed, 1977).

With this estimate of the mean, clear-sky insolation (joules $m^{-2}$ $sec^{-1}$) over the Gulf of Mexico, i.e., the equivalent radiation is 4.43 μEin $m^{-2}$ $sec^{-1}$ over the visible spectrum, the hourly light input to the model, $I_o(t)$, is assigned by

$$I_o(d) = \int_{i=1}^{\ell} I_o(t)dt \tag{23}$$

where $\ell$ is the photoperiod in hr. No attempt is made to simulate reduction of incoming radiation by clouds. The hourly cloud-free irradiance reaches a maximum, $I_m$, at local noon, i.e.,

$$I_o(t) = I_m \sin^3 [\pi(t - \lambda)\ell^{-1}] \tag{24}$$

where $\lambda$ is the hour of sunrise, defined by

$$\lambda = 12 - 0.5\ \ell \tag{25}$$

To complete our definition of the light field, we must obtain the photoperiod, $\ell$.

Using the relationship of the angle of solar elevation, e, to its declination angle, $\omega$ at a specific latitude of 25°N, given by Neuberger (1965) as

$$\sin(e) = \sin(25°N)\sin(\omega) + \cos(25°N)\cos(\omega)\cos(n) \tag{26}$$

where n is the hour angle difference from local solar noon (15° $hr^{-1}$), will allow computation of $\ell$. Solving eq. (26) for n, with a specified daily value

of $\omega$ and setting e=0, gives the time of sunrise, in hours from local noon. The photoperiod then is

$$\ell = 2n \tag{27}$$

In our biological model, the photoperiod was thus obtained from eqs. (26)-(27) and solar declination angles, $\omega$, for each day (Neuberger, 1965); it varied from 10.5 to 13.5 hr.

With knowledge of the daily photoperiod and incident PAR, the hourly mean irradiance, $\bar{I}_o(t)$, is defined as

$$\bar{I}_o(t) = I_o(d)\ \ell^{-1} \tag{28}$$

which allows calculation of the maximum irradiance at local noon by

$$I_m = \bar{I}_o(t)\ \ell \left\{ \int_{i=1}^{\ell} \sin^3\left[\pi(t - \lambda)\ell^{-1}\right] dt \right\}^{-1} \tag{29}$$

The monthly average of $I_m$ is presented in Table 2 as an index of the daily variation of light forcing in our coupled models. The last formulation of our models is the nitrogen dependence, $\chi$, of this daily light-regulated growth of phytoplankton.

In contrast to our model of the uncoupled spring food chain of the continental shelf ecosystem off New York (Walsh et al., 1988a), we assume here that nitrogen is not limiting the individual growth of a phytoplankton cell, i.e., there is no Michaelis-Menten expression for nutrient uptake in the present model. At a growth rate of 4 cell divisions $day^{-1}$, we assume that an individual algal cell is instead growing maximally on recycled nitrogen (Goldman et al., 1979), before consumption by a herbivore within a tightly coupled picoplankton-protozoan-bacterial food web (Azam et al., 1983). Nitrogen instead limits the amount of primary production, with the supply of new nitrogen determining the flux of possible export from the euphotic zone. The last term of eq. (20), $\chi$, thus defines the oligotrophic nature of the nutrient dynamics of the Gulf of Mexico, where as much as 90% of the nitrogen demand of daily primary production may be met by dissolved ammonium, urea, and amino acids (Eppley and Peterson, 1980).

In a model of new production, we must differentiate between the algal biomass grown on oceanic $NO_3$ and river effluent, i.e., N of eq. (18), and that synthesized from the recycled sources of nitrogen, by using $\chi$, the ratio of new to total nitrogen uptake by the phytoplankton. This ratio can be expressed as a fraction of the ambient new nitrogen (Platt and Harrison, 1985) by

$$\chi = \chi_m \left[ 1 - e^{-\left(\theta N \chi_m^{-1}\right)} \right] \tag{30}$$

where $\chi_m$ = 0.83 is the maximum ratio, i.e., assuming a minimal recycled production of 17%.

A nitrate concentration of 10 μg-at $NO_3$ $\ell^{-1}$ at the interface depth yields a $\chi$ of 0.83 in a region, where uptake of "new" nitrogen will be negligible as a result of light limitation. Near the mouth of the Mississippi River, uptake of new nitrogen will be the largest, however, where both light and nitrogen are abundant. Our value of $\theta$ = 0.74 $m^3$ mg-at$^{-1}$ simulates a subtropical oceanic habitat (Lewis et al., 1986), compared to 5.48 $m^3$ mg-at$^{-1}$ for coastal waters (Platt and Harrison, 1985). As another unitless fraction, eq. (30) replaces our prior formulation of

$$\chi = \frac{N}{k_N + N} \tag{31}$$

where $k_N$ was a half-saturation constant of this Michaelis-Menten expression for nutrient limitation (Walsh et al., 1988a).

4. Numerical techniques

Solutions to eqs. (2)-(4) and (18)-(19) are obtained numerically, using finite-difference approximations to their time and space derivatives. The numerical scheme for eqs. (2)-(4) is similar to that of Hulburt and Thompson (1980), except that our time differencing is fully explicit. The scheme for eqs. (18)-(19) consists of a semi-implicit Crank-Nicholson method for the

vertical mixing terms and an explicit, forward-in-time method for the remaining terms.

A staggered grid system is used for both the physical and biological models, with the state variables of layer thickness, $h_i$, pressure, $P_i$, nutrient, N, and phytoplankton, M, positioned in the center of each grid cell. The horizontal velocity component, $u_i$, is instead placed one-half grid increment to the east and west of each cell center, while $v_i$ is located one-half grid increment to the north and south. Similarly, the vertical transfer processes, effected by $K_z$ and $w_s$, are positioned one-half grid increment above and below the centroid of each of the 20 vertical cells.

The lateral boundaries of the models are drawn through either u or v points, where the appropriate normal velocity component is zero. Similar to eqs. (2)-(4), the flux boundary conditions for eqs. (18) and (19) then consist of zero orthogonal transfer of nitrogen and chlorophyll along the solid land-sea boundaries. Input of nitrogen from the Mississippi River is simulated as a continuous release into the three upper layers ($\sim$25 m) of each of the two cells of the biological model, immediately adjacent to its mouth (the • of Fig. 8), at a rate of $4.86 \times 10^{12}$ μg-at N $hr^{-1}$. Instantaneous mixing of the river effluent is assumed over the changing volumes of these surface layers at each time step. The other import of nitrate and chlorophyll through Yucatan Strait involves the product of the boundary inflows with changing depth profiles of $NO_3$ and chlorophyll. The dissolved and particulate fluxes through the outflow port of Florida Strait are instead self-determined,

using an upstream differencing formulation, which requires no external information (Walsh, 1988).

The fluxes at the surface of the sea are defined as

$$K_z \frac{\partial N}{\partial \phi} = K_z \frac{\partial M}{\partial \phi} = w_s M = 0 \qquad (32)$$

At the bottom of the upper layer of the circulation model, i.e., the twentieth layer of the biological model, the time-invariant boundary conditions are $N_b$ = 10 μg-at $NO_3$ $\ell^{-1}$ and again $K_z \frac{\partial M}{\partial \phi} = 0$. As in the case of export through Florida Strait, the vertical particulate flux, due to sinking through the interface to the sediments, is self-determined, using our upstream formulation of the finite-difference equations at the boundaries.

The finite difference forms of eqs. (2)-(4) involved a central difference operator in space and time (e.g., Hulburt and Thompson, 1980; Walsh, 1988). To avoid numerical instabilities of this technique (Haltiner, 1971), the horizontal turbulence terms of eqs. (2)-(3) were evaluated at a prior time step to that of the other terms. The use of this leap-frog scheme can also lead to decoupling of the numerical solution at odd and even time steps (e.g., O'Brien, 1986). Euler's backward scheme (Haltiner, 1971) was thus employed for two consecutive time steps, at intervals of 900 time steps, to prevent this time splitting.

Our time step of the circulation model was determined by the Courant, Freidricks, Lewy (CFL) stability condition (O'Brien, 1986) of

$$\Delta t \leq \frac{1}{2}\left[\gamma^2\left(\frac{1}{\Delta x^2}+\frac{1}{\Delta y^2}\right)\right]^{-\frac{1}{2}} \tag{33}$$

where $\gamma$ is the phase speed of the free surface gravity wave. With $\gamma = \sqrt{gD}$, where $D = h_1 + h_2$ is the total depth in the model, and using a maximum depth of 3800 m, eq. (33) leads to a time step of $\sim$50 sec. A time step of 48 sec was consequently used over a duration of 3 yr to simulate penetration and shedding of eddies by the Loop Current.

Within the biochemical model, an upstream finite difference scheme is used for the advective terms of eqs. (18)-(19), following Smolarkiewicz (1983). This scheme can be written, using eq. (18), as:

$$\begin{aligned}\left(h_{1i,j}N_{i,j}\right)^{t+\Delta t} - \left(h_{1i,j}N_{i,j}\right)^{t} = &\left[F\left(N^t_{i,j},N^t_{i+1,j},U^t_{i+\frac{1}{2},j}\right)\right. \\ &\left. - F\left(N^t_{i-1,j},N^t_{i,j},U^t_{i-\frac{1}{2},j}\right)\right]\frac{\Delta t}{2\Delta x} \\ &- \left[F\left(N^t_{i,j},N^t_{i,j+1},V^t_{1,j+\frac{1}{2}}\right) - F\left(N^t_{i,j-1},N^t_{i,j},V^t_{i,j-\frac{1}{2}}\right)\right]\frac{\Delta t}{2\Delta y}\end{aligned} \tag{34}$$

where $U_{i\pm\frac{1}{2},j} = u_{i\pm\frac{1}{2},j}\left(\frac{h_{1i,j} + h_{1i\pm1,j}}{2}\right)$

and $V_{i,j\pm\frac{1}{2}} = v_{i,j\pm\frac{1}{2}} \left(\frac{h_{1i,j} + h_{1i,j\pm1}}{2}\right)$.

The subscripts i and j are grid indices in the x and y directions respectively, while the superscripts, t and t+Δt, denote time levels. The general form of the operator F() is

$$F(N_{i,j},N_{i+1,j},U) = [(U + |U|)N_{i,j} + (U - |U|)N_{i+1,j}] \tag{35}$$

Although this first-order scheme introduces strong implicit diffusion, it is transportive, the phase errors are relatively small, it conserves mass, and is economical to use. The CFL stability condition for this scheme is

$$\Delta t \leq \frac{1}{2}\left(\frac{u^2_{i+\frac{1}{2},j}}{\Delta x^2} + \frac{v^2_{i,j+\frac{1}{2}}}{\Delta y^2}\right)^{-\frac{1}{2}} \tag{36}$$

This is easily satisfied with a time step of 1 hr for maximum velocities of 1 m $sec^{-1}$.

The Von Neumann stability condition for the vertical mixing terms in eqs. (18) and (19) is, however,

$$\Delta t \leq \frac{\Delta z^2}{2K_z} \tag{37}$$

A maximum value for $K_z$ of 66 $cm^2$ $sec^{-1}$ (Table 2), and the smallest $\Delta z$ of 5 m, suggests a time step of $\sim$0.5 hr. To remove this time restriction, a semi-implicit Crank-Nicholson (O'Brien, 1986) method was employed for these terms.

It consists of

$$\left(h_{1i,j}N_{i,j,k}\right)^{t+\Delta t} = \left(h_{1i,j}N_{i,j,k}\right)^{t} + \frac{1}{\bar{h}_{1i,j}\Delta\phi}\left[K^{t}_{i,j,k-\frac{1}{2}}\left(\bar{N}_{i,j,k-1} - \bar{N}_{i,j,k}\right)\right.$$

$$\left. - K^{t}_{i,j,k+\frac{1}{2}}\left(\bar{N}_{i,j,k} - \bar{N}_{i,j,k+1}\right)\right] \qquad (38)$$

where $\bar{N}_{i,j,k} = \dfrac{\left[\left(h_{1i,}N_{j\ i,j,k}\right)^{t+\Delta t} + \left(h_{1i,j}N_{i,j,k}\right)^{t}\right]}{2}$, and $\bar{h}_1 = \left(h_1^t + h_1^{t+\Delta t}\right)/2$. Here k is the grid index in the vertical dimension, with k = 1 being the topmost layer of the model. Equation (38), with appropriate boundary conditions, reduces to a tridiagonal matrix, which can be solved using standard methods (Walsh et al., 1988a).

The no-flux boundary conditions are incorporated in the model by assigning the values of N and M at fictitious exterior points to equal those just inside a particular boundary. The lower boundary value of N is incorporated using a one-sided, second-order approximation for the first derivatives of N at the interface depth. This becomes

$$\frac{\partial N}{\partial \phi} \simeq \frac{1}{3\Delta\phi} (-8N_b + 9N_{b-1} - N_{b-2}) \qquad (39)$$

where $N_b$ is the value of N at the interface, and $N_{b-1}$, $N_{b-2}$ are $\frac{1}{2}\Delta\phi$ and $\frac{3}{2}\Delta\phi$ above the interface depth. The remaining terms of eqs. (18)-(19) were approximated using an explicit, forward-in-time procedure (Walsh, 1988).

Consequently, numerical solutions of eqs. (18)-(19) were obtained with a time step of 1 hr over a duration of 1 yr within the coupled physical/biological models. The output of the third yr results of the circulation model was the time-dependent circulation field of the biological model. Interpolating between the monthly entries of $K_o$ and $I_o$ in Table 2, the values of vertical mixing and incident radiation were changed hourly, while the flow field was updated daily. The initial conditions of algal biomass and nitrate were derived from steady-state solutions of the one-dimensional, depth-dependent form of eqs. (18)-(19) for the month of May (Table 2). Day 0 of the coupled biological/physical models is thus May 1.

5. CZCS imagery

To provide an additional check on the validity of our calculation, time series of Coastal Zone Color Scanner (CZCS) images were compiled for two 3.5 x $10^4$ $km^2$ areas of the eastern (Location G of Figure 8) and western (Location H) Gulf of Mexico, as well as over the whole basin (Muller-Karger et al., 1988). Briefly, synoptic estimates of the concentration of pigments in surface waters

of the Gulf were obtained from approximately 300 individual scenes between January 1979 and July 1982. This preliminary CZCS time series consists of pigment concentrations derived from ratios of the blue (443 nm) or blue-green (520 nm) water-leaving radiances to the green radiance (550 nm) -- see Gordon et al., 1988, and references therein. The pigment estimates are actually the concentration of chlorophyll a, phaeopigments, and dissolved organic matter.

The CZCS data were first processed at 1/16 of their original 1 km spatial resolution by Otis Brown and Bob Evans at the University of Miami. These pigment concentrations were then binned spatially into 20 km x 20 km squares, with 30-day composites based on congruent images, mapped to a cylindrical equidistant projection. The arithmetic means of the monthly pigment concentrations are presented in Figure 25 for three areas of interest: the entire Gulf of Mexico, an eastern region centered at 24°N, 86°W, and a western one centered at 25°N, 93°W.

These CZCS time series provided an estimate of the average pigment concentration within the first optical depth of the water column (at most 10 m). Thus, we compared these satellite estimates with results of the model by taking the arithmetic mean each day at noon of the simulated chlorophyll concentration of the first layer over the same spatial domains. Shipboard validation data of these chlorophyll fields are available from cruises taken during February 1980 and 1981 (El-Sayed and Trees, 1980; Ortner et al., 1984).

## Results

After the formulation of the initial states and boundary conditions, the time-dependent inputs of N, as a result of circulation and river discharge, were either accumulated in the water column as N and M, remineralized, or transferred to the sediments as sinking losses of M. The phytoplankton, M, are not consumed by herbivores, since neither grazing pressure, nor metazoan excretion, are explicit processes of eqs. (18)-(19) for estimation of "new" production. Accordingly, fecal pellets do not exit the simulated water column. The coupled physical-biological models nevertheless provide an enormous 3-dimensional array of numbers, varying from 2-21 layers at 2193 active grid points over time steps of 48-3600 sec for 1-3 yr of simulated time. To digest our results and their implications, we present them in three sections: 2-dimensional output of the circulation model, 1-dimensional output of the biological model, and 3-dimensional output of the coupled physical-biological models. Locations of representative time series are shown in Figure 8.

### 1. Circulation model

Integration of eqs. (2)-(4) was performed over 1080 days of simulated time (Fig. 9), assuming an initial state of no motion throughout the basin. Inflow across Yucatan Strait was increased linearly for a period of 30 days to a value of 30 Sv. After this spinup, the circulation patterns exhibit a cycle of intrusion, westward bending, and finally eddy separation of the Loop Current in the Gulf. This is similar to the numerical results of Hulburt and

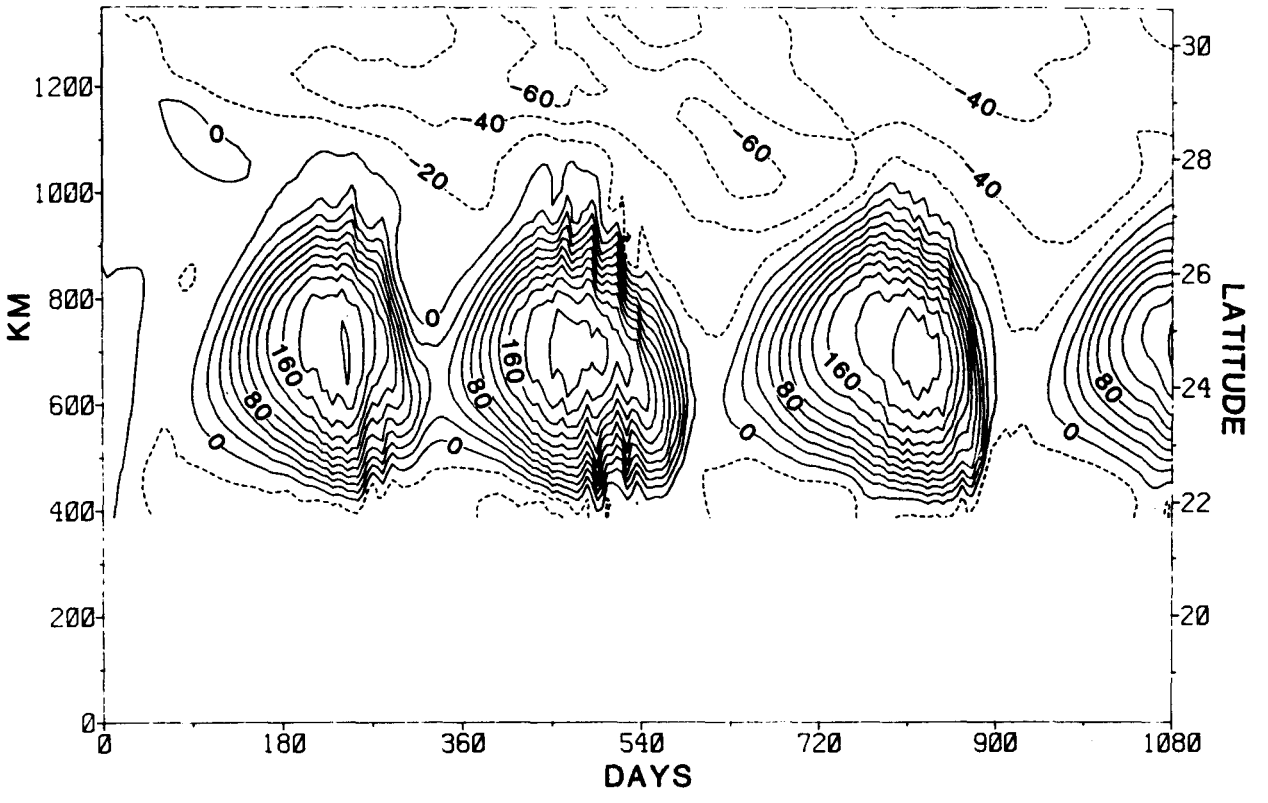


Fig. 9. Interannual variation in pycnocline height across a north-south section of the Gulf of Mexico, between the Yucatan peninsula and Pensacola, Florida--see Fig. 8.

Thompson (1980) and to the physical results of Sugimoto and Ichiye (1988). Flows of ∿90 cm $sec^{-1}$ were calculated for individual snapshots of the Loop Current and its anticyclonic eddies, while weaker currents of <10 cm $sec^{-1}$ were associated with cyclonic eddies at the margins of the basin (Fig. 10a).

Figure 9 is a plot of the relative pycnocline depth as a function of time along a north-south section, 40 km west of the inflow port (see Fig. 8 for location), over the 1080 days of simulated time. The pycnoclines in this and following figures are plotted as the deviation of the pycnocline from its initial position at 200 m, with positive values indicating a deeper pycnocline as a result of downwelling. The negative values of Figure 9 denote upwelling on Campeche Bank and the northwest Florida shelf. Figure 9 also shows approximately 3-1/2 cycles of Loop Current penetration and eddy shedding, with an average period of 309 days. Our near annual cycle of the simulated Loop Current conforms to mean hydrographic (Elliott, 1982) and satellite (Auer, 1987) estimates of an annual cycle of major eddy formation by the Loop Current.

A look at one such cycle, beginning at day 10 of the third annual event (Fig. 9), is shown in Figures 10b and 11. The pycnocline displacement field in Figure 10b shows the Loop Current with minimal penetration into the Gulf, similar to field observations in January 1952 (Fig. 4) and May 1972 (Fig. 15a). An anticyclonic eddy is centered just north of Campeche Bank; the eddy had detached from the Loop Current approximately 10 days earlier. The shape of this initial eddy is elliptical (Fig. 10b), becoming more so (Fig. 11b), as it approached the Mexican coast (Kirwan et al., 1988). Using

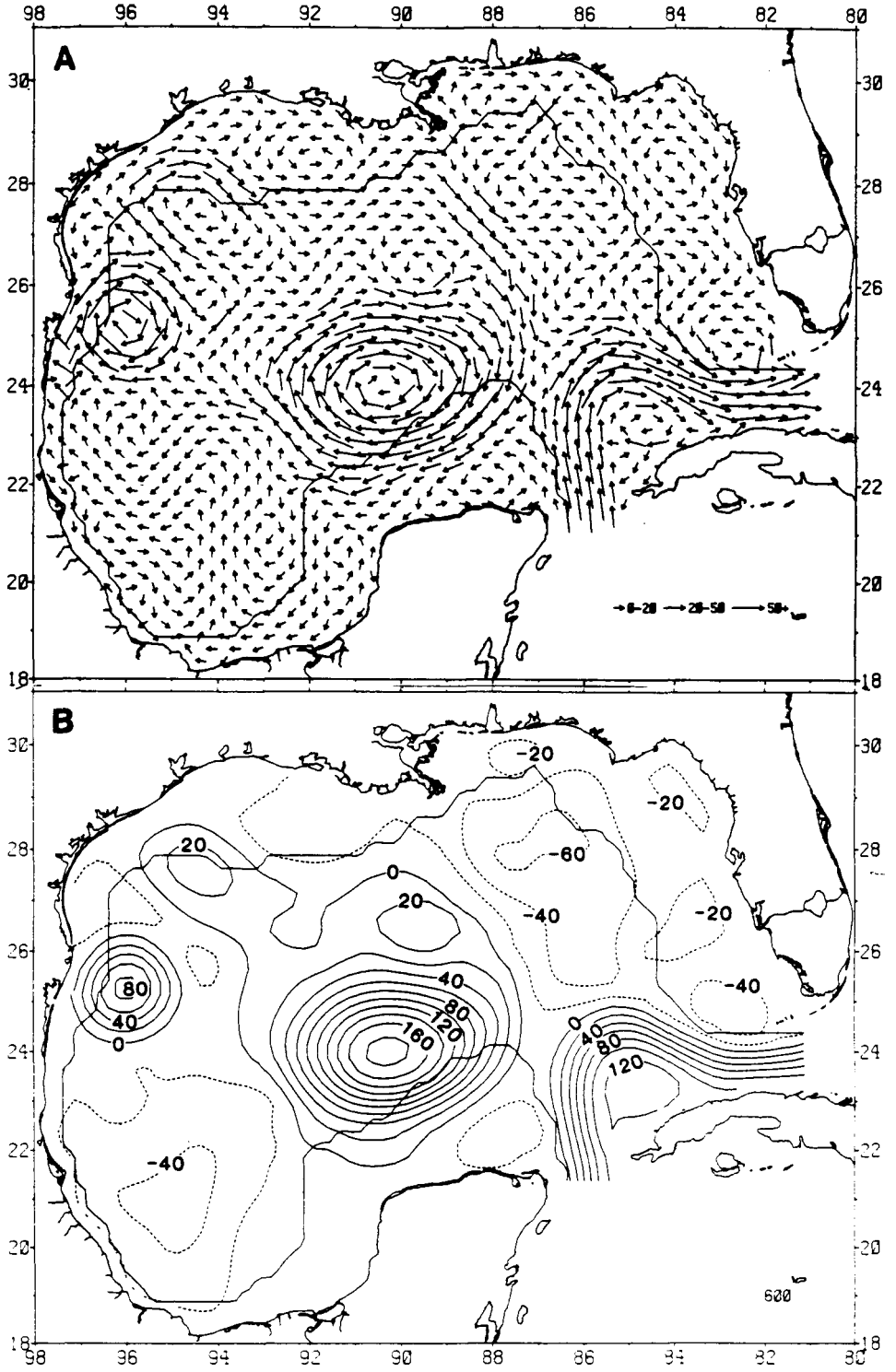


Fig. 10. The distribution of A) surface currents in relation to B) pycnocline height within the Gulf of Mexico during day 10 of the third penetration cycle of the Loop Current (see Fig. 9).

the distance between speed maxima, $V_m$ of Figure 10a, this recently-shed eddy had a north-south diameter of 232 km and an east-west diameter of 354 km. Elliott (1982) found rms radii of 183 km in a study of three anticyclones formed in 1966-1967, while Auer (1987) reported a mean initial diameter of 307 km in his study of 1981-85 Loop Current rings.

Hulburt and Thompson (1980) suggest that a typical north-south diameter for Loop Current eddies should be of the order $d = \sqrt{V_m/\beta} \simeq 225$ km, if a value of $V_m = 1$ m sec$^{-1}$ is used, where $\beta$ is defined in eq. (9). The upper layer velocity field (Fig. 10a) shows the dominant circulation patterns associated with the Loop Current and its newly formed anticyclonic eddy. A fairly strong anticyclonic cell is also evident along the Texas-Mexican coastline. This additional cell is a remnant of an eddy spawned during the second penetration cycle of the Loop Current (Fig. 9). Simulated currents within the Loop Current and the Campeche Bank anticyclonic eddy reach speeds of 90 cm sec$^{-1}$, similar to Hulburt and Thompson's (1980) formulation of a trajectory of constant absolute vorticity. These simulated flows are also in accord with near-surface geostrophic speeds of $\sim$100 cm sec$^{-1}$ calculated by Nowlin and Hubertz (1972) from hydrographic observations of both the Loop Current and an anticyclonic eddy.

Figure 11 shows subsequent pycnocline displacement fields at 80-day intervals from day 10 of the third penetration cycle (Fig. 10b); the associated currents are shown in Figure 20. At day 90, the Loop Current has penetrated approximately 150 km farther into the Gulf, with the pycnocline deepening to 340 m in the center of the Loop (Fig. 11a). The anticyclonic

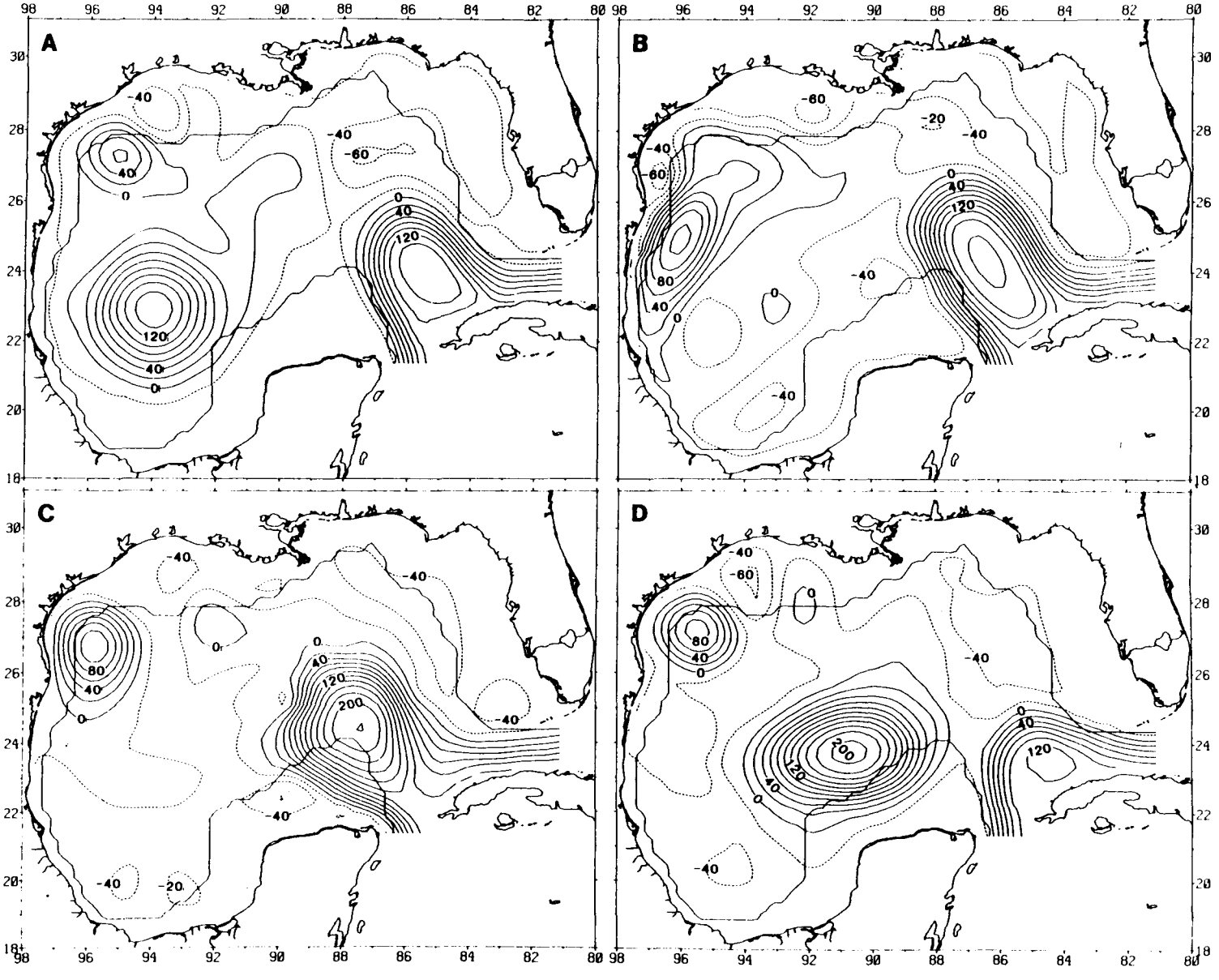


Fig. 11. Annual variation of pycnocline height within the Gulf of Mexico on days A) 90, B) 170, C) 250, and D) 330 during a penetration cycle of the Loop Current.

eddy, previously located north of Campeche Bank, moved 350 km west-southwest to the northern part of the Bay of Campeche. This movement corresponds to a translation speed of $\sim$5 cm $sec^{-1}$, similar to observations of 4-6 cm $sec^{-1}$ for 1980-85 Loop Current rings (Auer, 1987; Kirwan et al., 1988). This motion also corresponds to the nondispersive internal Rossby wave speed, c, approximated by $c = \beta g' h_1 / f^2$, where all terms are previously defined, if a value of $h_1$ = 300 m is used.

By day 170, (Fig. 11b), the Loop Current is near its maximum northern penetration into the Gulf, reaching 27°N, if the zero isopleth of the pycnocline displacement field is used. Within the center of the Loop Current, the pycnocline has been further depressed to a depth of 380 m, the same displacement as the center of the shed eddy on day 10 (Fig. 10b). Also, with westward movement no longer possible, the eddy previously in the Bay of Campeche has moved north to a position off the continental slope southeast of Brownsville, Texas, similar to observations of rings in 1980 and 1982 (Kirwan et al., 1988).

By day 250 (Fig. 11c), this eddy has moved to the northwestern corner of the Gulf. With the shelf turning eastward there, the eddy can move no farther and slowly dissipates (Fig. 11d). During its sojourn across the western Gulf of Mexico, the depressed center of the anticyclonic eddy rose from a depth of 380 m on day 10 (Fig. 10b) to 280 m on day 330 (Fig. 11d), yielding apparent upwelling rates of 0.3-0.4 m $day^{-1}$. Comparable upwelling rates of $\sim$1 m $day^{-1}$ occur within decaying warm core rings of the Gulf Stream (Franks et al.,

1986). Thus, the anticyclonic rings of the Loop Current may be loci of enhanced production in the oligotrophic western Gulf of Mexico.

Back in the eastern Gulf of Mexico, the Loop Current has moved westward a total distance of approximately 100 km by day 250 (Fig. 11c), with the closed center taking on a more circular shape. Several small waves can be seen on the eastern wall of the simulated Current, preceding the separation of the next anticyclonic ring. These have also been inferred from satellite imagery and hydrography (Vukovich and Maul, 1985). Satellite temperature data in October and December 1976 (Vukovich et al., 1979) were used to estimate the northward extension of the Loop Current in November 1976 (Fig. 12a), which is similar to day 250 of the simulation (Fig. 11c). Note the inferred wave at the cyclonic edge of the Loop Current, demarcated by the 100 m depth of the 22°C isotherm during the Researcher cruise (Fig. 12a).

By day 330 (Fig. 11d) the penetration cycle of the Loop Current is complete. The Loop Current, having extended farther to the west, has shed another eddy and retreated, leaving a circulation pattern very similar to that seen on day 10 (Fig. 10b). The areal extent of 40 m upward displacement of the pycnocline at the west Florida shelf-break is minimal under this situation, compared to more northward penetration of the Loop Current (Figs. 11a, 11b, and 11c). If light and wind forcing were minimal at this time as well, we might expect little primary production or export to the sediments. Since the shedding cycle of the Loop Current varies interannually from 4 to 16 months between generation events (Auer, 1987), however, we must first sort out the seasonal effects of incident radiation and vertical mixing

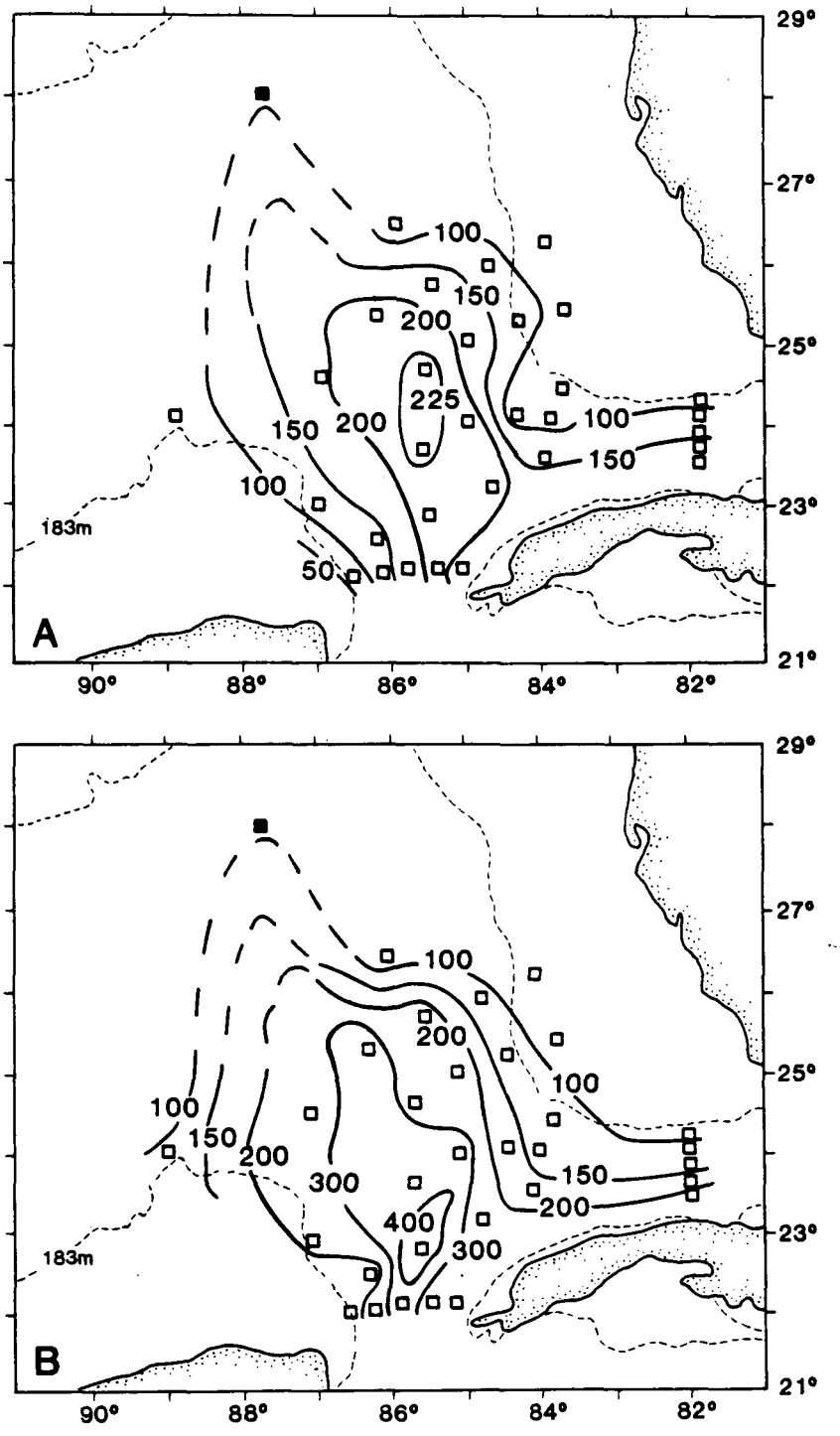


Fig. 12. The depths of A) the 22°C isotherm and B) the 5 μg-at $\ell^{-1}$ isopleth of nitrate within the eastern Gulf of Mexico during November 1976, based on shipboard and satellite (■) data.

on algal growth, before introducing the additional complexity of upwelling and downwelling events.

2. Biological Model

A monthly time series of temperature, phosphate, and chlorophyll was collected during 1960 (Alexander et al., 1962) in 800 m of water on the eastern side of the Florida Current (25°33'N, 79°25'W) near Cat Cay, Bahamas (Location E of Fig. 8), where upwelling, as a result of cyclonic eddies, should be minimal. The depth of the 22°C isotherm (recall Fig. 6) remained at 165-175 m throughout this time series, except for June 1960, when an upward vertical displacement of 25 m occurred. The 19°C isotherm moved up 60 m that month to a depth of 140 m.

Concomitantly, a subsurface chlorophyll maximum of >0.5 μg chl $\ell^{-1}$ and phosphate depletion occurred in June 1960. We deleted the data from this month in Figures 13b and 14b, in a comparison of the seasonal results from the biological model, where we held the depths of the interface constant at respectively 200 m (Figs. 13a and 14a) and 100 m (Figs. 13c and 14c). Using a Redfield dissolved N/P ratio of 15/1, we also converted their phosphate data of the aphotic zone to equivalent nitrate concentrations in Figure 14b.

Surface chlorophyll concentrations of 0.30 μg $\ell^{-1}$ in January and 0.03 μg $\ell^{-1}$ in August off Cat Cay (Fig. 13b) are reproduced by the model, when the interface depth is held constant at 200 m (Fig. 13a). Concordance of model and field results of the temporal change in algal biomass implies that the minimum chlorophyll concentration of ∿0.03 μg chl $\ell^{-1}$ is the "steady-state"

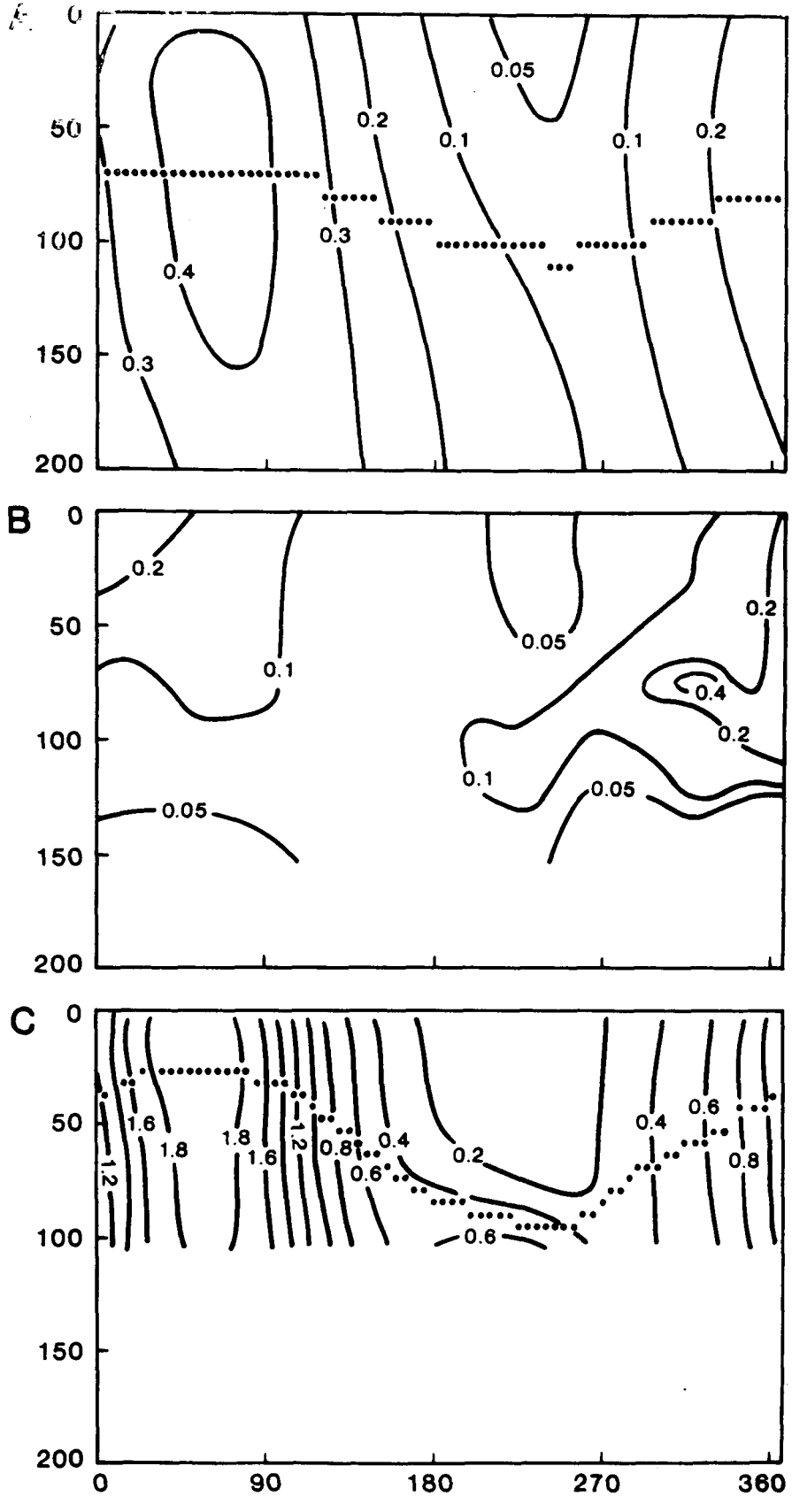


Fig. 13. Annual variation of chlorophyll both in the simulated Gulf of Mexico, when the pycnocline depth is held constant at A) 200 m and C) 100 m, and in B) the Florida Current off the Bahamas; the euphotic zone depth is denoted by •.

result of grazing and growth from recycled nitrogen. Addition of new nitrogen as nitrate by vertical mixing in the model, modified by eq. (30), leads to observed increases of algal biomass, which are not grazed, but available for export instead to the aphotic zone, demarcated by the dotted lines in Figures 13a and 13c.

Subsurface chlorophyll maxima of 0.4 μg $\ell^{-1}$ (Fig. 13b) are also reproduced by the model (Fig. 13a), but with poor phasing between observation and theory. Such discrepancy in the timing of midwater chlorophyll maxima may reflect inadequate sampling of the water column, both with bottle casts in 1960, and with vertical resolution of mixing in the model. For example, the mean depths of the 1.5 μg-at $NO_3$ $\ell^{-1}$ isopleth of nitrate, averaged over the year, are equivalent, ∿160 m, in the 200-m case of the model (Fig. 14a) and off Cat Cay (Fig. 14b). The apparent vertical excursion of the surrogate 1.5 μg-at $NO_3$ $\ell^{-1}$ isopleth from depths of >200 m to 125 m off Cat Cay (Fig. 14b) may reflect a time-dependent flux of nitrate across the pycnocline of the real ocean. In the model, the cross-pycnocline flux was held constant in these initial cases.

Upward movement of the model's interface depth, e.g., Figures 13c and 14c, allows greater nitrate concentration at shallower depths (Fig. 14c). A stronger seasonal signal in the depth of the 0.5 μg-at $NO_3$ $\ell^{-1}$ isopleth results from increased phytoplankton activity within the euphotic zone. When the depth of the interface is held constant at 100 m in this second case, however, the seasonal cycle of simulated algal biomass (Fig. 13c) continues to reflect the change of the mixed layer depth from 100 m in January to 24 m in

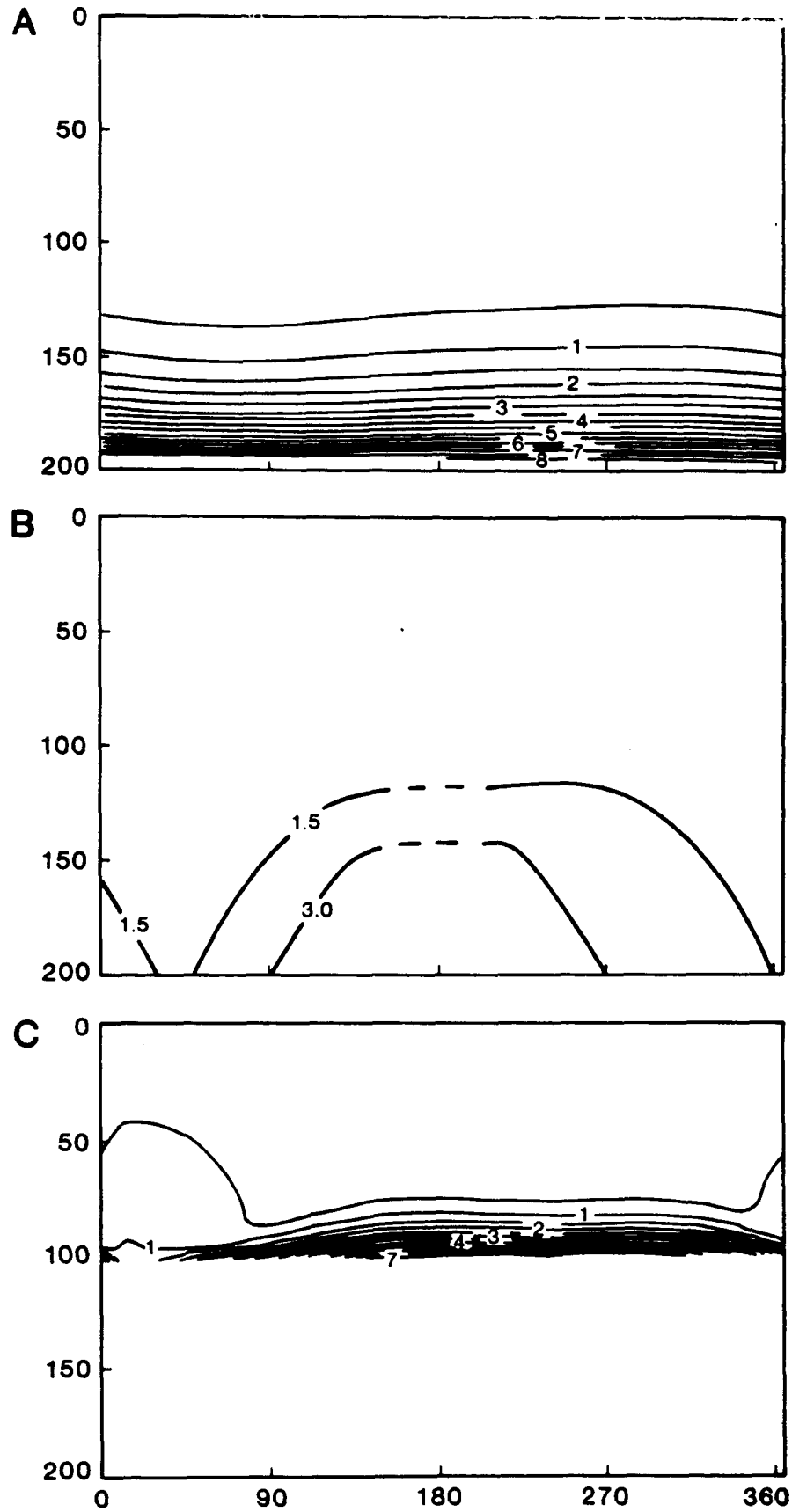


Fig. 14. Annual variation of surrogate nitrate (N/P = 15/1) both in the simulated Gulf of Mexico, when the pycnocline depth is held constant at A) 200 m and C) 100 m, and in B) the Florida Current off the Bahamas.

August, rather than the opposite seasonal variation of light, which is never less than a maximum daylight value of 696 μEin $cm^{-2}$ $hr^{-1}$ (Table 2).

With greater nitrate concentrations at the bottom of the euphotic zone in the second case (Fig. 14c), the simulated chlorophyll stocks increase about fivefold (Fig. 13c) over those of the first case (Fig. 13a). The seasonal cycle of the depth of the euphotic zone is also more pronounced, ranging from 25 m to 100 m. The annual sinking loss of algal biomass across the pycnocline in the first case of a 200-m interface depth was 0.2 g chl $m^{-2}$ $yr^{-1}$, compared to the much higher value of 1.0 g chl $m^{-2}$ $yr^{-1}$ after upward movement of the pycnocline to a constant depth of 100 m in the model. Using a range in C/chl ratio of 50/1 to 100/1 for living phytoplankton and detritus in the Florida Current (Steele, 1964), these annual inputs to the aphotic zone represent respective carbon fluxes of 10-20 and 50-100 g C $m^{-2}$ $yr^{-1}$.

About 160 miles farther north of the Cat Cay time series (Figs. 13b and 14b), a sediment trap was moored at 660 m near 27°42'N, 78°54'W during June 1977 (Hinga et al., 1979). Upwelling in the water column above this trap on the eastern side of the Florida Current near Walker's Cay, Bahamas, should be minimal. The flux of particulate organic carbon estimated at this sediment trap was 14.4 mg C $m^{-2}$ $day^{-1}$, or 5.2 g C $m^{-2}$ $yr^{-1}$, compared to 10-20 g C $m^{-2}$ $yr^{-1}$ exiting the euphotic zone of the biological model, where the interface depth is held constant at 200 m (Figs. 13a and 14a). Assuming a constant C/N ratio of 10/1 for particulate matter in the low carbon sediments on the upper slope of this region (Fig. 7), the equivalent nitrogen fluxes at 200 m in the model and 660 m in the sea are 1-2 and 0.5 g N $m^{-2}$ $yr^{-1}$. The observed C/N

ratio of the trapped particulate matter was 46/1, indicating significant remineralization of presumably slow sinking organic matter within the water column.

Another sediment trap mooring at a depth of 1345 m on the slope off Myrtle Beach, South Carolina, at 33°30'N, 76°15'W (Hinga et al., 1979), yielded 29.8 mg C $m^{-2}$ $day^{-1}$, or 10.8 g C $m^{-2}$ $yr^{-1}$. Despite the greater descent, the surviving particulate matter had a lower C/N ratio of 23/1. This mooring was located both near the western edge of the Florida Current, where cyclonic eddy-induced upwelling is expected (Lee et al., 1981), and downstream of the Charleston Bump, where topographic upwelling also prevails (Bane and Dewar, 1988). Using a generalized depth-flux relationship (Martin et al., 1987), we obtain possible fluxes of 21.6 g C $m^{-2}$ $yr^{-1}$ at 660 m and 86.4 g C $m^{-2}$ $yr^{-1}$ at 100 m in the water column above the trap at 1345 m. With the model's interface depth held constant at 100 m in the second case (Fig. 13c), reflecting increased upwelling, the predicted flux of 50-100 g C $m^{-2}$ $yr^{-1}$ at a depth of 100 m is similar to that extrapolated from the field data off South Carolina.

We thus expect two sources of variance in the results of the coupled physical/biological models: temporal as a result of seasonal vertical mixing effected by wind, and spatial as a result of upwelling effected by the Loop Current. For example, the nitrate flux across the pycnocline into the 20th layer of the biological model ranges from 0.1 to 0.6 g-at $NO_3$ $m^{-2}$ $yr^{-1}$ in respectively the 200-m and 100-m cases of constant interface depth (Figs. 14a and 14c). The former case is similar to microscale velocity shear estimates

of a nitrate flux of 0.05 g-at $NO_3$ $m^{-2}$ $yr^{-1}$ into the euphotic zone southeast of the Azores (Lewis et al., 1986), where mesoscale eddies are less energetic (Stommel, 1987). The latter case is equivalent to $^3He$ estimates of a nitrate flux of 0.6 g-at $NO_3$ $m^{-2}$ $yr^{-1}$ into the euphotic zone off Bermuda (Jenkins, 1988), where mesoscale upwelling events (Woods, 1988) may be the major supply mechanism.

If the biological model is run for a year with a constant interface depth of 400 m, however, i.e., in the center of an anticyclonic eddy, the nitrate flux into the 20th layer is only 0.05 g-at $NO_3$ $m^{-2}$ $yr^{-1}$; the simulated depth profile of nitrate then also approximates the field observations southeast of the Azores (Lewis et al., 1986). In this third case of the model, the winter maximum of algal biomass was tenfold less than that of the second case of a 100-m interface depth (Fig. 14c), while the seasonal variation was about threefold, from >0.15 μg $\ell^{-1}$ in January to <0.05 μg $\ell^{-1}$ in August. Upward movement of the interface depth from 400 m to 100 m thus leads to the same range of algal biomass variation as that effected by seasonal changes in wind forcing and vertical mixing (Table 2), when the interface depth is held constant at 200 m.

To distinguish between the biochemical consequences of the annual cycle of wind forcing and the subannual periodicity (∿310 days) of the Loop Current penetration and eddy shedding, we ran three cases of the coupled physical/biological model. Over the same cycle of Loop Current advance and retreat discussed in the first section of our results, the biological response to this time-dependent nutrient addition was explored with 1) a constant $K_o$

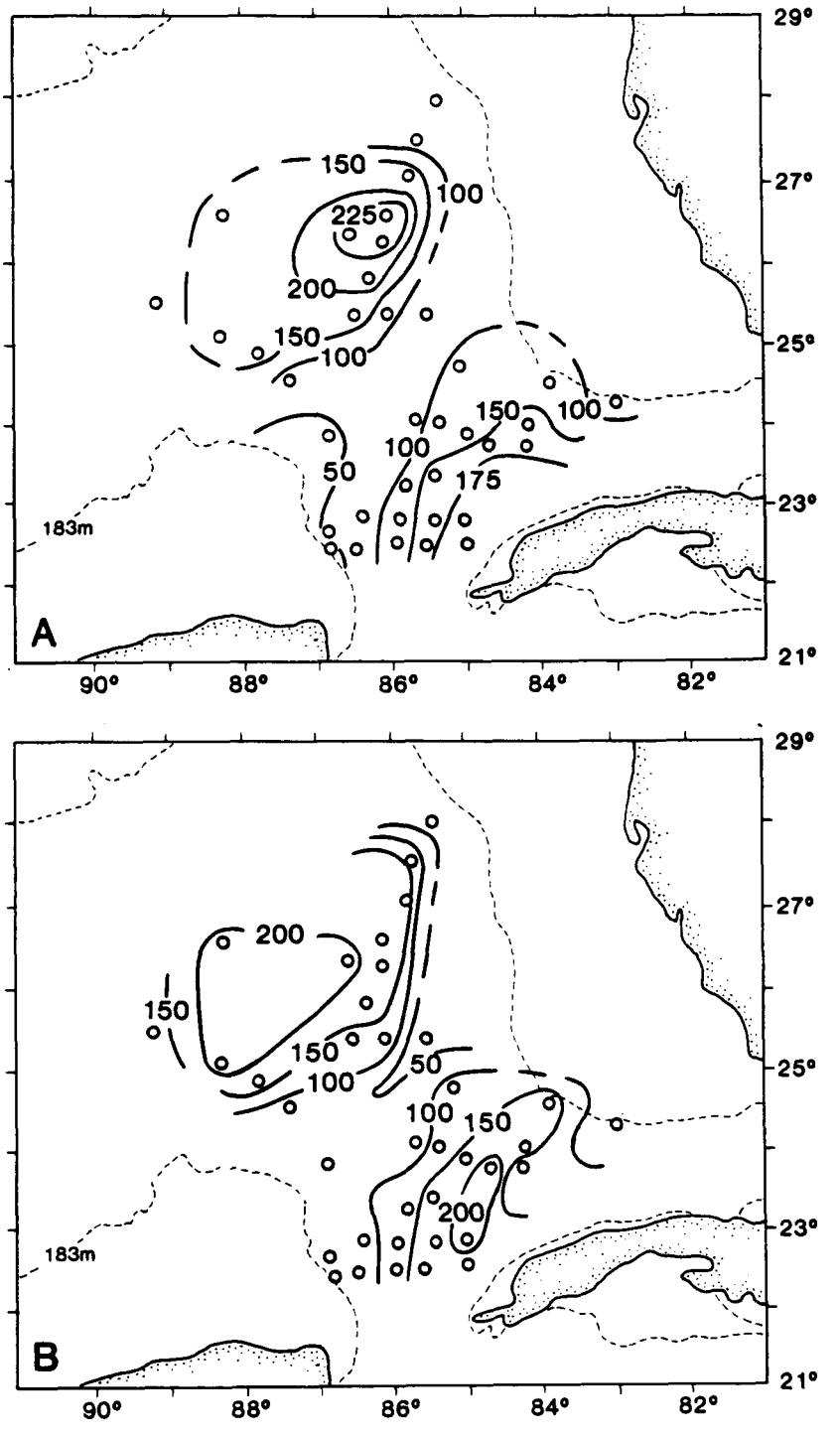


Fig. 15. The depths of A) the 22°C isotherm and B) the 5 μg-at $\ell^{-1}$ isopleth of nitrate within the eastern Gulf of Mexico during May 1972, based on shipboard data.

and $h_m$ of 50 $cm^2$ $sec^{-1}$ and 100 m, i.e. January; 2) a constant $K_o$ and $h_m$ of 25 $cm^2$ $sec^{-1}$ and 25 m, i.e. August; and 3) the monthly variation in both parameters using the values of Table 2. The April and November mixed layer depths and vertical eddy diffusivities are the same (Table 2), for example, such that the observed nitrate fields of early May 1972 (Fig. 15b) and November 1976 (Fig. 12b) reflect absence and presence of the Loop Current in the eastern Gulf of Mexico, rather than seasonal changes in vertical mixing. If the vertical mixing regimes of January or August were operative, however, the biological utilization rates would be different from those under April or November conditions.

3. Physical-biological models

The biological model is initialized using the circulation field on day 10 of the third cycle of Loop Current penetration (Fig. 10), and a May 1 value (Table 2) for daily incident radiation. For the seasonal wind mixing cases, May 1 values were used for the mixed-layer depth and eddy viscosity as well. Day 170 of the coupled physical/biological models thus represents October 8 in terms of daily incident radiation, mixed-layer depth, and eddy viscosity for the two seasonal wind mixing cases (Fig. 16a,b). In the winter and summer cases of constant mixing, however, day 170 instead represents January (16c) and August (16d) mixing regimes, coupled to October light conditions.

Without nutrient input from the Mississippi River, the simulated nitrate on day 170 of the first seasonal case (Fig. 16a) matches the observed nitrate distribution within the Loop Current during November 1976 (Fig. 12b). The

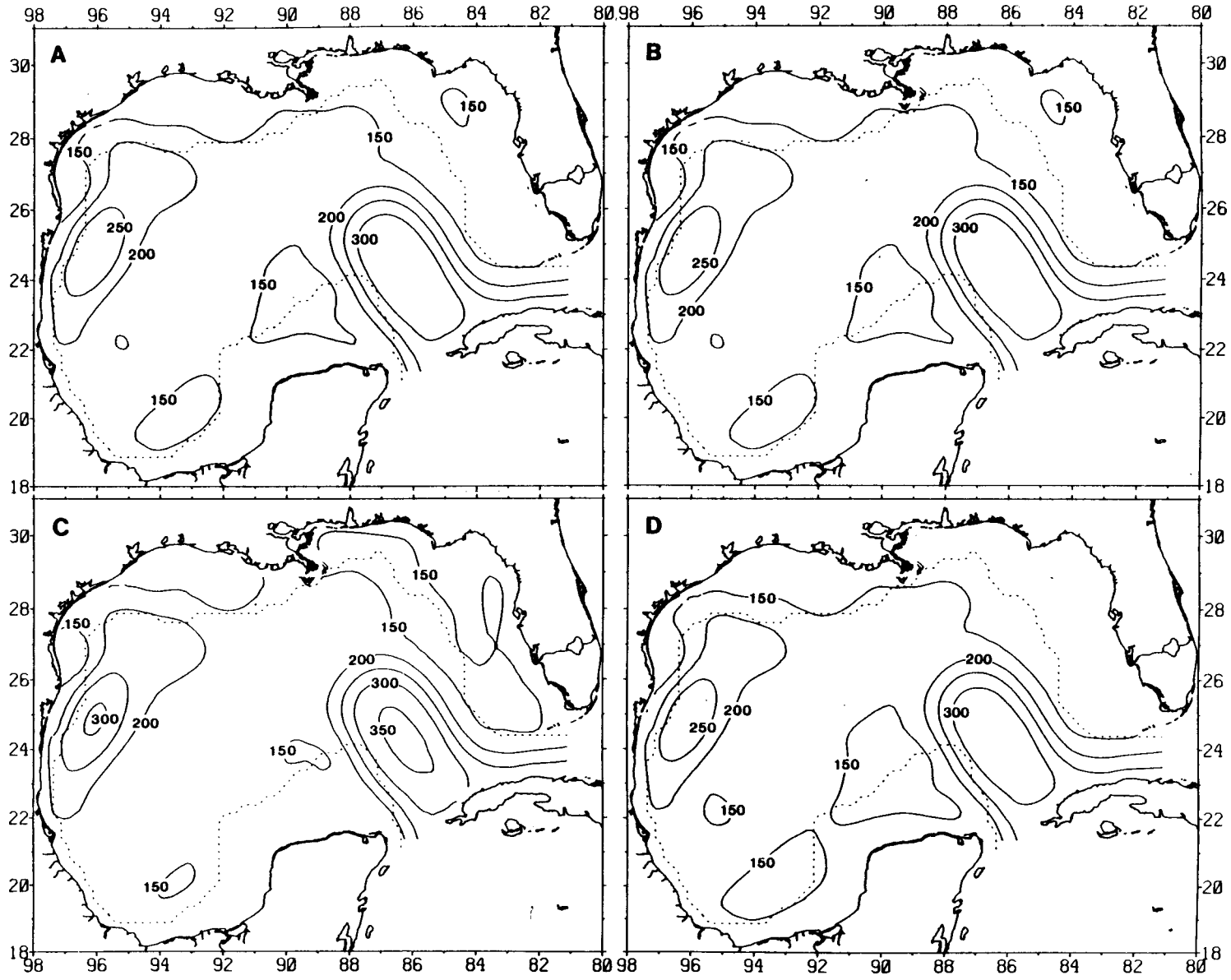


Fig. 16. The depth of the 5 μg-at $\ell^{-1}$ isopleth of nitrate within the Gulf of Mexico on day 170 when the simulated Loop Current is at 27°N, under A) seasonal wind forcing (Table 2), B) seasonal wind forcing and Mississippi River effluent, (C) January mixing and River, D) August mixing and River.

5 μg-at $\ell^{-1}$ isopleth of $NO_3$ is found at >300 m depths within the cores of the simulated (Fig. 16a) and observed (Fig. 12b) Loop Current, but at <150 m depths at the shelf-break off the Yucatan Peninsula and West Florida. Nitrogen from the Mississippi River stimulates phytoplankton growth in the second seasonal case of the model (Fig. 17b), such that little nitrate is found on the Louisiana shelf (Fig. 16b); otherwise the nitrate fields on day 170 of these two seasonal mixing cases are identical (Figs. 16a,b). The contour levels of Figure 17 are 0.05, 0.10, 0.25, 0.50, 1, 2, 3, 4, and 5 μg chl $\ell^{-1}$.

The depth of the surface mixed layer in January is twice that of October (Table 2), however, such that the January mixing case leads to greater nutrient uptake (Fig. 16c) and algal standing stock (Fig. 17c) than the seasonal October cases (Figs. 16 a,b and 17 a,b). The 5 μg-at $\ell^{-1}$ isopleth of the January case on day 170 is found deeper within the Loop Current, within the previously-shed anticyclonic rings off Mexico, and on the West Florida shelf (Fig. 16c), while 2- to 3-fold greater chlorophyll concentrations are simulated at the surface of the model (Fig. 17c).

In contrast, the August depth of the surface mixed layer is half that of October (Table 2), such that the August mixing case leads to smaller nutrient uptake (Fig. 16d) and algal standing stock (Fig. 17d) than the seasonal October cases (Figs. 16 a,b and 17 a,b). The regions of the simulated Gulf of Mexico on day 170, where the depth of the 5 μg-at $\ell^{-1}$ isopleth of nitrate is shallower than 150 m, are more extensive in the August case (Fig. 16d), while half the amount of chlorophyll is found in the Loop Current and its rings

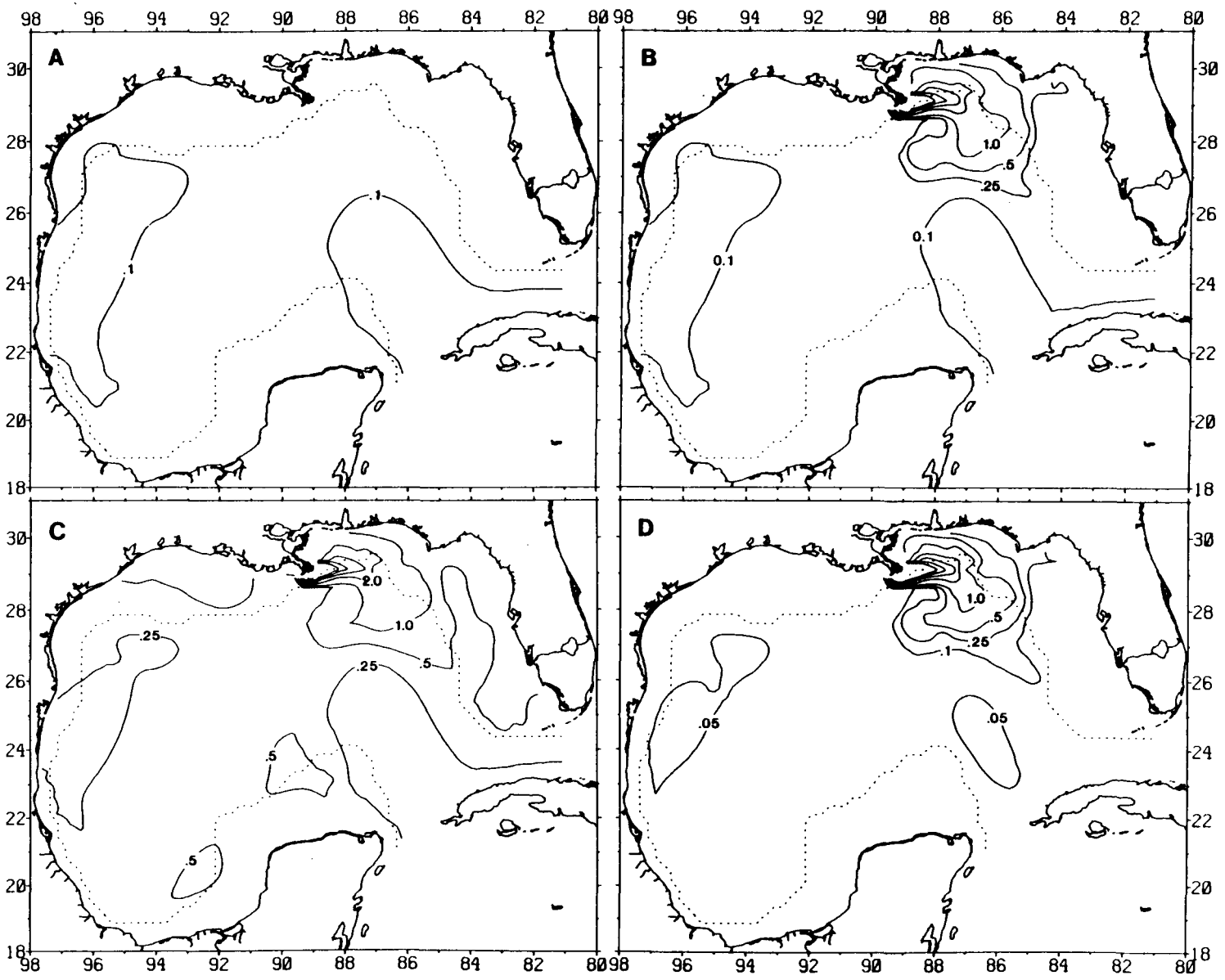


Fig. 17. The distribution of surface chlorophyll within the Gulf of Mexico on day 170 when the simulated Loop Current is at 27°N, under A) seasonal wind forcing (Table 2), B) seasonal wind forcing and Mississippi River effluent, (C) January mixing and River, D) August mixing and River.

(Fig. 17d). The observed distribution of surface chlorophyll in Florida Strait during October-November is ∿0.1 μg chl $\ell^{-1}$ (Fig. 13b), similar to only the seasonal mixing cases (Fig. 17a,b), suggesting that the time-invariant January (Fig. 17c) and August (Fig. 17d) mixing cases are unrealistic.

For example, day 330 in our coupled physical/biological simulation represents March 17, when the depth of the surface mixed layer is 86 m, similar to that in January, but almost 4-fold that of August (Table 2). The simulated nitrate fields of the seasonal wind mixing cases (Fig. 18 a,b) and the January case on day 330 (Fig. 18c) then more closely resemble each other than either the August case (Fig. 18d) or May observations (Fig. 15b), when the mixed layer depth is at 41 m (Table 2). The rest of our discussion is thus restricted to the results of the second seasonal mixing case, i.e., with inclusion of anthropogenic nutrients from the Mississippi River.

Day 90 of the seasonal mixing case with Mississippi River effluent (Fig. 19a) represents July 20, when the depth of the surface mixed layer is the same as in August (Table 2). The surface eddy viscosity of July is larger than August, however, such that the surface chlorophyll within the Loop Current and the western Gulf of Mexico is slightly higher on day 90 of the seasonal case (Fig. 19a), compared to day 170 of the time-invariant August case (Fig. 17d). Although the Loop Current had penetrated ∿150 km north into the Gulf of Mexico at this time (Fig. 11b), the vertical exchange processes were too weak on day 90 to allow a surface signal of enhanced chlorophyll abundance at the cyclonic edges of the western boundary current.

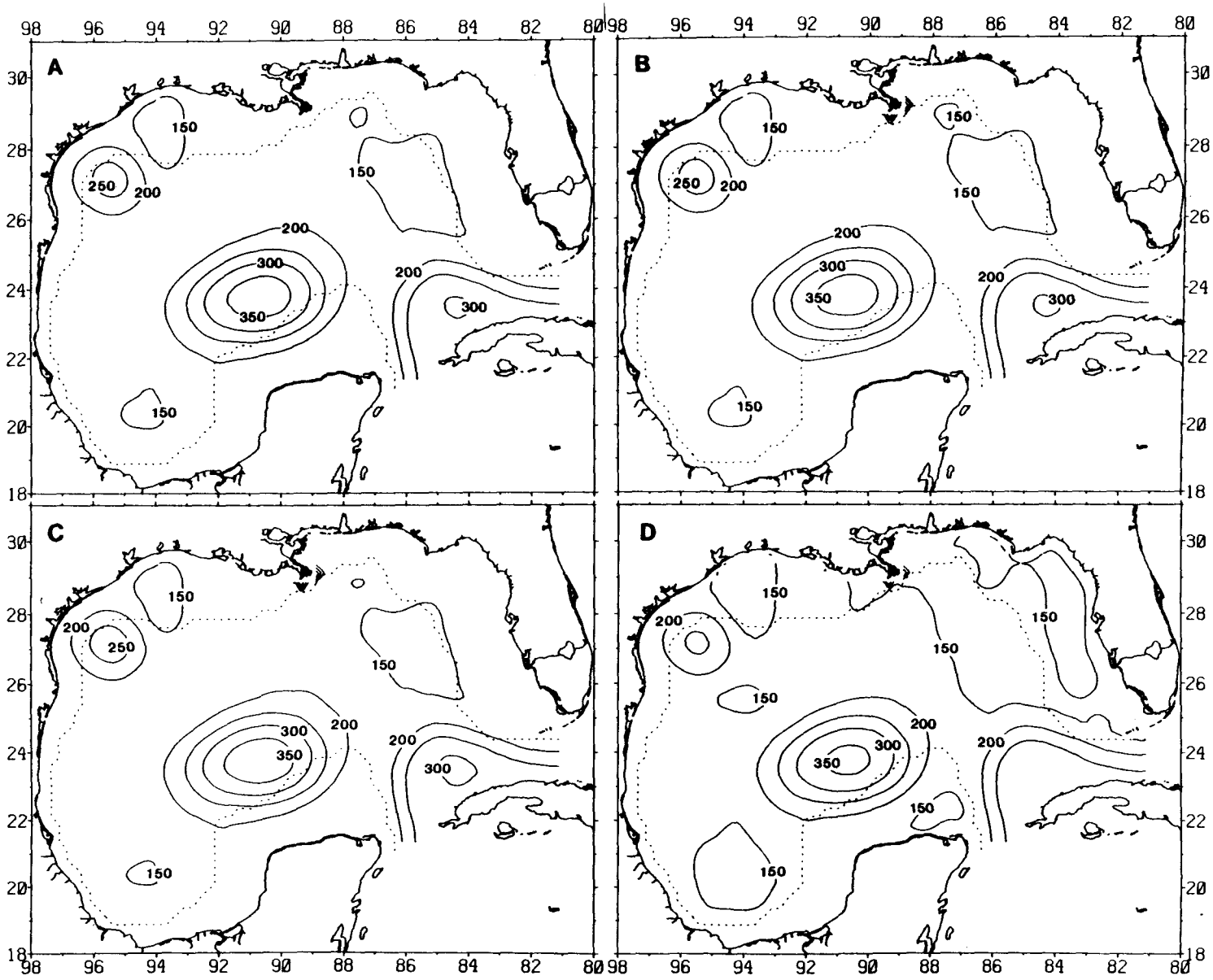


Fig. 18. The depth of the 5 μg-at $\ell^{-1}$ isopleth of nitrate within the Gulf of Mexico on day 330 when the simulated Loop Current is at 25°N, under A) seasonal wind forcing (Table 2), B) seasonal wind forcing and Mississippi River effluent, (C) January mixing and River, D) August mixing and River.

By day 170, i.e., October 8, the Loop Current had reached 27°N (Fig. 11c), the surface mixed layer had deepened twofold (Table 2), and the cyclonic edges of the Loop Current were demarcated by the 0.1 μg chl $\ell^{-1}$ isopleths at the surface in the eastern Gulf of Mexico (Fig. 19b). As a result of strong southeastward flow, e.g. day 170 (Fig. 20b), along the shelf-break, from the mouth of the Mississippi River to off Tampa Bay [in contrast to days 10 (Fig. 10a) and 90 (Fig. 20a)], the 1.0 μg chl $\ell^{-1}$ isopleth of the Mississippi phytoplankton plume had also moved southeast 100 km along the shelf-break between day 90 (Fig. 19a) and day 170 (Fig. 19b). Within the western Gulf, the cyclonic edges of the shed eddy (Fig. 11b, Fig. 20b) were similarly demarcated by the 0.1 μg chl $\ell^{-1}$ isopleth (Fig. 19b).

Over the next 80 days, the depth of the surface mixed layer reached its seasonal maximum, yielding surface concentrations of 0.3-0.4 μg chl $\ell^{-1}$ (Fig. 19c) on day 250, or December 27, at the edge of the calving Loop Current and within the cyclonic circulation cells in the Bay of Campeche and on the west Texas shelf (Figs. 11c, 20c). Continued southeastward flow at the shelf-break below Tampa Bay (Fig. 20c) advected the 1 μg chl $\ell^{-1}$ isopleth associated with the Mississippi River plume, another 100 km to the southeast between day 170 (Fig. 19b) and day 250 (Fig. 19c). Boluses of fresh water (Atkinson and Wallace, 1975), escaped buoys (Schroeder et al., 1987), red-tide trajectories (Murphy et al., 1975), and CZCS imagery (Trees, 1985) all support this simulated southeastward export of surface waters along the west Florida shelf-break.

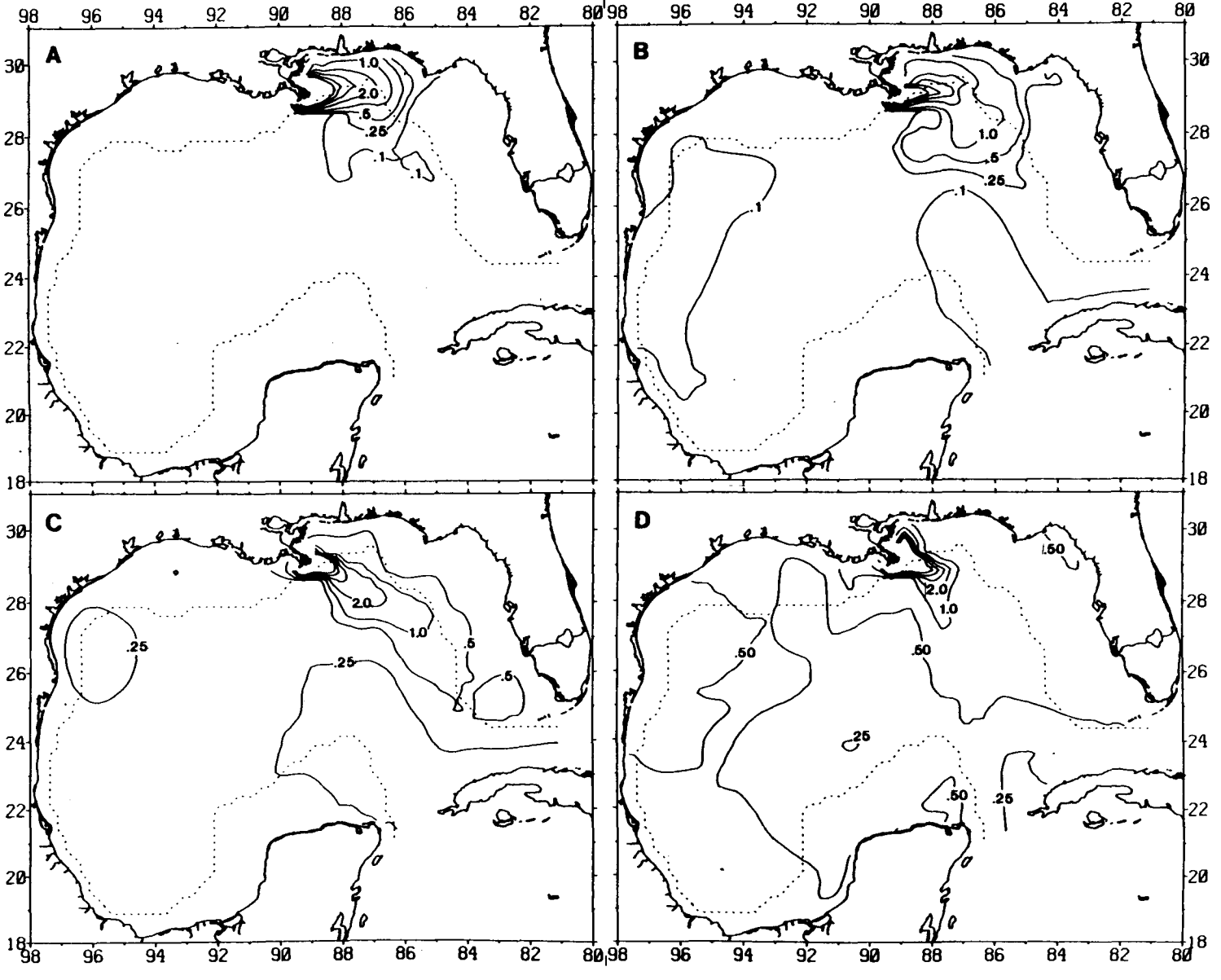


Fig. 19. Annual variation of surface chlorophyll within the Gulf of Mexico under seasonal wind forcing (Table 2) and Mississippi River effluent on days A) 90, B) 170, C) 250 and D) 330 during a penetration cycle of the Loop Current.

By day 330, or March 17, an anticyclonic eddy of the Loop Current had shed and offshore flows prevailed west of Tampa Bay (Figs. 11d, 20d). As a consequence, the 1 μg chl $\ell^{-1}$ isopleth retreated ∿250 km to the northwest (Fig. 19d), suggesting a seasonal modulation of estuarine export from the Gulf of Mexico. Continued deep mixing within the surface layer (Table 2) led to lower nutrient (18b, 21a) and higher chlorophyll (19d) concentrations of 0.4-0.5 μg chl $\ell^{-1}$ on day 330 at the cyclonic edges of the shriveled Loop Current and recently-shed eddy. This surface signature of the combination of wind mixing and upwelling is reflected at depth in the model as well, with 0.5 μg chl $\ell^{-1}$ found near 150 m within the central part of the Gulf of Mexico for days 315-330 (Fig. 22a).

More detailed time series of nitrate (Fig. 21) and chlorophyll (Fig. 22) over the upper 20 layers of the coupled physical/biological models are shown for 4 representative areas (Table 3) of the central Gulf of Mexico and the shelf-break off west Florida, Louisiana, and Texas (Locations A, B, C, and D of Fig. 8). The central Gulf time series at 25°53'N, 89°53'W, for example, shows little impact of the Loop Current until day 225 (Fig. 21a). With westward movement of the Current between days 170 (Fig. 11b) and 250 (Fig. 11c), the depth of the 2 μg-at $\ell^{-1}$ isopleth of nitrate (Fig. 21a) dropped below 150 m on day 225, while the interface depth (shown as a dashed line in Figs. 21 and 22) was then >200 m. Separation of the anticyclonic eddy and its southwestward movement by day 330 (Fig. 11d) resulted in shoaling of the depths of both the 2 μg-at $NO_3$ $\ell^{-1}$ isopleth and the interface as early as day 295 (Figs. 21a, 22a).

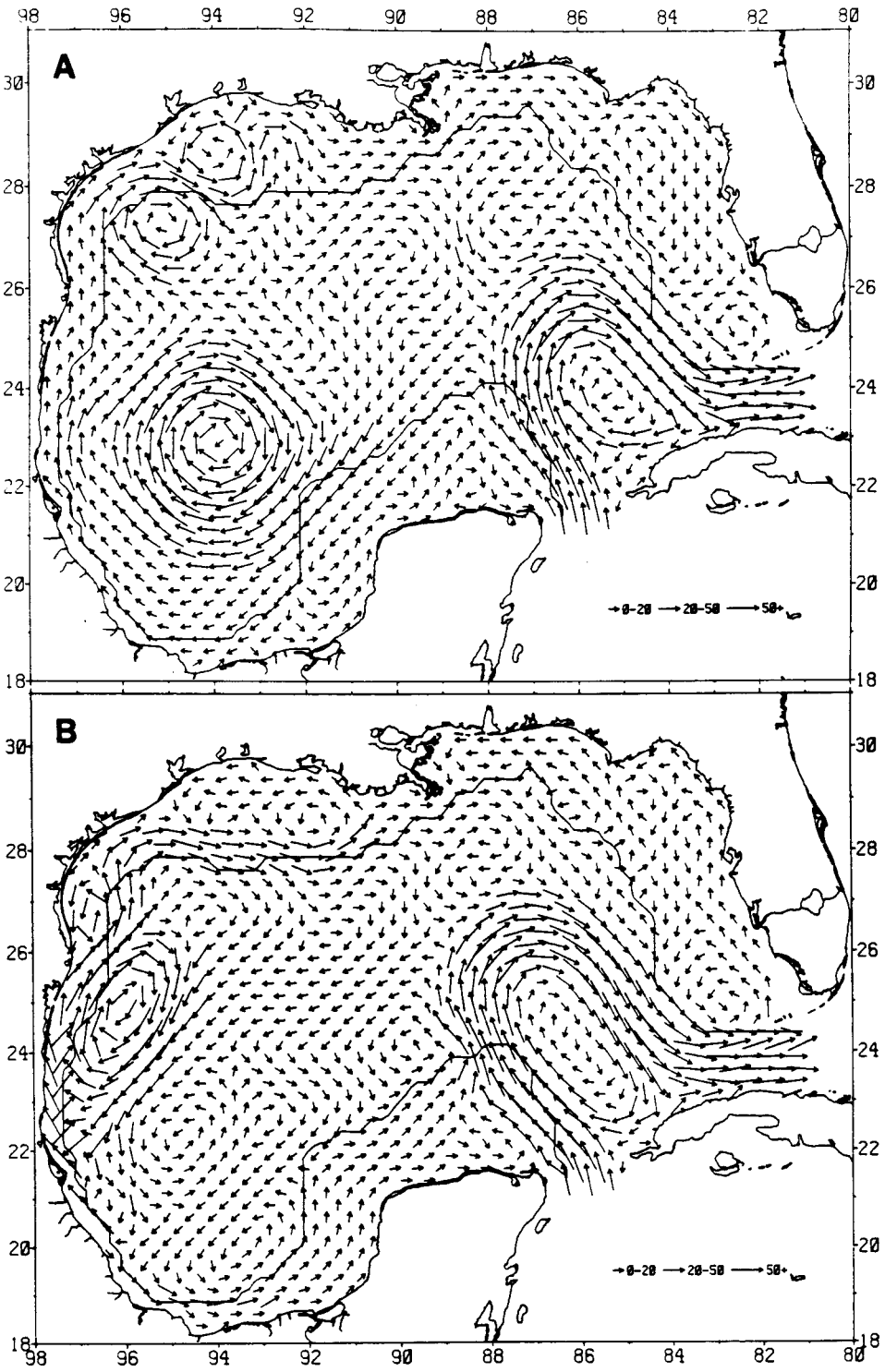


Fig. 20. Annual variation of currents within the surface layer of the circulation model on days A) 90, B) 170, C) 250, and D) 330 during a penetration cycle of the Loop Current.

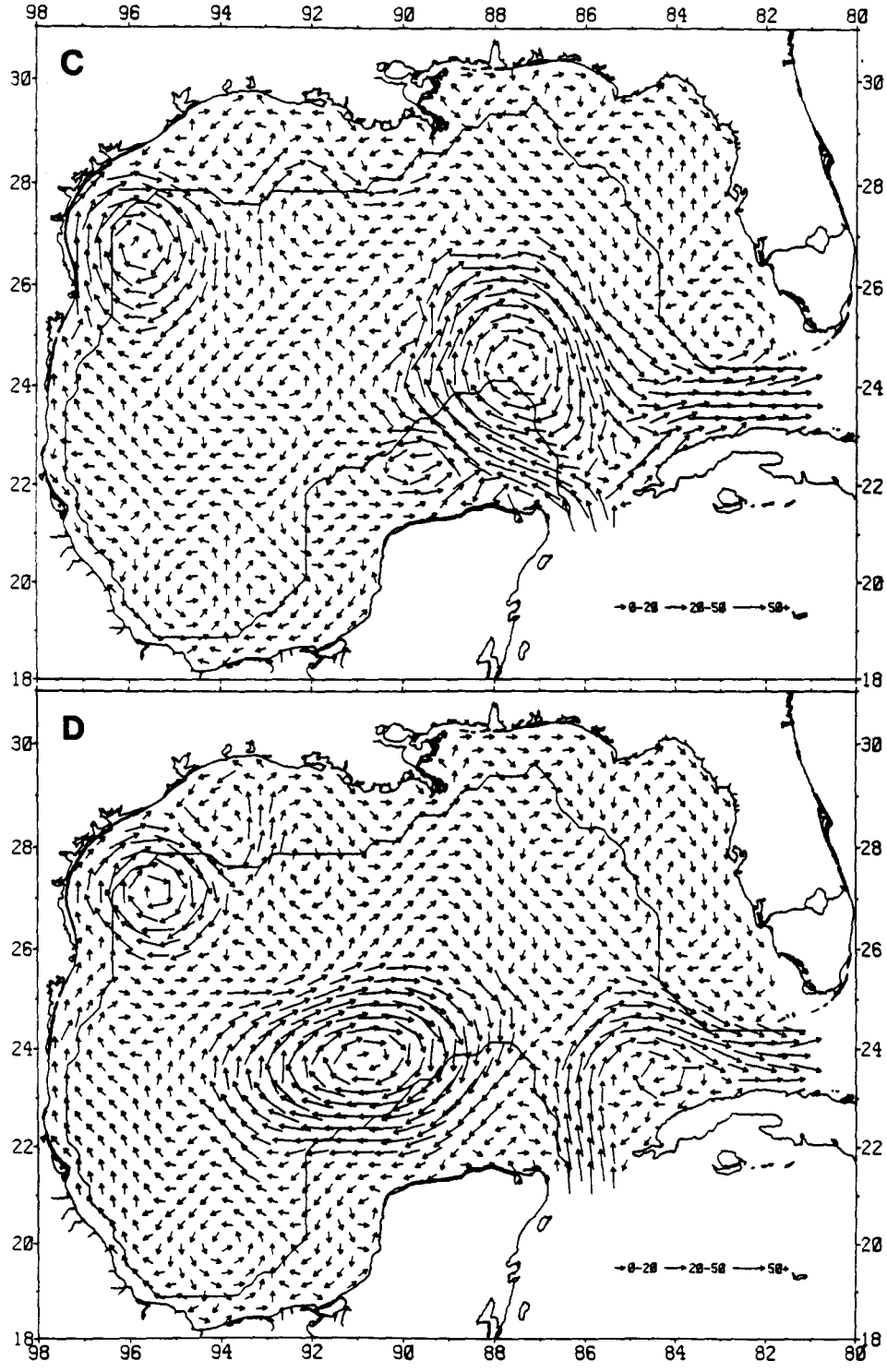


Fig. 20. Annual variation of currents within the surface layer of the circulation model on days A) 90, B) 170, C) 250, and D) 330 during a penetration cycle of the Loop Current.

The highest concentrations of chlorophyll in the central Gulf were simulated during the presence of the Loop Current (Fig. 22a), however. These results imply that the depth of the surface mixed layer (Table 2) was more important than a 45-day downwelling episode of less nutrient availability within the core of the Loop Current. In this region of the Gulf, the annual nitrate input of 132.6 mg-at $m^{-2}$ $yr^{-1}$ and a remineralization of 56.7 mg-at $m^{-2}$ $yr^{-1}$ produced a mean standing crop of 52.1 mg chl $m^{-2}$ over an average upper layer of 174 m extent, containing a 1% light depth of 81.7 m, a "new" primary production of 19.1 g C $m^{-2}$ $yr^{-1}$ (assuming a C/chl ratio of 50/1), and an export at the interface depth of 257.9 mg chl $m^{-2}$ $yr^{-1}$ after partial decomposition of the sinking phytodetritus (Table 3).

Farther to the east at 25°8'N, 84°8'W above the Florida shelf-break (Fig. 8), only the cyclonic impact of the simulated Loop Current was observed (Fig. 21b). The depth of the 2 μg-at $\ell^{-1}$ isopleth of nitrate was always <150 m, shoaling to 125 m between days 165 and 235, while the interface depth remained above 200 m throughout the year (Fig. 22b). A nitrate input of 159.5 mg-at $m^{-2}$ $yr^{-1}$ (Table 3), somewhat larger than that derived from the case of a constant interface depth of 200 m (Fig. 14a), should have led to a mean chlorophyll content of 51.6 mg chl $m^{-2}$ and a "new" primary production of 26.6 g C $m^{-2}$ $yr^{-1}$ (Case A of Table 3).

Instead, chlorophyll abundances of 122 mg chl $m^{-2}$ were found within the 174 m upper layer above the southwest Florida shelf-break on days 280 and 315 (Fig. 22b), after the maximum southward excursion of the Mississippi River-derived plume on day 260 (Fig. 19c). About 700 km southeast of the

Table 3. Annual nitrate fluxes, mean chlorophyll content, "new" primary production, remineralization, and sinking losses within 4 regions of the Gulf of Mexico under A) seasonal wind mixing and no Mississippi discharge (M), compared to Mississippi discharge with B) seasonal, C) winter and D) summer vertical mixing regimes.

| | Central Gulf 25°53'N, 89°53'W | West Florida 25°8'N, 84°8'W | Louisiana 29°8'N, 88°23'W | Texas 27°38'N, 95°38'W |
|---|---|---|---|---|
| Nitrate input to upper layer ($mg\text{-}at\ m^{-2}\ yr^{-1}$) | | | | |
| A. Seasonal | 132.6 | 160.8 | 188.4 | 119.3 |
| B. Seasonal + M | 132.6 | 159.5 | 176.9 | 119.3 |
| C. Winter + M | 195.2 | 242.0 | 289.0 | 175.9 |
| D. Summer + M | 99.8 | 115.0 | 124.8 | 90.8 |
| Chlorophyll content of upper layer ($mg\ m^{-2}$) | | | | |
| A. Seasonal | 51.5 | 51.6 | 53.8 | 55.5 |
| B. Seasonal + M | 52.1 | 58.8 | 479.9 | 55.5 |
| C. Winter + M | 69.7 | 78.3 | 477.8 | 73.3 |
| D. Summer + M | 26.5 | 31.5 | 482.8 | 26.3 |
| Primary production of upper layer ($g\ C\ m^{-2}\ yr^{-1}$) | | | | |
| A. Seasonal | 19.0 | 26.6 | 26.2 | 15.6 |
| B. Seasonal + M | 19.1 | 27.7 | 332.4 | 15.6 |
| C. Winter + M | 24.7 | 36.1 | 318.1 | 21.2 |
| D. Summer + M | 11.3 | 16.1 | 284.6 | 8.8 |
| Particle export of upper layer ($mg\ chl\ m^{-2}\ yr^{-1}$) | | | | |
| A. Seasonal | 254.2 | 294.8 | 363.0 | 247.2 |
| B. Seasonal + M | 257.9 | 350.7 | 1497.0 | 247.4 |
| C. Winter + M | 352.9 | 453.8 | 1827.7 | 337.7 |
| D. Summer + M | 174.5 | 249.6 | 1103.0 | 157.5 |
| Particle export of lower layer ($mg\ chl\ m^{-2}\ yr^{-1}$) | | | | |
| A. Seasonal | 27.5 | 158.8 | 190.9 | 141.8 |
| B. Seasonal + M | 28.0 | 185.7 | 723.7 | 141.8 |
| C. Winter + M | 44.9 | 267.2 | 955.3 | 214.7 |
| D. Summer + M | 22.7 | 144.6 | 545.6 | 100.5 |
| Remineralization of upper layer ($mg\text{-}at\ m^{-2}\ yr^{-1}$) | | | | |
| A. Seasonal | 56.2 | 56.3 | 58.6 | 60.5 |
| B. Seasonal + M | 56.7 | 64.1 | 522.4 | 60.5 |
| C. Winter + M | 76.0 | 85.3 | 520.2 | 79.9 |
| D. Summer + M | 28.9 | 34.4 | 525.7 | 28.7 |

mouth of the Mississippi River at 25°8'N, 84°8'W, the mean algal standing crop was 58.8 mg chl $m^{-2}$, with an associated "new" primary production of 27.7 g C $m^{-2}$ $yr^{-1}$ and an export of 350.7 mg chl $m^{-2}$ $yr^{-1}$ (Case B of Table 3). At 29°8'N, 88°23'W on the southeast Louisiana slope within 50 km of the mouth of the Mississippi River (Fig. 8), and thus much closer to this estuarine source of nutrients (Fig. 21c), the phytoplankton biomass accordingly increases tenfold (Fig. 22c). Note that the contour interval is 1.0 μg chl $\ell^{-1}$ in Figure 22c and 0.1 μg chl $\ell^{-1}$ in Figures 22a,b and 22d.

Upwelling at the Louisiana shelf-break (Fig. 11) would input 188.4 mg-at $NO_3$ $m^{-2}$ $yr^{-1}$ in the absence of river discharge (Case A of Table 3). The interface depth remains at 159 m, but in sharp contrast to the southwest Florida slope (Fig. 21b), about 1 μg-at $NO_3$ $\ell^{-1}$ is at times left above the 1% light depth of 19 m near the mouth of the Mississippi River (Fig. 21c). The combined anthropogenic and natural nutrient input yields a mean chlorophyll content of 479.9 mg chl $m^{-2}$, with an associated "new" primary production of 332.4 g C $m^{-2}$ $yr^{-1}$ and an export at the interface of 1497 mg chl $m^{-2}$ $yr^{-1}$ (Table 3). As a result of remineralization of plankton grown on anthropogenic nitrogen sources in the upper layer, more nitrate is added to the upper layer from nitrification (522.4 mg-at $NO_3$ $m^{-2}$ $yr^{-1}$) than from upwelling (176.9 mg-at $NO_3$ $m^{-2}$ $yr^{-1}$). Assuming a maximum f ratio of 0.83, a total production of 400.5 g C $m^{-2}$ $yr^{-1}$ is inferred.

At 2 stations near the 420-m isobath of the southwest Louisiana slope (Location F of Fig. 8), i.e., outside of the Mississippi River plume (Fig. 19), mean <u>in situ</u> concentrations of nitrate were 0.79 μg-at $NO_3$ $\ell^{-1}$ and

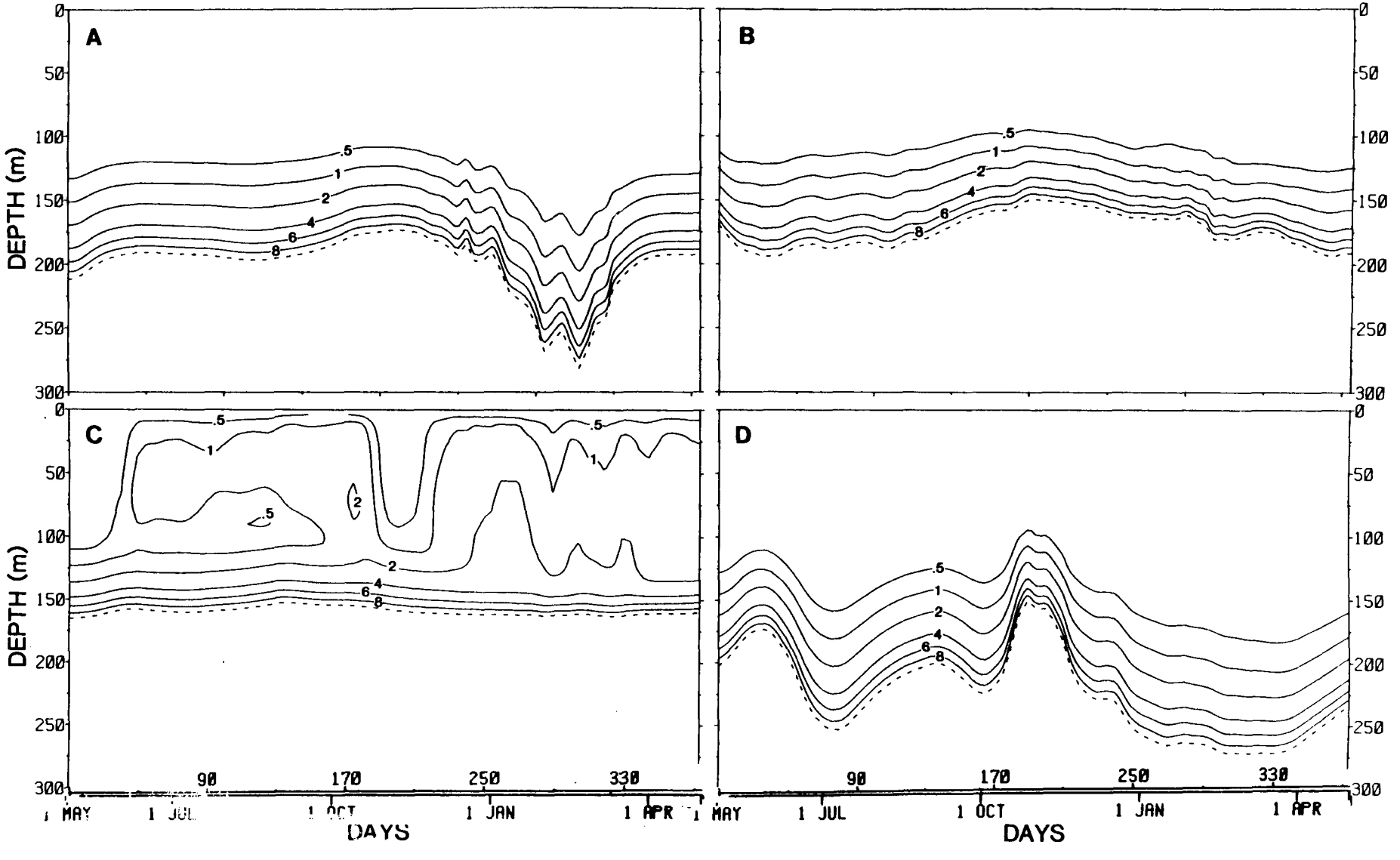


Fig. 21. Annual variation of nitrate under seasonal wind forcing (Table 2) and Mississippi River effluent in A) the central Gulf of Mexico, and at the edge of B) the west Florida, C) the Louisiana, and D) the Texas shelves.

of chlorophyll were 0.74 μg chl $\ell^{-1}$ over the upper 100 m of the 8-9 December 1982 water column (M. Dagg, personal communication). With southward movement of the algal plume on the southeast Louisiana slope on day 170 (Figs. 19b, 20b), the simulated nitrate (Fig. 21c) and chlorophyll (Fig. 22c) concentrations at 29°8'N, 88°23'W during days 180-230, i.e., October 18 to December 7, matched the observations at 28°33'N, 89°53'W (Dagg et al., 1987). Similarly over an annual cycle, observed total primary production of 250-350 g C $m^{-2}$ $yr^{-1}$ within 50 km of the Mississippi River (Thomas and Simmons, 1960; Fucik, 1974) suggest that our coupled models accurately depict some of the consequences of eutrophication in the northern Gulf of Mexico.

Farther to the west at 27°38'N, 95°38'W on the Texas shelf-break, the depth of the interface remains below 200 m for 125 days (Fig. 21d), as a result of downwelling within anticyclonic eddies, shed by the Loop Current. Consequently, the annual nutrient input of 119.3 mg-at $NO_3$ $m^{-2}$ $yr^{-1}$ allows a mean algal biomass of only 55.5 mg $m^{-2}$, with annual "new" production of 15.6 g C $m^{-2}$ $yr^{-1}$ and export of 247.4 mg chl $m^{-2}$ $yr^{-1}$ (Table 3). On days 35 and 205, chlorophyll stocks increase to 0.25 mg chl $m^{-3}$ (Fig. 22d) in response to upwelling at the edge of the eddies (Figs. 11, 20), but the seasonal mixing signal dominates the annual cycle beyond day 230 in this region of the Gulf of Mexico. Like the central part of the Gulf, the computed export at the interface depth here is the smallest on the continental margin of the basin (Figs. 23a,c).

In the absence of Mississippi River discharge, the largest input of organic matter to the sediments occurs off Tampa Bay at the west Florida

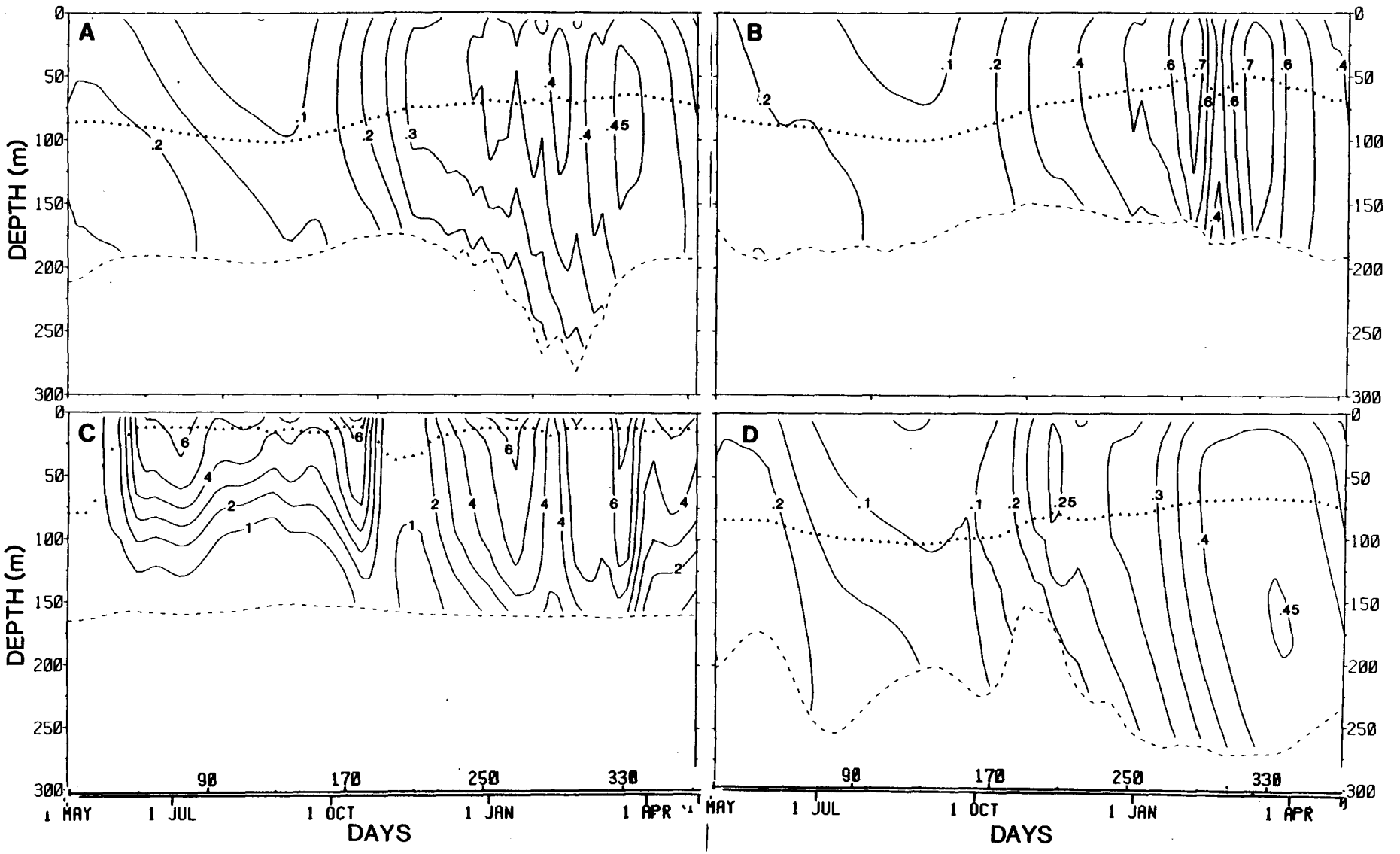


Fig. 22. Annual variation of subsurface chlorophyll under seasonal wind forcing (Table 2) and Mississippi River effluent in A) the central Gulf of Mexico, and at the edge of B) the west Florida, C) the Louisiana, and D) the Texas shelves.

shelf-break. A flux of 0.40 g chl $m^{-2}$ $yr^{-1}$ occurs at the interface depth (Fig. 23a) and 0.1 g chl $m^{-2}$ $yr^{-1}$ arrives at the slope bottom (Fig. 23c). Advection of organic matter to the southeast from the Louisiana shelf leads to a doubling of the detrital loading in this depocenter, i.e., 0.8 g chl $m^{-2}$ $yr^{-1}$ at the interface and 0.2 g chl $m^{-2}$ $yr^{-1}$ at the bottom (Figs. 23b,d). Assuming again a C/chl ratio of 50/1-100/1 for phytodetritus (Steele, 1964), the full range of carbon input from the water column west of Tampa Bay becomes 20-80 g C $m^{-2}$ $yr^{-1}$ at the interface depth and 5-20 g C $m^{-2}$ $yr^{-1}$ at the slope bottom.

In contrast, our previous range of estimates of carbon accumulation within the Gulf of Mexico sediments (Fig. 7) from eq. (1) was 0.4-7.8 g C $m^{-2}$ $yr^{-1}$. Since our minimum bottom depth (D) in the model, was 500 m, the changing depths of the interface from 160 m to 280 m (Figs. 21, 22) more realistically represent the bottom topography of the outer shelf, where the >1.0% dw carbon deposits are found (Fig. 7). A depth-weighted composite of Figures 23a and 23c, or Figures 23b and 23d, may then be a more reasonable estimate of carbon input to the bottom. At a depth range of 160-280 m, for example, an input of 20-80 g C $m^{-2}$ $yr^{-1}$ to the bottom, together with a survival rate of 10% for phytodetritus within the outer shelf benthic community (Walsh et al., 1988b), yields a maximum accumulation rate of 8 g C $m^{-2}$ $yr^{-1}$. This estimate coincides with our previous calculation of 7.8 g C $m^{-2}$ $yr^{-1}$ for the 1.5% dw carbon sediments.

Within deeper regions, at bottom depths of 1600-2800 m, where >0.5% carbon deposits are found (Fig. 7), an input of 5-20 g C $m^{-2}$ $yr^{-1}$ and a 10%

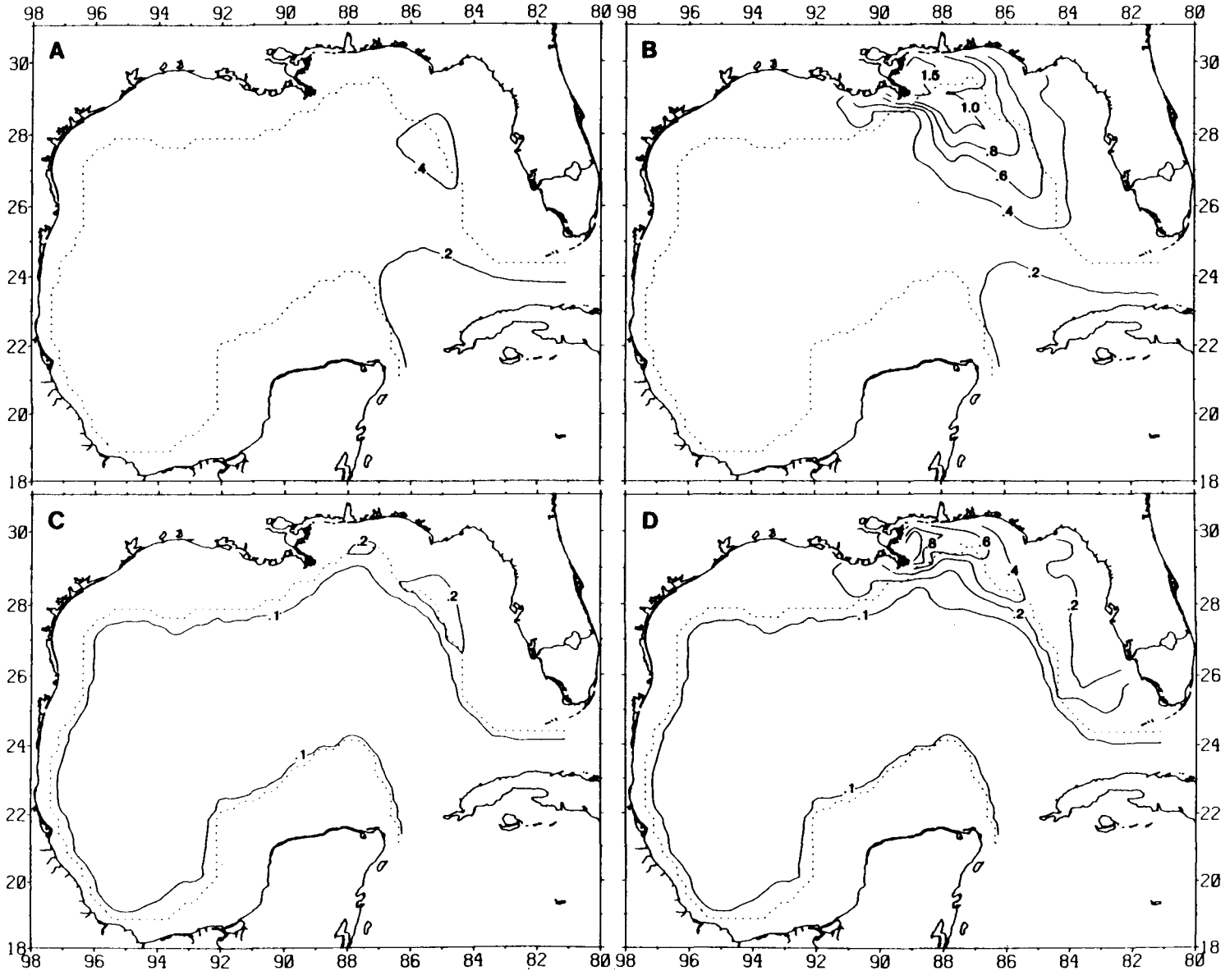


Fig. 23. Annual input of chlorophyll to the surficial sediments of the Gulf of Mexico from the upper (A,B) and lower (C,D) layers of the circulation model, with nutrient loading from oceanic (A,C) and additional terrestrial (B,D) sources.

survival rate on the bottom implies a minimum accumulation rate of 0.5 g C $m^{-2}$ $yr^{-1}$. This agrees with our previous calculation of 0.4 g C $m^{-2}$ $yr^{-1}$ for 0.75% dw carbon sediments, where lower sedimentation rates were assumed. Higher sinking rates of 30-300 m $day^{-1}$, resulting from seasonal aggregation processes, instead of 3 m $day^{-1}$ used in the model, could yield a larger input of carbon to the continental margins of the Gulf of Mexico, if these settling velocities prevailed throughout the year.

## Conclusions

Seasonal succession of phytoplankton species and possible aggregation processes, leading to the rapid sinking of diatoms (Lampitt, 1985) and picoplankton (Lochte and Turley, 1988), are beyond the scope of our present physical and biological models of the Gulf of Mexico. Without a realistic depiction of mesoscale plankton dynamics at the species level, we may thus have underestimated the nitrogen burial and evasion losses in the Gulf. Furthermore, if wind-induced upwelling contributes additional supplies of "new" nitrogen, beyond that parameterized by Loop Current-induced upwelling, we may have underestimated the "new" production and again the sinking losses out of the water column.

Oceanic forcing, in the form of a western boundary current, has been a major focus of this study. This forcing may be responsible for some of the longshore currents on the outer West Florida shelf (Sturges and Evans, 1983). Local wind forcing is highly coherent with flows over bottom depths <45 m on the West Florida (Mitchum and Sturges, 1982) and Texas-Louisiana (Cochrane and

Kelly, 1986) shelves, however, and may lead to local regions of intensified upwelling in the Gulf of Mexico (Wallcraft, 1986). Although we used seasonal changes of wind stress to calculate both the depth of the surface mixed layer and the vertical eddy viscosity (Table 2) of the biological model, the circulation model was, of course, unable to replicate either the wind-induced upwelling, or the westward advection of Mississippi and Atchafalaya River effluent (Cochrane and Kelly, 1986; Dinnel and Wiseman, 1986).

Coupling of a local shelf model, with increased vertical resolution of the circulation, description of the wind response, and inclusion of phytoplankton species succession, to our present basin-scale calculations is the goal of our future research. We do not expect burial of organic matter in shallow shelf waters (<50 m) to have an important impact, however, on our conclusions from a nitrogen budget for the larger Gulf of Mexico. An underestimate of the burial loss would again be the consequence of poorly resolved coastal regions. The nitrogen budget of Table 4 attempts to address these deficiencies by consideration of various scenarios of increased burial rather than remineralization losses.

The simulated fluxes of nitrate in through Yucatan Strait and out via Florida Strait (Fig. 24) have a weak time dependency related to the penetration cycle of the Loop Current. On day 170, when the Loop Current has reached 27°N (Fig. 16b), the depth of the interface on the cyclonic side of the Current is $\sim$10 m deeper in Yucatan Strait (Fig. 24a) and $\sim$5 m deeper in Florida Strait (Fig. 24b) than on day 330 (Figs. 24c,d). More upwelling occurs within these Straits on day 330, when the Loop Current retreated to

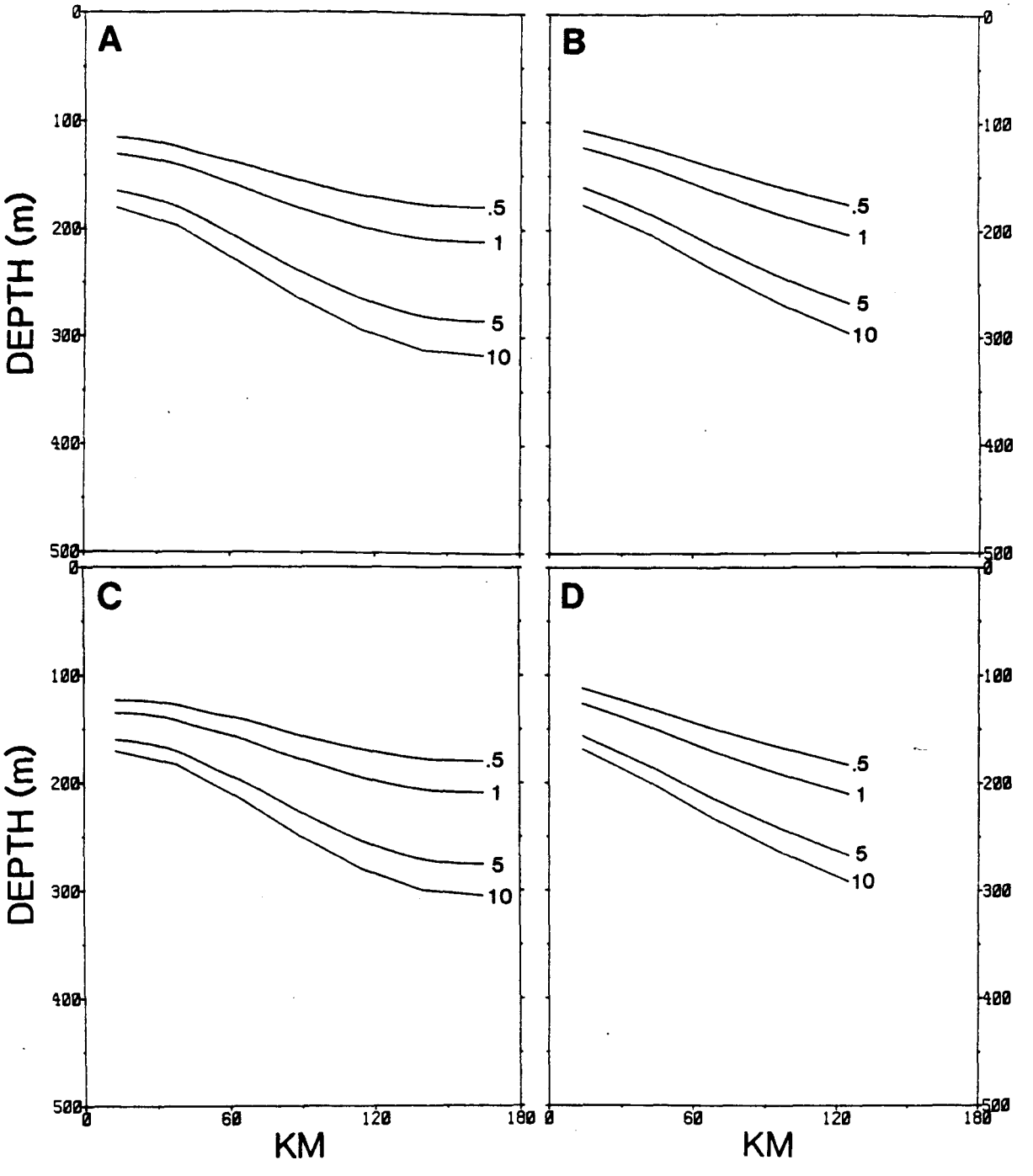


Fig. 24. The simulated distribution of nitrate across Yucatan Strait (A,C) and Florida (B,D) Strait on days 170 and 330 under seasonal wind forcing and Mississippi River effluent.

25°N (Fig. 18b), similar to nitrate sections in January 1952 (Fig. 2) and October 1977 (Fig. 3) rather than during November 1976 (Fig. 4).

As a result of less biological utilization, however, the 0.5 μg-at $\ell^{-1}$ isopleth of nitrate is ∿5 m higher in the water column on day 170 than 330 within both Yucatan and Florida Straits (Fig. 24), such that the flux differences are minimal. During deep penetration of the Loop Current, the influx of nitrate in the upper layer across Yucatan Strait was actually 373.8 kg $NO_3$-N $sec^{-1}$ on day 170, compared to 372.1 kg $NO_3$-N $sec^{-1}$ on day 330. Similarly, the efflux of nitrate across Florida Strait was 365.7 kg $NO_3$-N $sec^{-1}$ on day 170, instead of 363.2 kg $NO_3$-N $sec^{-1}$ on day 330.

On both days, more dissolved nitrogen entered the Gulf of Mexico in the upper layer across Yucatan Strait than departed via Florida Strait (Fig. 24). On an annual basis, 1.16 x $10^{10}$ kg $NO_3$-N, or 368.7 kg $NO_3$-N $sec^{-1}$, entered Yucatan Strait above a mean interface depth of 248.1 m. Continued upwelling led to a mean interface depth of 236.1 m within Florida Strait, but an efflux of only 1.13 x $10^{10}$ kg $NO_3$-N $yr^{-1}$, or 359.2 kg $NO_3$-N $sec^{-1}$, occurred (Table 4). A comparable average of January 1952 and October 1977 observations for the 0-10 μg-at $NO_3$ $\ell^{-1}$ layers is 440 kg $NO_3$-N $sec^{-1}$ within Yucatan Strait and 435 kg $NO_3$-N $sec^{-1}$ within Florida Strait (Table 1). Addition of the particulate nitrogen influx through Yucatan Strait in the form of chlorophyll (0.09 x $10^{10}$ kg chl-N $yr^{-1}$) and its outflux through Florida Strait (0.12 x $10^{10}$ kg chl-N $yr^{-1}$) to the annual nitrogen budget of Table 4 yields a balanced total of ∿1.25 x $10^{10}$ kg N $yr^{-1}$.

Table 4. Annual nitrogen budget of surface waters of the Gulf of Mexico.

Eutrophication case

| Nitrogen sources ($\times 10^{10}$ kg N $yr^{-1}$) | | Nitrogen sinks ($\times 10^{10}$ kg N $yr^{-1}$) | |
|---|---|---|---|
| Yucatan dissolved | 1.16 | Florida dissolved | 1.13 |
| Yucatan particulate | 0.09 | Florida particulate | 0.12 |
| Mississippi effluent | 0.12 | Sinking detritus after remineralization | 0.45 |
| Upwelling/diffusive | 0.32 | Total | 1.70 |
| | 1.69 | | |

Natural case

| Nitrogen sources ($\times 10^{10}$ kg N $yr^{-1}$) | | Nitrogen sinks ($\times 10^{10}$ kg N $yr^{-1}$) | |
|---|---|---|---|
| Yucatan dissolved | 1.16 | Florida dissolved | 1.13 |
| Yucatan particulate | 0.09 | Florida particulate | 0.11 |
| Upwelling/diffusive | 0.32 | Sinking detritus | 0.37 |
| Total | 1.57 | Total | 1.61 |

After one year of simulated time, the model solutions are not quite those at equilibrium, such that in the natural case of Table 4, the detrital loss of particulate nitrogen is somewhat larger (3%) than the upwelled/diffusive input of nitrate. The $0.05 \times 10^{10}$ kg chl-N $yr^{-1}$ additional sink of particulate nitrogen is derived from initial nitrate stocks in the water column. Addition of anthropogenic nitrogen to the surface waters of the model allows a faster approach to equilibrium solutions, with only a $0.01 \times 10^{10}$ kg chl-N $yr^{-1}$ discrepancy between supply and loss of nitrogen in surface waters. The additional nitrogen inputs of Mississippi River effluent ($0.12 \times 10^{10}$ kg N $yr^{-1}$) and vertical exchange from the lower layer ($0.32 \times 10^{10}$ kg $NO_3$-N $yr^{-1}$) are now converted into sinking detrital nitrogen ($0.45 \times 10^{10}$ kg chl-N $yr^{-1}$), with only a small export of particulate matter still derived from the initial nitrate stocks.

At the equilibrium state of the eutrophication case, the particulate export will be just maintained by an input of $0.12 \times 10^{10}$ kg $NO_3$-N $yr^{-1}$ from the Mississippi River and of $0.32 \times 10^{10}$ kg $NO_3$-N $yr^{-1}$ from the lower layer of the Loop Current and its anticyclonic rings. In the absence of eutrophication and upwelling at the cyclonic edges of these western boundary currents in the Gulf of Mexico basin, however, only $0.11\text{-}0.21 \times 10^{10}$ kg $NO_3$-N $yr^{-1}$ would have instead entered the upper layers of the coupled models, i.e., with constant interface depths of respectively 400 and 200 m in the biological model (Fig. 14). The "total" nitrogen production and carbon fixation of the Gulf, other than cyanobacteria, would then be a function of the operant f ratio at a particular depth and time.

Assuming a tempo-spatial average f ratio of 0.06 over the mean 1% light depth of 80 m, where the nitrate content was 0.09 μg-at $NO_3$ $\ell^{-1}$ for case A, i.e., seasonal wind mixing and no Mississippi discharge, the total nitrogen uptake would be 5.3 x $10^{10}$ kg N $yr^{-1}$ as a result of Loop Current-induced upwelling. The total uptake would be only 1.8-3.5 x $10^{10}$ kg N $yr^{-1}$ in its absence, i.e., constant interface depths of 400 and 200 m. With a C/N ratio of 6/1, the higher total primary production of 32 x $10^{10}$ kg C $yr^{-1}$, spread over a basin of 1.53 x $10^6$ $km^2$ extent, yields an annual average of 209 g C $m^{-2}$, instead of 72-137 g C $m^{-2}$ $yr^{-1}$ in the absence of upwelling.

Inclusion of either clouds to reduce the incident radiation, or greater sinking rates to reflect aggregates, would have reduced the algal biomass and the amount of "new" production, with an increase of nitrate stocks left behind in the water column. Consequently the f ratio would increase, yielding lower total primary production. Over the 0.1% light depth of 119 m in Case A, for example, the average nitrate content was 0.23 μg-at $NO_3$ $\ell^{-1}$ and the mean f ratio was instead 0.12. An f ratio of 0.12 over the deeper water column would imply a mean annual production of 105 g C $m^{-2}$ $yr^{-1}$ in the absence of Mississippi River effluent.

With few *in situ* estimates of primary production, the validity of the model's results can be tested with preliminary satellite time series (Muller-Karger *et al.*, 1988). In Case A with no Mississippi discharge, the simulated chlorophyll mean over the whole basin of the Gulf of Mexico underestimates the satellite estimate of the same spatial domain, containing eutrophic coastal waters, for most of the time during 1979-82 (Fig. 25a).

This comparison implies an underestimate of the f ratio and total production by the model as well.

In the middle of the western Gulf (Fig. 25c), however, the model overestimates the seasonal maxima of the CZCS pigment concentration by threefold each year -- see Figure 8 for locations of the pigment time series G and H. Within the Loop Current region of the eastern Gulf, greater interannual variability of algal biomass evidently occurs, such that the model exactly reproduced the maximum amount of the seasonal satellite signal in 1981, but not in other years (Fig. 25b). Note that both the satellite data and the model overestimate by threefold (Fig. 25b) the shipboard observations of 0.11-0.13 μg chl $\ell^{-1}$ within surface waters of the Loop Current during early February 1981 (Ortner et al., 1984). However, only the satellite data coincide with shipboard observations of 0.05-0.07 μg chl $\ell^{-1}$ in surface waters of the Loop Current during late February 1980 (El-Sayed and Trees, 1980). The model apparently overestimates by fivefold (Fig. 25b) the observed 1980 chlorophyll biomass in the region of the Loop Current, but only by twofold (Fig. 25c) the 0.2-0.3 μg chl $\ell^{-1}$ measured in the western area during February 1980 (El-Sayed and Trees, 1980).

Pending future resolution of the quality of these data sets, it appears that the model may either equal or overestimate by at least two- to threefold the chlorophyll content and ensuing "new" production in most of the Gulf of Mexico. The total primary production, depending on concomitant changes in f ratios, may thus be as much as 70-210 g C $m^{-2}$ $yr^{-1}$ in the oligotrophic parts of the basin, in contrast to prior estimates of ∿25 g C $m^{-2}$ $yr^{-1}$ (El-Sayed,

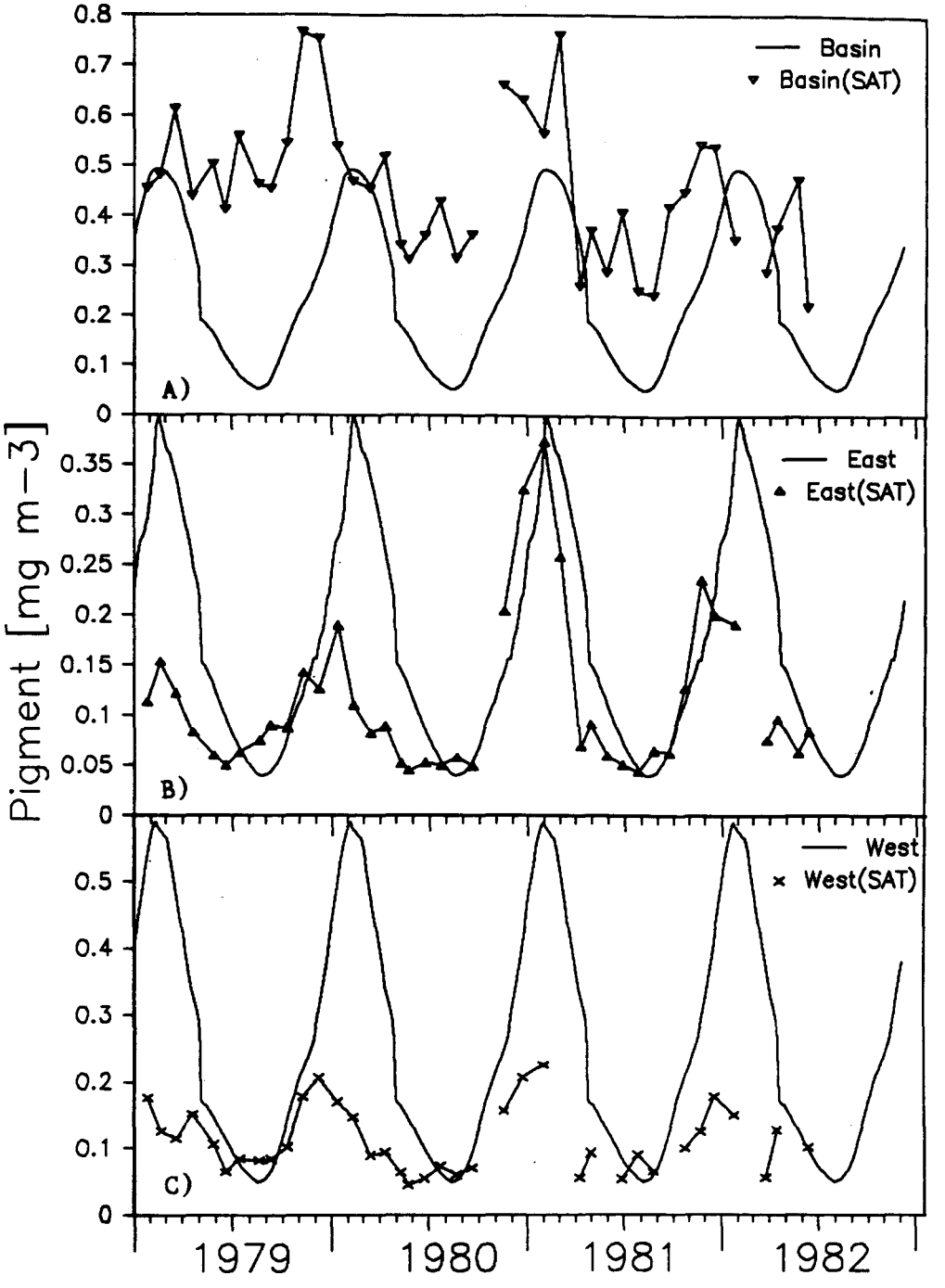


Fig. 25. Annual variation of simulated surface chlorophyll under only seasonal wind forcing, with respect to 1979-82 CZCS estimates of pigment A) over the whole basin, B) within the eastern Gulf of Mexico, and C) within the western Gulf -- see Fig. 8 for locations of the aggregated satellite and model time series.

1972). The mean of the equivalent carbon fixation of the "new" production of Case A (Table 3) at the 4 representative time series (21.9 g C $m^{-2}$ $yr^{-1}$) actually includes some recycled production, since it is based on both upwelled nitrate and local remineralized nitrate.

The remineralization rate of 0.005 $day^{-1}$ in the model results in nitrification values of 0.001 to 0.010 mg-at N $m^{-3}$ $day^{-1}$ over the upper 264 m of the simulated water column (Table 3). They are somewhat lower than those observed (0.016-0.068 mg-at N $m^{-3}$ $day^{-1}$) within eutrophic waters off southern California (Ward et al., 1982) and in the nitrite maximum layer of the equatorial North Pacific (Wada and Hattori, 1972). The model's results are comparable to those computed at 100 m for open waters (0.003-0.023 mg-at N $m^{-3}$ $day^{-1}$) of the North Pacific (Martin et al., 1987), however, suggesting that our estimates of bacterial decomposition of particulate matter in the upper layer are reasonable.

With no further decomposition, 45 x $10^8$ kg chl-N $yr^{-1}$ of detrital nitrogen would arrive on the bottom of the Gulf of Mexico, compared to 6 x $10^8$ kg N $yr^{-1}$ required from our previous estimates of burial and denitrification. Application of the smaller decomposition rate of 0.0025 $day^{-1}$ within the lower layer of the model results in a nitrification of 9 x $10^8$ kg $NO_3$-N $yr^{-1}$ beneath the interface and a particle flux of 15 x $10^8$ kg chl-N $yr^{-1}$ to the bottom sediments.

Increasing the nitrate flux across the interface by 50% to 0.47 x $10^{10}$ kg $NO_3$-N $yr^{-1}$ in the January mixing case, i.e., simulating additional upwelling by local winds, yields sinking fluxes of 58 x $10^8$ kg chl-N $yr^{-1}$ at the

interface and 22 x $10^8$ kg chl-N $yr^{-1}$ at the bottom. Removal of the Mississippi River input from Table 4 results in decreased remineralization rates as well, with sinking fluxes of 37 x $10^8$ kg chl-N $yr^{-1}$ at the interface and 12 x $10^8$ kg chl-N $yr^{-1}$ at the bottom, i.e., similar to the eutrophication case of 15 x $10^8$ kg chl-N $yr^{-1}$ at the sediment interface. In all of these situations, the input of particulate nitrogen to the sea floor (12-22 x $10^8$ kg chl-N $yr^{-1}$) exceeds the estimated burial flux of 3.5 x $10^8$ kg N $yr^{-1}$, allowing loss of nitrogen as both $N_2$ and reduced nitrogen compounds.

Within the uncertainties of the assumptions in our physical and biological models, we are pleased that the budgets of Table 4 are in fair agreement after one year of simulated time. Additional in situ and satellite data, together with inclusion of second-order processes in another simulation model, will advance our understanding of the way carbon and nitrogen are cycled on the margins of the ocean. For example, arguments about unbalanced global nitrogen budgets have been advanced in the past (McElroy, 1983) and hinge on uncertainties about the amount of both sinks and sources (Fogg, 1982; Walsh, 1984), particularly nitrogen fixation, which we have neglected.

In a first-order approximation, however, it would appear that less than 25% of man's accelerated inputs of nitrogen are possibly stored in bottom sediments on the continental margin. The remainder may be dispersed in dissolved form, after initial uptake in the euphotic zone and remineralization beneath the pycnocline. On a relative basis, the presence of a western boundary current in the Gulf of Mexico may increase the "new" and total production by two- to threefold that of the other oligotrophic regions in the

ocean. As concomitant ocean color and thermal data from satellite imagery continue to become available, we will refine the above calculations to both extend the spatial domain of these models to regions of open boundary conditions, and to resolve apparent interannual temporal variations of primary production. The fate of this fixed carbon and the nature of the organisms involved await the next generation of coupled physical/biological models.

## Acknowledgements

This research was supported by the Office of Naval Research under grant N00014-87-G-0218, by the National Aeronautics and Space Administration under grant NAGW-678, and by the Department of Energy under grant DE-FG05-85ER60285. We thank George Berberian, Mike Dagg, Otis Brown, and Bob Evans for the unpublished data used in this analysis.

## References Cited


Alexander, J. E., J. H. Steele and E. F. Corcoran. 1962. The seasonal cycle of chlorophyll in Florida Straits. Proc. Annu. Gulf Caribb. Fish. Inst., 14, 63-67.

Armstrong, D. W. 1974. Some dynamics of carbon, nitrogen, and phosphorus in the marine shelf environment of the Mississippi Fan. M.S. Thesis, Texas A&M Univ., College Station, pp. 1-79.

Atkinson, L. P. and D. Wallace. 1975. The source of unusually low surface salinities in the Gulf Stream off Georgia. Deep-Sea Res., 22, 913-916.

Atkinson, L. P., D. W. Menzel and K. A. Bush. 1985. Oceanography of the southeastern U.S. continental shelf. Coast. Estuar. Sci., 2, American Geophysical Union, Washington, pp. 1-156.

Auer, S. J. 1987. Five-year climatological study of the Gulf Stream system and its associated rings. J. Geophys. Res., 92, 11709-11726.

Azam, F., T. Fenchel, J. G. Field, J. S. Gray, L. A. Meyer-Reed and F. Thingstad. 1983. The ecological role of water-column microbes in the sea. Mar. Ecol. Prog. Ser., 10, 257-263.

Bane, J. M. and W. K. Dewar. 1988. Gulf Stream bimodality and variability downstream of the Charleston Bump. J. Geophys. Res., 93, 6695-6710.

Bannister, T. T. and A. D. Weidemann. 1984. The maximum quantum yield of phytoplankton photosynthesis in situ. J. Plankton Res., 6, 275-294.

Berberian, G. A. and R. B. Starr. 1978. The circulation between the Cayman Sea and the Gulf of Mexico as deduced from nutrient distributions, in Cooperative Investigations of the Caribbean and Adjacent Regions, H. B. Stewart, ed., FAO Fisheries Report 200, Rome, pp. 255-266.

Berger, W. H., K. Fischer, G. Lai and G. Wu. 1987. Ocean productivity and organic carbon flux. SIO Ref. 87-30, Univ. of California, San Diego, pp. 1-67.

Berryhill, H. L. 1977. Environmental studies, South Texas Outer Continental Shelf, 1975: An atlas and integrated study. Prepared for the Bureau of Land Management, Contract 08550-MU5-20, pg. 240.

Bienfang, P. K., J. Szyper and E. Laws. 1983. Sinking rate and pigment responses to light limitation of a marine diatom: implications to dynamics of chlorophyll maximum layers. Oceanol. Acta, 6, 55-62.

Blumberg, A. F. and G. L. Mellor. 1983. Diagnostic and prognostic numerical evaluation studies of the South Atlantic Bight. J. Geophys. Res., 88, 4579-4592.

Blumberg, A. F. and G. L. Mellor. 1985. A simulation of the circulation in the Gulf of Mexico. Israel J. Earth Sci., 34, 122-144.

Brooks, I. H. and P. P. Niiler. 1975. The Florida Current at Key West: summer 1972. J. Mar. Res., 33, 83-92.

Bryan, K. and M. D. Cox. 1972. The circulation of the world ocean: a numerical study. 1. A homogeneous model. J. Phys. Oceanogr., 2, 319-335.

Capone, D. G. and E. J. Carpenter. 1982. Nitrogen fixation in the marine environment. Science, 217, 1140-1142.

Christensen, J. P. 1981. Oxygen consumption, denitrification, and sulfate reduction in coastal marine sediments. Ph.D. Thesis, Univ. of Washington, Seattle, pp. 1-231.

Cochrane, J. D. and F. J. Kelly. 1986. Low-frequency circulation on the Texas-Louisiana continental shelf. J. Geophys. Res., 91, 10645-10659.

Cox, M. D. 1975. A baroclinic numerical model of the world ocean, in Numerical Models of Ocean Circulation, National Academy of Science, Washington, pp. 107-120.

Csanady, G. T. 1976. Mean circulation in shallow seas. J. Geophys. Res., 81, 5389-5399.

Csanady, G. T. 1986. Mass transfer to and from small particles in the sea. Limnol. Oceanogr., 31, 237-248.

Csanady, G. T. and P. Hamilton. 1988. Circulation of slopewater. Cont. Shelf Res., 8, 565-624.

Cullen, J. J. and R. W. Eppley. 1981. Chlorophyll maximum layers of the southern California Bight and possible mechanisms of their formation and maintenance. Oceanol. Acta, 4, 23-32.

Dagg, M. J., P. B. Ortner and F. Al-Yamani. 1987. Winter-time distribution and abundance of copepod nauplii in the northern Gulf of Mexico. Fish. Bull., 86, 319-330.

Dinnel, S. P. and W. J. Wiseman. 1986. Fresh water on the Louisiana and Texas shelf. Cont. Shelf Res., 6, 765-784.

Elliott, B. A. 1982. Anticyclonic rings in the Gulf of Mexico. J. Phys. Oceanogr., 12, 1291-1309.

El-Sayed, S. Z. 1972. Primary productivity and standing crop of phytoplankton, in Chemistry, Primary Productivity, and Benthic Algae of the Gulf of Mexico, V. C. Bushnell, ed., Ser. Atlas Mar. Environ., Am. Geogr. Soc., 22, 8-13.

El-Sayed, S. Z. and C. C. Trees. 1980. Ecological studies of phytoplankton in the Gulf of Mexico during NOAA/NMFS Oregon II cruise. Texas A&M Tech. Rep. 80-8-T, pp. 1-53.

Eppley, R. W. 1972. Temperature and phytoplankton growth in the sea. Fish. Bull., 70, 1063-1085.

Eppley, R. W., E. H. Renger and W. G. Harrison. 1979. Nitrate and phytoplankton production in southern California coastal waters. Limnol. Oceanogr., 24, 483-494.

Eppley, R. W. and B. J. Peterson. 1980. Particulate organic matter flux and planktonic new production in the deep ocean. Nature, 282, 677-680.

ESE and LGL. 1985. Southwest Florida shelf benthic communities study. Year 4 annual report submitted by Environmental Science and Engineering, Inc., and LGL Ecological Research Associates, Inc., to Marine Minerals Service, Metairie, Louisiana. Contract No. 14-12-0001-30071, pg. 94.

Etter, P. C. 1983. Heat and freshwater budgets in the Gulf of Mexico. J. Phys. Oceanogr., 13, 2058-2069.

Fogg, G. E. 1982. Nitrogen cycling in sea water. Philos. Trans. R. Soc. London, B 296, 511-570.

Franks, P. J., J. S. Wroblewski and G. R. Flierl. 1986. Prediction of phytoplankton growth in response to the frictional decay of a warm-core ring. J. Geophys. Res., 91, 7603-7610.

Fucik, K. W. 1974. The effect of petroleum operations on the phytoplankton ecology of the Louisiana coastal waters. M.S. thesis, Texas A&M, College Station, pp. 1-82.

Furnas, M. J. and T. J. Smayda. 1987. Inputs of subthermocline waters and nitrate onto the Campeche Bank. Cont. Shelf Res., 7, 161-175.

Gearing, P. J. 1975. Stable carbon isotope ratios of continental margin sediments. Ph.D. Thesis, Univ. of Texas, Austin, pp. 1-154.

Gearing P., J. N. Gearing, T. F. Lytle and J. S. Lytle. 1976. Hydrocarbons in 60 northeast Gulf of Mexico shelf sediments: a preliminary survey. Geochim. Cosmochim. Acta, 40, 1005-1017.

Gearing, P., F. E. Plucker and P. L. Parker. 1977. Organic carbon stable isotope ratios of continental margin sediments. Mar. Chem., 5, 251-266.

Geider, R. J. and B. A. Osborne. 1986. Light absorption, photosynthesis, and growth of Nannochloris atomus in nutrient-saturated cultures. Mar. Biol., 93, 351-360.

Goldman, J. C., J. J. McCarthy and D. G. Peavey. 1979. Growth rate influence on the chemical composition of phytoplankton in oceanic waters. Nature, 279, 210-215.

Gordon, A. L. 1967. Circulation of the Caribbean Sea. J. Geophys. Res., 77, 62-73.

Gordon, H. R., O. B. Brown, R. H. Evans, J. W. Brown, R. C. Smith, K. S. Baker and D. K. Clarke, 1988. A semianalytic radiance model of ocean color. J. Geophys. Res., 93, 10909-10924.

Haines, J. R., R. M. Atlas, R. P. Griffiths and R. Y. Morita. 1981. Denitrification and nitrogen fixation in Alaska continental shelf sediments. Appl. Environ. Microbiol., 41, 412-421.

Haltiner, G. J. 1971. Numerical weather predictions. J. Wiley & Sons, New York, pp. 1-317.

Hamilton, P. and M. Rattray. 1978. A numerical model of the depth dependent, wind driven circulation on a continental shelf. J. Phys. Oceanogr., 8, 437-457.

Hansen, D. V. and R. L. Molinari. 1979. Deep currents in the Yucatan Strait. J. Geophys. Res., 84, 359-362.

Hathaway, J. C. 1971. WHOI data file, Continental Margin program, Atlantic coast of the United States. WHOI Technical Report 77-15.

Hedges, J. I. and P. L. Parker. 1976. Land-derived organic matter in surface sediments from the Gulf of Mexico. Geochim. Cosmochim. Acta, 40, 1019-1029.

Hinga, K. R., J. M. Sieburth and G. R. Heath. 1979. The supply and use of organic matter at the deep-sea floor. J. Mar. Res., 37, 557-579.

Hofmann, E. E. and S. J. Worley. 1986. An investigation of the circulation of the Gulf of Mexico. J. Geophys. Res., 91, 14221-14236.

Holland, W. R. and A. D. Hirschman. 1972. A numerical calculation of the circulation of the North Atlantic Ocean. J. Phys. Oceanogr., 5, 642-669.

Holland, W. R. and L. B. Lin. 1975. On the origin of mesoscale eddies and their contribution to the general circulation of the ocean. I. A preliminary numerical experiment. J. Phys. Oceanogr., 5, 642-657.

Hulburt, H. E. and J. D. Thompson. 1980. A numerical study of Loop Current intrusions and eddy shedding. J. Phys. Oceanogr., 10, 1611-1651.

Jassby, A. D. and T. Platt. 1976. Mathematical formulation of the relationship between photosynthesis and light for phytoplankton. Limnol. Oceanogr., 21, 540-547.

Jenkins, W. J. 1988. Nitrate flux into the euphotic zone near Bermuda. Nature, 331, 521-523.

King, F. D. and A. H. Devol. 1979. Estimates of vertical eddy diffusion through the thermocline from phytoplankton uptake rates in the mixed layer of the eastern tropical Pacific. Limnol. Oceanogr., 24, 645-651.

Kirwan, A. D., J. K. Lewis, A. W. Indest, P. Reinersman and I. Quintero. 1988. Observed and simulated kinematic properties of Loop Current rings. J. Geophys. Res., 93, 1189-1198.

Kullenberg, G. E. 1976. On vertical mixing and the energy transfer from the wind to the water. Tellus, 28, 159-165.

Lampitt, R. S. 1985. Evidence for seasonal deposition of detritus to the deep-sea floor and its subsequent resuspension. Deep-Sea Res., 32, 885-898.

Lee, T. N., L. P. Atkinson and R. Legeckis. 1981. Observation of a Gulf Stream frontal eddy on the Georgia continental shelf, April 1977. Deep-Sea Res., 28, 347-378.

Leipper, D. F. 1970. A sequence of current patterns in the Gulf of Mexico. J. Geophys. Res., 75, 637-657.

Levitus, S. 1982. Climatological atlas of the world ocean. NOAA Prof. Pap. No. 13, 1-173.

Lewis, M. R., W. G. Harrison, N. S. Oakey, D. Hebert and T. Platt. 1986. Vertical nitrate fluxes in the oligotrophic ocean. Science, 234, 870-873.

LGL Ecological Research Associates. 1986. Gulf of Mexico continental slope study annual report: year 2. Submitted to Marine Minerals Management Service, Metairie, Louisiana, Contract No. 14-12-0001-30212, pp. B10 - B-19.

Lochte, K., and C. M. Turley. 1988. Bacteria and cyanobacteria associated with phytodetritus in the deep sea. Nature, 333, 67-69.

Malone, T. C. and P. J. Neale. 1981. Parameters of light-dependent photosynthesis for phytoplankton size fractions in temperate estuarine and coastal environments. Mar. Biol., 61, 289-297.

Martin, J. H., G. A. Knauer, D. M. Karl and W. M. Broenkow. 1987. VERTEX: carbon cycling in the northeast Pacific. Deep-Sea Res., 34, 267-285.

Maul, G. A. 1977. The annual cycle of the Gulf Loop. Part I. Observations during a one-year time series. J. Mar. Res., 35, 219-247.

Maul, G. A. 1978. The 1972-73 cycle of the Gulf Loop Current. Part II: mass and salt balances of the basin, in Cooperative Investigations of the Caribbean and Adjacent Regions, H. B. Stewart, ed., FAO Fisheries Report 200, Rome, pp. 597-619.

Maul, G. A., G. C. Thomas and T. A. Nelsen. 1979. Hydrographic data from the NOAA ship Researcher during the October 1977 ocean color and circulation cruise in the Gulf of Mexico. NOAA Data Report ERL AOML-1, Miami, pp. 1-31.

McElroy, M. B. 1983. Marine biological controls on atmospheric $CO_2$ and climate. Nature, 302, 328-329.

Mellor, G. L. and T. Yamada. 1974. A hierarchy of turbulence closure models for planetary boundary layers. J. Atmos. Sci., 31, 1791-1806.

Merrell, W. J., J. M. Morrison, W. D. Nowlin, R. L. Molinari, I. H. Brooks and R. Yager. 1978. A description of the circulation observed in the eastern Gulf of Mexico during CICAR survey month II, May 1972, in Cooperative Investigations of the Caribbean and Adjacent Regions, H. B. Stewart, ed., FAO Fisheries Report 200, Rome, pp. 51-61.

Mitchum, C. T. and W. Sturges. 1982. Wind-driven currents on the West Florida shelf. J. Phys. Oceanogr., 12, 1310-1317.

Molinari, R. L. and R. E. Yager. 1977. Upper layer hydrographic conditions at the Yucatan Strait during May 1972. J. Mar. Res., 35, 11-20.

Montgomery, R. 1941. Transport of the Florida Current off Habana. J. Mar. Res., 4, 198-220.

Morrison, J. M. and W. D. Nowlin. 1977. Repeated nutrient, oxygen, and density sections through the Loop Current. J. Mar. Res., 35, 105-126.

Muller, P. J. and E. Suess. 1979. Productivity, sedimentation rate, and sedimentary organic matter in the ocean. I. Organic carbon preservation. Deep-Sea Res., 26, 1347-1362.

Muller-Karger, F. E., J. J. Walsh, D. A. Dieterle and R. H. Evans. 1988. The seasonal cycle of the circulation in the western North Atlantic: the interplay between the open ocean, the Caribbean Sea, and the Gulf of Mexico. EOS, 69, 1113.

Munk, W. H. 1950. On the wind-driven ocean circulation. J. Meteorol., 7, 79-93.

Munk, W. H. and E. R. Anderson. 1948. Notes on a theory of the thermocline. J. Mar. Res., 7, 277-295.

Murphy, E. B., K. A. Steidinger, B. S. Roberts, J. Williams and J. W. Jolley. 1975. An explanation for the Florida east coast Gymnodinium breve red tide of November 1972. Limnol. Oceanogr., 20, 481-486.

Neuberger, H. 1965. Introduction to physical meteorology. Pennsylvania State Univ. Press, University Park, pp. 1-271.

Niiler, P. P. 1975. Deepening of the wind-mixed layer. J. Mar. Res., 33, 405-422.

Niiler, P. P. and W. S. Richardson. 1973. Seasonal variability of the Florida Current. J. Mar. Res., 31, 144-167.

Nowlin, W. D. and H. J. McLellan. 1967. A characterization of the Gulf of Mexico waters in winter. J. Mar. Res., 25, 24-59.

Nowlin, W. D. and J. M. Hubertz. 1972. Contrasting summer circulation patterns for the eastern Gulf Loop Current versus anticyclonic ring. Texas A&M Univ. Oceanogr. Stud. 2, L. R. Capurro and R. O. Reid, eds., Gulf Publishing Co., Houston, pp. 119-138.

O'Brien, J. J. 1971. A two-dimensional model of the wind-driven North Pacific. Invest. Pesq., 35, 331-349.

O'Brien, J. J. 1986. The hyperbolic problem, in Advanced Physical Oceanographic Numerical Modelling, J. J. O'Brien, ed., Reidel, Dordrecht, pp. 165-186.

O'Brien, J. J. and H. E. Hulburt. 1972. A numerical model of coastal upwelling. J. Phys. Oceanogr., 2, 14-26.

O'Brien, J. J. and G. W. Heburn. 1983. The state-of-the-art in coastal ocean modelling: a numerical model of coastal upwelling off Peru--including mixed layer dynamics, in Coastal Ocean Modelling, H. G. Gade, A. Edwards and H. Svendsen, eds., Plenum, New York, pp. 113-164.

Ortner, P. B., R. L. Ferguson, S. R. Piotrowicz, L. Chesal, G. A. Berberian and A. V. Palumbo. 1984. Biological consequences of hydrographic and atmospheric advection within the Gulf Loop Intrusion. Deep-Sea Res., 31, 1101-1120.

Parker, R. A. 1977. Radiocarbon dating of marine sediments. Ph.D. Thesis, Texas A&M Univ., College Station, pp. 1-128.

Paskausky, D. F. and R. O. Reid. 1972. A barotropic prognostic numerical circulation model, in Contributions on the Physical Oceanography of the Gulf of Mexico, Volume II, L. R. Capurro and R. O. Reid, eds., Gulf Publishing Company, Houston, pp. 163-176.

Platt, T. and A. D. Jassby. 1976. The relationship between photosynthesis and light for natural assemblages of coastal marine phytoplankton. J. Phycol., 12, 421-430.

Platt, T. and W. G. Harrison. 1985. Biogenic fluxes of carbon and nitrogen in the ocean. Nature, 318, 55-58.

Reed, R. K. 1977. On estimating insolation over the ocean. J. Phys. Oceanogr., 7, 482-485.

Rowe, G. T. and D. W. Menzel. 1971. Quantitative benthic samples from the deep Gulf of Mexico. Bull. Mar. Sci., 21, 556-566.

Scholl, D. W. 1963. Sedimentation in modern coastal swamps, southwestern Florida. Am. Assoc. Pet. Geol. Bull., 47, 1581-1603.

Schroeder, W. W., S. P. Dinnel, W. J. Wiseman and W. J. Merrell. 1987. Circulation patterns inferred from the movement of detached buoys in the eastern Gulf of Mexico. Cont. Shelf Res., 7, 883-894.

Shokes, R. F. 1976. Rate-dependent distribution of lead-210 and interstitial sulfate in sediments of the Mississippi River delta. Ph.D. Thesis, Texas A&M Univ., College Station, pp. 1-123.

Smetacek, V. S. 1985. Role of sinking in diatom life-history cycles: ecological, evolutionary, and geological significance. Mar. Biol., 84, 239-251.

Smolarkiewicz, P. K. 1983. A simple positive definite advection scheme with small implicit diffusion. Mon. Wea. Rev., 111, 479-486.

Steele, J. H. 1964. A study of production in the Gulf of Mexico. J. Mar. Res., 22, 211-222.

Stetson, H. C. and P. D. Trask. 1953. The sedimentation of the western Gulf of Mexico. Pap. Phys. Oceanogr. Meteorol., 12, 1-46.

Stommel, H. 1965. The Gulf Stream, Univ. of California Press, Berkeley, pp. 1-248.

Stommel, H. 1987. A View of the Sea. Princeton University Press, Princeton, pp. 1-165.

Sturges, W. and J. C. Evans. 1983. On the variability of the Loop Current in the Gulf of Mexico. J. Mar. Res., 41, 639-653.

Sugimoto, T. and T. Ichiye. 1988. On seasonal and year-to-year variations of the Loop Current and eddy formation in the Gulf of Mexico based on rotating model experiments. Deep-Sea Res., 35, 569-594.

SUSIO. 1977. Baseline monitoring studies, Mississippi, Alabama, Florida, outer continental shelf, 1975-76. Volume III. Results. Compiled by the State University System of Florida Institute of Oceanography, St. Petersburg, for the Bureau of Land Management. Contract No. 08550-CTS-30. U.S. Document PB-282 803, Springfield, pg. 361.

Sverdrup, H. U., M. W. Johnson and R. H. Fleming. 1942. The Oceans, Prentice-Hall, Englewood Cliffs, pp. 1-1060.

Thomas, W. H. and G. Simmons. 1970. Phytoplankton production in the Mississippi Delta, in Recent Sediments, Northwest Gulf of Mexico, F. P. Shepard, F. B. Phleger, and T. H. van Andel, eds., Am. Assoc. Petrol. Geol., Tulsa, 103-116.

Thompson, J. D. 1974. The coastal upwelling cycle on a beta-plane. Hydrodynamics and thermodynamics. Ph.D. thesis, Florida State Univ., Tallahassee, p. 1-141.

Trask, P. D. 1953. The sediments of the western Gulf of Mexico, Part II. Chemical studies of sediments in the western Gulf of Mexico. Pap. Phys. Oceanogr. Meteorol., 12, 47-120.

Trees, C. C. 1985. Remote sensing of ocean color in the northern Gulf of Mexico. Ph.D. thesis, Texas A&M University, College Station, pp. 1-258.

Upshaw, C. F., W. B. Creath and F. L. Brooks. 1966. Sediments and microfauna off the coasts of Mississippi and adjacent states. Miss. Geol. Econ. Topogr. Sur. Bull., 106, 1-127.

Vasilev, G. D. and Y. A. Torin. 1969. Oceanographic and fishing-biological characteristics of the Gulf of Mexico and the Caribbean Sea, in Soviet-Cuban Fishery Research, A. S. Bogdanov, ed., Israel Programs for Scientific Translation, Jerusalem, pp. 225-250.

Vukovich, F. M. and G. A. Maul. 1985. Cyclonic eddies in the eastern Gulf of Mexico. J. Phys. Oceanogr., 15, 105-117.

Vukovich, F. M., B. W. Crissman, M. Bushnell and W. J. King. 1979. Some aspects of the oceanography of the Gulf of Mexico using satellite and in situ data. J. Geophys. Res., 84, 7749-7768.

Wada, E. and A. Hattori. 1972. Nitrite distribution and nitrate reduction in deep sea waters. Deep-Sea Res., 19, 123-132.

Wallcraft, A. 1986. Gulf of Mexico circulation modeling study. Progress report by JAYCOR to Minerals Management Service, Metairie, Louisiana. Contract No. 14-12-0001-30073, pp. 1-94.

Walsh, J. J. 1983. Death in the sea: enigmatic phytoplankton losses. Prog. Oceanogr., 12, 1-86.

Walsh, J. J., 1984. The role of the ocean biota in accelerated ecological cycles: a temporal view. Bioscience, 34, 499-507.

Walsh, J. J. 1988. On the Nature of Continental Shelves, Academic Press, New York, pp. 1-520.

Walsh, J. J., G. T. Rowe, R. L. Iverson and C. P. McRoy. 1981. Biological export of shelf carbon is a neglected sink of the global $CO_2$ cycle. Nature, 291, 196-201.

Walsh, J. J., E. T. Premuzic, J. S. Gaffney, G. T. Rowe, G. Harbottle, R. W. Stoenner, W. L. Balsam, P. R. Betzer and S. A. Macko. 1985. Organic storage of $CO_2$ on the continental slope off the mid-Atlantic bight, the southeastern Bering Sea, and the Peru coast. Deep-Sea Res., 32, 853-883.

Walsh, J. J., D. A. Dieterle and M. B. Meyers. 1988a. A simulation analysis of the fate of phytoplankton within the Mid-Atlantic Bight. Cont. Shelf Res., 8, 757-788.

Walsh, J. J., P. E. Biscaye and G. T. Csanady. 1988b. The 1983-84 Shelf Edge Exchange Processes (SEEP)-I experiment: hypotheses and highlights. Cont. Shelf Res., 8, 435-456.

Ward, B. B., R. J. Olsen and M. J. Perry. 1982. Microbial nitrification rates in the primary nitrite maximum off southern California. Deep-Sea Res., 29, 247-255.

Wennekens, M. P. 1959. Water mass properties of the Straits of Florida and related waters. Bull. Mar. Sci., 9, 1-52.

Woods, J. D. 1988. Mesoscale upwelling and primary production, in Towards a theory of biological-physical interaction in the world ocean, B. J. Rothschild, ed., D. Reidel, Dordrecht (in press).

Wroblewski, J. S. and J. G. Richman. 1987. The nonlinear response of plankton to wind mixing events--implications for larval fish survival. J. Plankton Res., 9, 103-123.

Wüst, G. 1964. Stratification and Circulation in the Antillean-Caribbean Basins, Columbia University Press, New York, pp. 1-201.